MOLECULAR INTERACTIONS BETWEEN VARIOUS MODEL CELL MEMBRANES AND MEMBRANE ACTIVE PEPTIDES STUDIED BY SUM FREQUENCY GENERATION VIBRATIONAL SPECTROSCOPY

by

Lauren Soblosky

A dissertation submitted in partial fulfillment
of the requirements for the degree of
Doctor of Philosophy
(Chemistry)
in the University of Michigan
2014

Doctoral Committee:

Professor Zhan Chen, Chair
Professor Kristina I. Håkansson
Professor Ayyalusamy Ramamoorthy
Professor John J. G. Tesmer

To Mom and Dad

ACKNOWLEDGEMENTS

The research included in this dissertation would not have been possible without my research advisor, Professor Zhan Chen. I am grateful for his support and to have had the opportunity to work in his lab for the past five years. I would also like to thank my committee, Professor Kristina Håkansson, Professor Ayyalusamy Ramamoorthy, and Professor John Tesmer for their feedback and suggestions.

I am also thankful for all of the great lab mates who have helped me and provided support over my five years here. The other four students in my year, Chi Zhang, Josh Jasensky, Bei Ding and Yuwei Liu were a wonderful group to work and progress through the program with. I am especially grateful for the discussions with Bei Ding pertaining to our collaborative work in Chapter 4. I would also like to thank Dr. Pei Yang for his technical knowledge and maintenance of the laser as well as Dr. Andrew Boughton for his help early on and discussions throughout my time here.

Funding for the work in this thesis was provided by NIH.

I would like to thank my friends and family who have encouraged and supported me even when I was discouraged. Special thanks to my parents, Joseph and Lorraine Soblosky; my sisters, Katie and Monica; and Richard Sutherland.

TABLE OF CONTENTS

LIST OF FIGURES

LIST OF TABLES

ABSTRACT

MOLECULAR INTERACTIONS BETWEEN VARIOUS MODEL CELL MEMBRANES AND MEMBRANE ACTIVE PEPTIDES STUDIED BY SUM FREQUENCY GENERATION VIBRATIONAL SPECTROSCOPY

by

Lauren Soblosky

Chair: Zhan Chen

Since the use of native cell membranes for biophysical studies is difficult, membrane mimetics are often used. For example, they are frequently used to study the interaction between membrane active peptides and cell membranes. However, if the model is too simple, it may not be able to provide physiologically meaningful information. As a result, it is important to move toward models that are more similar to native cell membranes in order to study interactions in an environment that is more relevant to the native state. In this thesis work, we utilized sum frequency generation vibrational spectroscopy (SFG) to study how peptides interact with three different model membranes representing the mammalian plasma cell membrane, the bacterial plasma cell membrane, and the Gram-negative bacterial outer cell membrane.

The mammalian plasma cell membrane was modeled by using a solid supported lipid bilayer prepared with 1-palmitoyl-2-oleoyl-*sn*-glycero-3-phosphocholine (POPC):cholesterol (1:1) mixture. We compared how the antimicrobial peptide LL-37 interacted with this bilayer

and a pure POPC bilayer. It was found that the addition of cholesterol inhibited the ability of LL-37 peptide to interact with the phospholipid bilayers as evidenced by the absence of SFG signal from bilayer associated peptide. This is possibly due to the cholesterol causing the fluid disordered bilayer to become more ordered which makes it more difficult for the peptide to interact through hydrophobic interactions with the lipid acyl chains. The hydrophobic interactions are important for this system because there would be little interaction between the cationic peptide and the zwitterionic lipid head groups. Similarly, for a POPC:POPG mixed lipid bilayer, the introduction of cholesterol also reduced the interactions between LL-37 and the lipid bilayer.

Native bacterial plasma cell membrane was modeled by using bilayers of 1,2-dipalmitoyl-d62-*sn*-glycero-3-phosphoglycerol (dDPPG)-*E. coli* polar lipid extract. The interactions of selected peptides with these bilayers and those containing dDPPG-1-palmitoyl-2-oleoyl-*sn*-glycero-3-phosphoglycerol (POPG) were compared. These peptides include MSI-594, ovispirin-1 G18, magainin 2, melittin, and LL-37. It was found that while POPG lipids are able to model some aspects of the interaction, such as peptide association with the lipid bilayer, a more complex lipid mixture is able to provide information that is more similar to interactions with a native cell membrane. Additionally, the use of asymmetric lipid bilayers with these two systems was able to show that the more complicated interaction mechanisms, such as interaction kinetics observed by lipid bilayer leaflet signal changes after peptide addition, can be studied with the *E. coli* polar lipid extract but were not easily observed in the POPG lipid system. This is at least in part due to the difference in charge of the two different lipid systems; the POPG system is entirely anionic while the *E. coli* polar lipid bilayer is approximately one third the charge of a POPG bilayer. This difference in charge will cause the overall peptide-lipid bilayer

interaction to be different because the charge interactions may interfere with other interactions, such as hydrophobic-hydrophobic interactions, that are likely important after initial peptide association.

The bacterial outer cell membrane was modeled using dDPPG-Kdo 2 Lipid A bilayer and dDPPE:dDPPG (3:1)-Lipid A from *Salmonella minnesota* R595 bilayer. We studied the interaction of isotope-labeled ovispirin-1 peptides with these membranes and compared them to their interaction with phospholipid bilayers composed of pure 1,2-dipalmitoyl-*sn*-glycero-3-phosphoglycerol (DPPG) or of a 1,2-dipalmitoyl-*sn*-glycero-3-phosphoethanolamine (DPPE)/DPPG mixture. It was found that these peptides interact similarly with both of these lipid membrane systems. Because the peptide interacted similarly in systems that primarily differed in the number of sugars extending past the head group region, it can be determined that there is no effect on peptide interaction at 50 μg/ml with a lipid A region with no extra sugars versus one with two sugars attached extending "outside" of the cell. Therefore, the higher resistance of Gram-negative bacteria cannot be explained by the presence of the inner core oligosaccharide region sugars. Additionally, we found through isotope labeling that the ovispirin-1 is lying down at the lipid head group-acyl chain interface, which is the same as its orientation when associated with DPPG bilayers, as observed in a previous study. From this data it was determined that the extra sugars did not change the orientation of the ovispirin-1 with the lipid bilayer.

The studies presented here characterize peptide-lipid interactions at model lipid bilayers that are more physiologically relevant than relatively simple phospholipid environments. This demonstrates the importance of bilayer choice in studying antimicrobial peptide interactions and characterizing their bilayer disruption mechanisms. With the knowledge obtained about peptide

activity at these more realistic bilayers, future studies in other areas focusing on predicting antimicrobial effectiveness or designing new antimicrobial molecules will more accurate and progress more quickly compared to studies utilizing simple model bilayers.

CHAPTER 1

INTRODUCTION

1.1 Motivation

Cell membranes are incredibly varied and complex biological structures. The idea of a "fluid mosaic model" was developed by S. J. Singer and says that these membranes can be thought of as fluid phospholipid matrices containing randomly distributed amphipathic globular integral proteins [1]. Basically, the cell membrane is regarded as a bilayer of phospholipids containing proteins and other structures that serve various functions. The overall function of the bilayer is to contain the internal portion of the cell while being selectively permeable and facilitating cell communication. The lipid composition varies depending on the organism and the cell type [2-5]. Proteins such as ion channels, cell recognition proteins, and receptor proteins are integrated into the lipid bilayer and allow the cell to function [3, 6-8]. Obviously, cell membranes are inherently complex.

Antibiotic resistance is a well-documented problem that has appeared after years of utilizing antibiotics to combat infection. The resulting infections caused by antibiotic resistant strains are difficult and expensive to treat which has caused antibacterial resistance to be a concern for the healthcare industry and the general population. As a result, there has been an increased effort to find new and better alternatives to antibiotics.

In general, antibiotics target systems in the bacteria that are vital to their ability to function such as cell wall synthesis, protein synthesis, DNA replication, RNA synthesis and folate synthesis [9-12]. The drug targets in the cell that influence these systems include enzymes, ribosomes, RNA, and less often, bacterial cell membranes [13]. Over time, bacteria become resistant to antibacterial drugs through different mechanisms such as adapting to make it harder for a drug to enter the cell, gaining the ability to expel the molecule from the cell [14, 15], changing the target molecule such that the antibiotic molecule cannot interact with it [16, 17], or altering the antibiotic drug to render it inactive [9, 11, 18-20]. This adaption is often achieved through either passing on a gene for the resistance feature to daughter cells, or through the passing of the genes directly to other bacteria through horizontal gene transfer of plasmids [18, 21, 22].

One well known antibiotic is penicillin [23]. Penicillins are β-lactam antibiotics [13]. As an antibiotic in this family, it affects the cell wall synthesis mechanism. The β-lactam binds to transpeptidase (penicillin binding protein, PBP), an enzyme that crosslinks the peptidoglycan units of the cell wall [24-26]. With the enzyme bound, it cannot crosslink the peptidoglycan and the cell wall integrity suffers and the cell eventually lyses [27]. However, bacteria have developed resistances against β-lactam antibiotics. One mechanism of resistance is the hydrolyzation of amide bond in the β-lactam ring of the drug by β-lactamase enzymes, which causes the drug to become inactive [28, 29]. Another mechanism of resistance is altering the peptidoglycan enzyme target so that the PBP has a lower affinity for β-lactam or is less sensitive [27, 30-33]. Defects in porins contribute to the outer membrane becoming less permeable which leads to increased resistance [34, 35]. Also, for Gram-negative bacteria in particular, drug efflux pumps that transport drugs out of the cell increase resistance as well [36, 37]. Given that there

are several different ways that bacteria can develop antimicrobial resistance, it is important that we continue to try to design or discover new or alternative therapies that are less prone to opposition so we can continue to treat infections.

One alternative is the use of antimicrobial peptides (AMPs). AMPs have been shown to target cell membranes, rather than particular proteins or other features of a bacterial cell. It is thought that cell membranes are much more difficult to change to develop resistance compared to those other features [38, 39]. Because they target a structure that is not as easy to modify, AMPs are an attractive alternative to traditional antibiotics and extensive research has been performed to develop antimicrobial peptide molecules with broad spectrum activities that are not toxic to human cells. As part of this process, it is important to understand the anti-microbial mechanism of these natural peptide molecules. These molecules will be interacting with complex bacterial cell membranes. However, it is difficult to study peptide-bilayer interaction in actual cells. Instead, model cell membranes are used to investigate the association, interaction and kinetics of peptide-bilayer interactions and this knowledge is then used to guide peptide development and help explain the interactions with real bacterial cells. Because we are using the interactions with these model membranes to learn about the potential interactions on actual membranes, we should work toward making the model membranes as realistic as possible. However, as more components are added, the system becomes more complex and potentially more difficult to study.

Techniques such as nuclear magnetic resonance (NMR) spectroscopy and Fourier transform infrared spectroscopy (FTIR) have been used to study peptide-bilayer interactions. NMR is a powerful technique that can give us orientation information about the peptide as well as information about the bilayer's order [40-47]. However, its sensitivity is low and relatively

large amounts of peptide are required for studies. As a result, it is sometimes difficult to study peptides at their physiological concentrations. FTIR is a vibrational spectroscopy and attenuated total reflectance (ATR-FTIR) can probe orientation information of membrane associated peptides and proteins [48-53]. Again, it has limited sensitivity for these applications and its "surface sensitivity" is attributed to the short penetration depth of the evanescent wave. However, ATR-FTIR actually probes deeper than just the surface (or lipid membrane/lipid bilayer). Also, because it probes more than just surfaces/interfaces, it generally has a large water background that must be subtracted during data processing.

Sum frequency generation vibrational spectroscopy (SFG) is an inherently surface sensitive vibrational technique. SFG has microgram sensitivity and has very low or, in many cases, no bulk signal background contributions. It has been shown to be a powerful tool in elucidating peptide-bilayer interaction and orientation [54-63]. In this work, we used SFG to investigate several examples in which the model cell membrane was made more complex by the addition of certain components and compare the interaction of peptides with those models to the interaction with commonly used simpler models. We elucidated the molecular interactions between peptides and model cell membranes to help design and guide development of antimicrobial peptides with improved antimicrobial properties.

1.2 Sum Frequency Generation Vibrational Spectroscopy

1.2.1 Brief Overview

Sum frequency generation vibrational spectroscopy (SFG) is based on a second order nonlinear optical process in which a fixed visible beam and a tunable infrared (IR) beam overlap in space and time, which results in a third beam produced at a frequency which is a sum of the

first two ($\omega_{vis}+ \omega_{IR} = \omega_{SF}$) [64, 65]. The sum frequency process is actually a combination of IR absorption and anti-stokes Raman scattering. When the incident IR frequency, ω_{IR}, matches a vibrational transition, the intensity of the sum frequency beam (ω_{SF}) is enhanced. This enhancement is observed as a peak in the spectrum. The resulting data is shown as a function of incident ω_{IR}, which is similar to an IR or Raman spectrum.

SFG signal is generated by a second order nonlinear optical process. Therefore, it does not exist in materials with inversion symmetry under the electric dipole approximation due to the selection rule. Most bulk materials possess inversion symmetry, while surfaces and interfaces do not [64-68]. As a result, SFG is a very powerful technique that has been used to study surfaces and interfaces. Additionally, orientation information can be obtained by using certain input and output beam polarizations [63, 67, 68]. SFG has successfully been used to study the structure and orientation of a variety of polymers at different interfaces [69-77], lipid bilayer systems [78-80], and biological molecules such as proteins and peptides [54-62, 81-86].

1.2.2 Theory

The polarization, also called dipole moment per unit volume, is the sum of the individual dipoles in a material and is proportional to the strength of the electric field, E. The relation is:

$$P = \chi^{(1)} E \qquad 1.1$$

Here, P is the polarization, $\chi^{(1)}$ is the first-order linear susceptibility of the material. However, when the electric field increases in intense light, the non-linear terms become larger and must be considered. The new polarization, under the dipole approximation, is now written:

$$P = P^{(1)} + P^{(2)} + P^{(3)} + ... = \chi^{(1)} E + \chi^{(2)} : EE + \chi^{(3)} : EEE + ... \qquad 1.2$$

Here, $\chi^{(2)}$ is the second order nonlinear optical susceptibly, a third rank tensor, and $\chi^{(3)}$ is the third order nonlinear optical susceptibility, a fourth rank tensor [67, 68]. $\chi^{(2)}$ is associated with SFG, as well as difference frequency generation (DFG) and second harmonic generation (SHG). $\chi^{(3)}$ is a process that is associated with methods such as coherent anti-stokes Raman scattering (CARS), a four wave mixing process. We are interested in SFG and $\chi^{(2)}$. The second order nonlinear polarization for this process with two incident beams of frequencies ω_1 (visible) and ω_2 (IR) with amplitudes of E_1 and E_2 is [65]:

$$P^{(2)} = \varepsilon_0 \chi^{(2)} : E_1 \cos(\omega_1 t) E_2 \cos(\omega_2 t) \qquad 1.3$$

By applying trigonometric identities, equation 1.3 can be rearranged to:

$$P^{(2)} = \varepsilon_0 \frac{1}{2} \chi^{(2)} : E_1 E_2 [\cos(\omega_1 + \omega_2)t + \cos(\omega_1 - \omega_2)t] \qquad 1.4$$

Equation 1.4 shows that there are two oscillating dipoles generated at frequencies $(\omega_1 + \omega_2)$ and $(\omega_1 - \omega_2)$, corresponding to the SFG and DFG processes [67, 68]. The intensity of this emitted SFG beam, I, is dependent on $\left|P^{(2)}\right|^2$ and is related to:

$$I(\omega_{SF}) \propto \left|\chi^{(2)}\right|^2 I(\omega_1) I(\omega_2) \qquad 1.5$$

Where $\omega_{SF} = \omega_1 + \omega_2$, $I(\omega_1) = \left|E_1\right|^2$, and $I(\omega_2) = \left|E_2\right|^2$.

Since SFG is the focus of this work, the measurement of $\chi^{(2)}$, the second order nonlinear susceptibility, is important. One of the main advantages of SFG and measuring $\chi^{(2)}$ is the fact that this process is surface and interface selective and there is no signal generated in a

centrosymmetric environment. This surface/interface sensitivity results from $\chi^{(2)}$ being a third rank polar tensor. For a centrosymmetric environment, the inversion operator says that:

$$\chi_{ijk}^{(2)} = \chi_{-i-j-k}^{(2)} \quad 1.6$$

where i, j and k refer to the laboratory frame of reference. For a third rank polar tensor, the inversion changes the sign of the tensor [64, 87]:

$$\chi_{ijk}^{(2)} = -\chi_{-i-j-k}^{(2)} \quad 1.7$$

For both of these to be true, $\chi^{(2)}$ must be zero; thus there is no SFG signal in materials with centrosymmetry. Most bulk materials have centrosymmetry and do not produce SFG signal. When the centrosymmetry is broken at an interface, SFG signal can be produced [68]. Thus SFG is an inherently surface/interface sensitive technique.

In addition to the non centrosymmetric requirement, to generate sum frequency signal, there needs to be an overlap of the two incoming visible and IR beams in space and time. Conservation of momentum can help to calculate the angle of the generated SF beam:

$$n_{1,SF}\omega_{SF}\sin\beta_{SF} = n_{1,vis}\omega_{vis}\sin\beta_{vis} \pm n_{1,IR}\omega_{IR}\sin\beta_{IR} \quad 1.8$$

$$n_{1,SF}k_{SF}\sin\beta_{SF} = n_{1,vis}k_{vis}\sin\beta_{vis} \pm n_{1,IR}k_{IR}\sin\beta_{IR} \quad 1.9$$

Here, n is the refractive index for the material, ω is the frequency of the light, β is the angle of the beam relative to the surface normal, and k is equal to ω/c with c being the speed of light [67]. The positive sign is used in cases of the two input beams arriving in the same direction

(such as in Figure 1.1), while the negative sign is used when they are arriving from opposite x-directions.

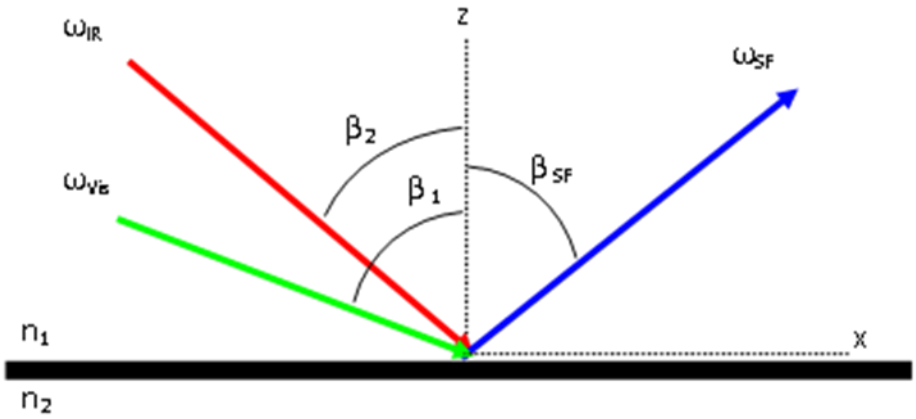

Figure 1.1: Co-propagating visible (incident angle β_1) and IR (incident angle β_2) beams generate SF signal at an angle β_{SF} versus the surface normal.

The SFG signal intensity collected from the reflection during an experiment is [88]:

$$I(\omega_{SF}) = \frac{8\pi_3\omega_2 \sec^2\beta_{SF}}{c^3 n_1(\omega_{SF}) n_1(\omega_1) n_1(\omega_2)} \left|\chi_{eff}^{(2)}\right|^2 I_1(\omega_1) I_2(\omega_2) \qquad 1.10$$

Where $n_i(\omega)$ is the refractive index of material i at frequency ω, β_{SF} is the angle of generated SF beam, I_1 and I_2 are the intensities of the input IR and visible beams. It is seen that:

$$I_{SFG} \propto \left|\chi_{eff}^{(2)}\right|^2 I_{IR} I_{vis} \qquad 1.11$$

$\chi_{eff}^{(2)}$, the effective second order nonlinear optical susceptibility, is obtained experimentally and is composed of a resonant and non-resonant term:

$$\chi_{eff}^{(2)} = \chi_{NR}^{(2)} + \sum_q \frac{A_q}{\omega_{IR} - \omega_q + i\Gamma_q} \qquad 1.12$$

$\chi_{NR}^{(2)}$ is the non-resonant contribution from the sample, A_q is the signal amplitude, ω_q is the frequency of the vibrational mode, and Γ_q is the linewidth. The resonant portion is used to fit the SFG peaks which can be obtained in different polarization combinations to calculate orientation information about the molecules. The relationship between $\chi_{eff}^{(2)}$ and $\chi^{(2)}$ defined in the lab-fixed coordinate system is given by [88]:

$$\chi_{eff}^{(2)} = \left[\hat{e}(\omega SF)\cdot L(\omega SF)\right]\cdot \chi(2) : \left[L(\omega_1)\cdot \hat{e}(\omega_1)\right]\left[L(\omega_2)\cdot \hat{e}(\omega_2)\right] \qquad 1.13$$

In this equation, $\hat{e}(\omega)$ is the unit polarization vector and L(ω) is the Fresnel factor at frequency ω. Information about $\chi^{(2)}$ can be obtained from the $\chi_{eff}^{(2)}$ measured from experiments. $\chi^{(2)}$, being a rank three tensor, has 27 terms. However, if it is assumed that the interface (in the x,y plane) is azimuthally isotropic, there are only seven non-zero terms, four of which are unique. These are $\chi_{xxz} = \chi_{yyz}$, $\chi_{xzx} = \chi_{yzy}$, $\chi_{zxx} = \chi_{zyy}$, and χ_{zzz} [67]. The x,y,z terms refer to the fixed lab coordinate frame. Information about these susceptibility terms can be discerned by collecting SFG signals while utilizing different polarization combinations of the input and output laser beams. The polarizations used in SFG are ssp (s polarized SFG beam, s polarized visible beam, p polarized IR beam), sps, pps and ppp, although we only use ssp and ppp in the studies reported later. The following expressions relate the $\chi_{eff}^{(2)}$ in these polarization combinations to non-zero $\chi^{(2)}$ terms [88]:

$$\chi_{eff,ssp}^{(2)} = L_{yy}(\omega_{SF})\,L_{yy}(\omega_{vis})\,L_{zz}(\omega_{IR})\sin\theta_{IR}\cdot\chi_{yyz}^{(2)} \qquad 1.14a$$

$$\chi_{eff,sps}^{(2)} = L_{yy}(\omega_{SF})\,L_{zz}(\omega_{vis})\,L_{yy}(\omega_{IR})\sin\theta_{vis}\cdot\chi_{yzy}^{(2)} \qquad 1.14b$$

$$\chi^{(2)}_{eff,pss} = L_{zz}(\omega_{SF})L_{yy}(\omega_{vis})L_{yy}(\omega_{IR})\sin\theta_{SFG}\cdot\chi^{(2)}_{zyy} \qquad 1.14c$$

$$\begin{aligned}\chi^{(2)}_{eff,ppp} = &-L_{xx}(\omega_{SF})L_{xx}(\omega_{vis})L_{zz}(\omega_{IR})\cos\theta_{SFG}\cos\theta_{vis}\sin\theta_{IR}\cdot\chi^{(2)}_{xxz}\\ &-L_{xx}(\omega_{SF})L_{zz}(\omega_{vis})L_{xx}(\omega_{IR})\cos\theta_{SFG}\sin\theta_{vis}\cos\theta_{IR}\cdot\chi^{(2)}_{xzx}\\ &+L_{zz}(\omega_{SF})L_{xx}(\omega_{vis})L_{xx}(\omega_{IR})\sin\theta_{SFG}\cos\theta_{vis}\cos\theta_{IR}\cdot\chi^{(2)}_{zxx}\\ &+L_{zz}(\omega_{SF})L_{zz}(\omega_{vis})L_{zz}(\omega_{IR})\sin\theta_{SFG}\sin\theta_{vis}\sin\theta_{IR}\cdot\chi^{(2)}_{zzz}\end{aligned} \qquad 1.14d$$

$L_{ii}(i = x,y,z)$ are the Fresnel factors which depend on the refractive index and input angles, ω is the frequency for the IR or visible beam, θ_{IR} and θ_{vis} are input angles versus the surface normal and θ_{SFG} is the output angle versus the surface normal. The Fresnel factors are as follows:

$$\begin{aligned}L_{xx}(\omega) &= \frac{2n_1(\omega)\cos\gamma}{n_1(\omega)\cos\gamma + n_2(\omega)\cos\theta},\\ L_{yy}(\omega) &= \frac{2n_1(\omega)\cos\theta}{n_1(\omega)\cos\theta + n_2(\omega)\cos\gamma},\\ L_{zz}(\omega) &= \frac{2n_2(\Omega)\cos\theta}{n_1(\omega)\cos\gamma + n_2(\omega)\cos\theta}\left(\frac{n_1(\Omega)}{n'(\Omega)}\right)^2\end{aligned} \qquad 1.15$$

In these equations, $n'(\omega)$ is the refractive index of the surface, θ is the incident beam input angle, γ is the refracted angle such that $n_1(\omega)\sin\theta = n_2(\omega)\sin\gamma$.

$\chi^{(2)}$ can be related to the molecular second order nonlinear polarizability (or hyperpolarizability), $\beta_{ijk}^{(2)}$, through a coordinate transformation [89]:

$$\chi^{(2)}_{IJK} = \frac{N}{\varepsilon_0}\sum_{IJK=x,y,z}\left\langle R_{Ii}R_{Jj}R_{Kk}\right\rangle\beta^{(2)}_{ijk} \qquad ijk = a,b,c \qquad 1.16$$

In this equation, N is the number of surface molecules, ε_0 is the vacuum permittivity, R is a transformation matrix to change from the molecular frame to the laboratory frame. The macroscopic susceptibility is therefore an average of the molecular hyperpolarizability of all the molecules.

If the IR frequency is near a vibrational resonance mode, the molecular hyperpolarizability can be written as:

$$\beta^{(2)} = \beta_{NR}^{(2)} + \sum_q \frac{\beta_q^{(2)}}{\omega_2 - \omega_q + i\Gamma_q} \qquad 1.17$$

A similar equation for the second order nonlinear susceptibility is also applicable, and was introduced in equation 1.12. β_q is the resonant intensity, ω_q is the resonant frequency and Γ_q is the resonant linewidth [67, 90]. Assuming the molecular hyperpolarizability of a functional group is known, one can use equation 1.12 to fit the spectrum and extract orientation information using $\chi^{(2)}$ ratios [67, 68, 90].

Additionally, the resonant part of the molecular hyperpolarizability tensor can be expressed as:

$$\beta_{ijk,q} \propto \frac{\partial \alpha_{ij}^*}{\partial Q_q} \frac{\partial \mu_k}{\partial Q_q} \qquad 1.18$$

Here, $\frac{\partial \alpha_{ij}^*}{\partial Q_q}$ and $\frac{\partial \mu_k}{\partial Q_q}$ are the IR transition dipole moment and Raman polarizability tensor derivatives for the qth vibrational mode in the molecular frame. This shows that for SFG signal, a molecule must be both IR and Raman active.

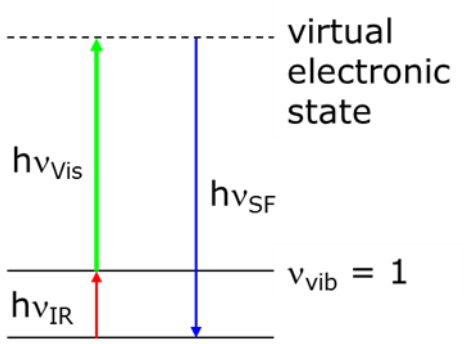

Figure 1.2: SFG energy diagram, shows IR absorption and anti-stokes Raman transition

1.2.3 Experimental System

The instrument used in this work to collect spectra is a SFG spectrometer from EKSPLA (Vilnius, Lithuania). It is comprised of four parts: picosecond Nd:YAG laser, harmonics unit, optical parametric generation/optical parametric amplification/difference frequency generation (OPG/OPA/DFG) unit, and the sample/detection system. Figure 1.3 shows a schematic of the laser system.

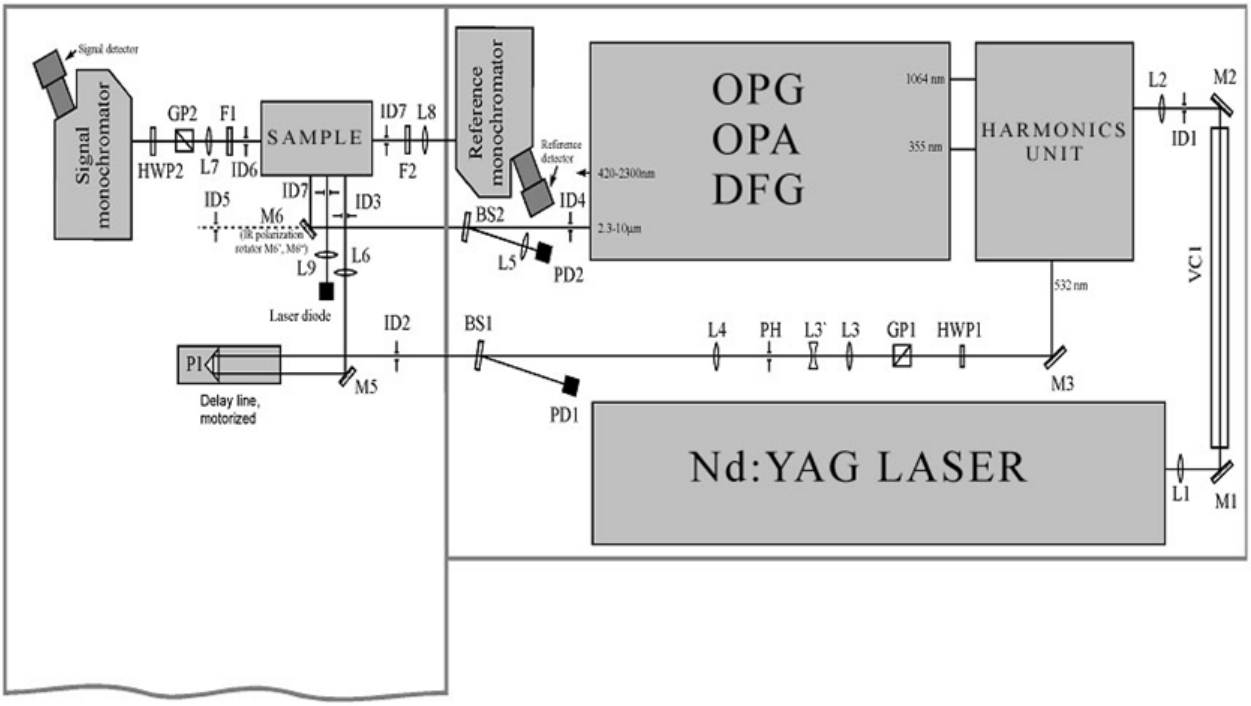

Figure 1.3: Schematic of the SFG system, including Nd:YAG, harmonics unit, OPG/OPA/DFG unit, sample and monochromator.[91]

The fundamental 1064 nm (20 picosecond pulse width) beam is produced by Nd:YAG mode locked laser. The repetition rate is 20 Hz. The Nd:YAG crystal is pumped by flashlamps and the mode locking is achieved by using a dye as a saturable absorber. The fundamental beam then goes to the harmonics unit.

The main purpose of the harmonics unit is to generate the second and third harmonics, 532 nm and 355 nm, respectively. This is achieved by passing the fundamental 1064 nm beam through KD*P nonlinear crystals. The input must be at a particular angle to the crystal to satisfy the phase matching condition and obtain the most efficient conversion. Visible 532 nm light is sent from the harmonics unit to the sample stage. 355 nm light is sent from the harmonics unit, along with fundamental 1064 nm light, to the OPG/OPA/DFG unit.

The purpose of the OPG/OPA/DFG unit is to produce the frequency tunable IR beam. The 355 nm beam passes through a LBO nonlinear crystal and produces a signal (420 to 680 nm) beam and an idler (740 to 2300 nm) beam whose wavelengths are determined by the phase matching condition and can be changed depending on the orientation of the crystal. The signal beam is filtered out of the output beam. The idler is sent through a $AgGaS_2$ nonlinear crystal with the fundamental and DFG produces the tunable IR beam which is sent to the sample. This mid IR is tunable from 1000 cm^{-1} to 4000 cm^{-1}.

At the sample, the visible 532 nm and the tunable IR beams overlap in space and time. The incident angles for the visible and IR are 60° and 54° versus the surface normal, respectively. The spot size of both beams is ~ 500 µm and the pulse energy for both beams is approximately 100 µJ at the sample. The SFG signal passes through a monochromator and is collected by a photomultiplier tube. The power of both beams is collected onto two photodiodes and this power information is later used for data normalization.

The sample geometry used in all of these studies is a near total internal reflection prism geometry.

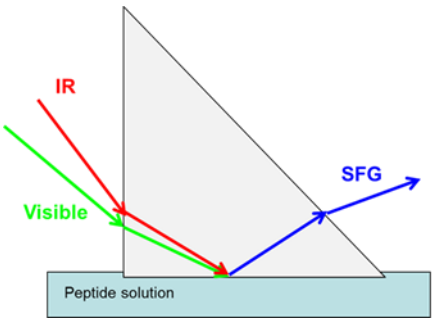

Figure 1.4: Near TIF prism geometry for SFG experiments

1.3 Presented Research

While most of the work in our lab has been with peptides and proteins interacting at relatively simple lipid bilayers, the work presented investigates several antimicrobial peptides at more complicated lipid bilayers. SFG was used to compare peptide-bilayer interactions at the simple and the more complicated model bilayer systems.

Chapter 2 investigates the effect of adding cholesterol (CHO) into 1-palmitoyl-2-oleoyl-*sn*-glycero-3-phosphocholine (POPC) and mixed POPC: 1-palmitoyl-2-oleoyl-*sn*-glycero-3-phospho-(1'-*rac*-glycerol) (POPG) bilayers. The interaction between the antimicrobial peptide, LL-37, and these bilayers is compared to the interaction between LL-37 and bilayers without cholesterol. It was found that before the addition of cholesterol, LL-37 oriented on POPC to be parallel with the bilayer. There were enough peptides on the bilayer to see amide I range signal from the peptide CO groups. After the addition of cholesterol, results suggested that there were some peptides associated with the bilayer, but they were much fewer in number. A mixed POPC:POPG:CHO (0.7:0.3:1) was also tested. Before the addition of cholesterol, the LL-37 molecules were inserted into the bilayer. However, LL-37 did not insert into the cholesterol-containing mixed bilayer. The results suggest that there were more LL-37 molecules associated with the bilayer compared to the POPC:CHO case. However, we only detected very small amide I signal in the ppp polarization and none in the ssp polarization. From these studies, it was concluded that cholesterol attenuates LL-37's ability to interact with POPC and mixed POPC/POPG bilayers. This could be due to the cholesterol molecules inducing a more condensed and ordered phase in the bilayer, resulting in a decrease in the hydrophobic-hydrophobic interactions between the peptide and lipid bilayer.

Chapter 3 investigates the interaction of a variety of peptides including MSI-594, Ovispirin-1 G18, magainin 2, melittin and LL-37 with dDPPG-*E. coli* polar lipid extract and dDPPG-POPG lipid bilayers. MSI-594 interacted more quickly with POPG lipids over the *E. coli* extract lipids and results suggest that it greatly disrupted or destroyed both bilayers. The amide I signal for MSI-594 for both systems was similar, suggesting the number and orientation of the associated peptides did not vary significantly between the two systems. The quick peptide association is likely due to electrostatic interactions. It is possible that at the concentration used, that the maximum number of peptides were associated and we would see a higher association at the more negative POPG bilayer if the peptide was at a higher concentration.

For ovispirin-1 G18, the peptide interacted more quickly with the POPG leaflet versus the *E. coli* extract leaflet. Additionally, the ovispirin-1 G18 severely disrupted or destroyed the dDPPG-POPG bilayer but could only slightly disrupt the dDPPG-*E. coli* extract bilayer. However, the amide I peptide signal was similar for both systems. These results suggest a similar amount and orientation of the ovispirin-1 G18 molecules on the two different systems. The dDPPG-*E. coli* extract bilayer might eventually be disrupted if left to interact for a long enough time. However, our observations at the current conditions showed that the ovispirin-1 G18 association is similar in both cases, but its ability to disrupt the bilayer is significantly hindered when interacting with the *E. coli* lipids.

Magainin 2 was studied at a low and a high concentration on the two systems. Magainin 2 can disrupt the outer leaflet of the dDPPG-POPG system at both 800 nM and 2 μM. It can only slightly disrupt the outer leaflet of dDPPG-*E. coli* lipid extract at 2 μM. The amide I signal for the two systems suggest there are more peptides associating at the POPG leaflet versus the E.

coli lipid leaflet. The data suggests that the interactions are different and it could likely be at least partly due to electrostatic effects.

Melittin was also studied at two concentrations for both systems. For both concentrations, both bilayer systems were roughly disrupted the same amount and the amide I peptide signal was not significantly different considering the difference in the bilayer charge. It was concluded that melittin interacts very similarly with the two systems, possibly related to the fact that it is not strictly selective for bacterial membranes like the other peptides in this study.

We also studied LL-37 at the dDPPG-POPG and dDPPG-*E. coli* lipid extract bilayers. According to our data, the LL-37 did associate with the bilayer but did not disrupt it. The amide I spectrum intensities were different, probably because of the electrostatic effects resulting in more peptide at the POPG leaflet. However, other than the number of peptides associated at the bilayer, LL-37 interacts with both bilayers similarly at the studied concentration.

Overall, after studying several peptides it seems that for these peptides POPG is an acceptable simple model for a bacterial membrane for many peptides because the main interactions between the peptides, represented by surface coverage and orientation, are similar for the two systems. However, some differences were observed in interaction time and in the ability to resist bilayer disruption/destruction between the two systems. We believe that the lipid bilayer containing the *E. coli* polar extract can better represent the real bacterial cell membrane.

Chapter 4 investigates the interaction of ovispirin-1 G18 with dDPPG-Kdo2 lipid A and dDPPG:dDPPE (4:1) – Lipid A from *Salmonella minnesota R595.* These lipid bilayer systems are meant to mimic the outer cell walls of gram negative bacteria. Both of the lipid A variants we chose had no outer core polysaccharides or an O-antigen chain. We also used ovispirin-1 G8 and

I7 to determine what environment the peptide was in on the Kdo2 lipid A leaflet compared to DPPG. It was determined that the ovispirin-1 is in the same environment in the Kdo2 lipid A leaflet as it is on DPPG. We also believe that the ovispirin-1 G18 is interacting similarly with dDPPG:dDPPE (4:1) – Lipid A from *Salmonella minnesota R595* compared to dDPPG:dDPPE (4:1)- dDPPG:dDPPE (4:1). From these results at the presented concentrations, we can conclude that when using ovispirin-1, a peptide that is suspected to act through the carpet mechanism, it interacts the same with lipid A leaflets as it does with phospholipid leaflets.

Using more complex lipid bilayers in this thesis research, we elucidated molecular interactions between peptides and cell membranes in more detail. Our results showed the importance of using more complex lipid bilayers as model cell membranes. In the future, research regarding peptide-bilayer interaction and the design of new antimicrobial molecules will be aware of the potential drawbacks of using simple membrane models for initial mechanistic studies. Additionally, our studies showed a reliable method to monitor time dependent molecular interactions of antimicrobial peptides with asymmetric lipid bilayers. The time to interact is very important to consider when developing new molecules and our method can help evaluate newly designed molecules.

1.5 References

1. Singer, S.J.; Nicolson, G.L. *Science* **1972**, *175*, 720-731.
2. Locher, R.; Neyses, L.; Stimpel, M.; Kuffer, B.; Vetter, W. *Biochemical and Biophysical Research Communications* **1984**, *124*, 822-828.
3. Holthuis, J.C.; Levine, T.P. *Nat Rev Mol Cell Biol* **2005**, *6*, 209-220.
4. Lange, Y.; Swaisgood, M.H.; Ramos, B.V.; Steck, T.L. *Journal of Biological Chemistry* **1989**, *264*, 3786-3793.
5. Zegers, M.M.P.; Hoekstra, D. *Biochemical Journal* **1998**, *336*, 257-269.
6. Varady, G.; Cserepes, J.; Nemeth, A.; Szabo, E.; Sarkadi, B. *Biomarkers in Medicine* **2013**, *7*, 803-819.

7. Vogler, O.; Barcelo, J.M.; Ribas, C.; Escriba, P.V. *Biochimica Et Biophysica Acta-Biomembranes* **2008**, *1778*, 1640-1652.
8. Devaux, P.F.; Herrmann, A.; Ohlwein, N.; Koziov, M.M. *Biochimica Et Biophysica Acta-Biomembranes* **2008**, *1778*, 1591-1600.
9. Lambert, P.A. *Advanced Drug Delivery Reviews* **2005**, *57*, 1471-1485.
10. Drlica, K.; Malik, M.; Kerns, R.J.; Zhaol, X.L. *Antimicrobial Agents and Chemotherapy* **2008**, *52*, 385-392.
11. Bockstael, K.; Van Aerschot, A. *Central European Journal of Medicine* **2009**, *4*, 141-155.
12. Kohanski, M.A.; Dwyer, D.J.; Collins, J.J. *Nature Reviews Microbiology* **2010**, *8*, 423-435.
13. Lange, R.P.; Locher, H.H.; Wyss, P.C.; Then, R.L. *Current Pharmaceutical Design* **2007**, *13*, 3140-3154.
14. Nikaido, H. *Science* **1994**, *264*, 382-388.
15. McMurry, L.; Petrucci, R.E.; Levy, S.B. *Proceedings of the National Academy of Sciences of the United States of America-Biological Sciences* **1980**, *77*, 3974-3977.
16. Bussiere, D.E.; Muchmore, S.W.; Dealwis, C.G.; Schluckebier, G.; Nienaber, V.L.; Edalji, R.P.; Walter, K.A.; Ladror, U.S.; Holzman, T.F.; Abad-Zapatero, C. *Biochemistry* **1998**, *37*, 7103-7112.
17. Bugg, T.D.H.; Wright, G.D.; Dutkamalen, S.; Arthur, M.; Courvalin, P.; Walsh, C.T. *Biochemistry* **1991**, *30*, 10408-10415.
18. Davies, J. *Science* **1994**, *264*, 375-382.
19. Wright, G.D. *Current Opinion in Microbiology* **1999**, *2*, 499-503.
20. Murray, I.A.; Shaw, W.V. *Antimicrobial Agents and Chemotherapy* **1997**, *41*, 1-6.
21. Molina, L.; Udaondo, Z.; Duque, E.; Fernandez, M.; Molina-Santiago, C.; Roca, A.; Porcel, M.; de la Torre, J.; Segura, A.; Plesiat, P.; Jeannot, K.; Ramos, J.L. *Plos One* **2014**. *9*, e81604, DOI: 10.1371/journal.pone.0081604.
22. Andersson, D.I. *Current Opinion in Microbiology* **2003**, *6*, 452-456.
23. Fleming, A. *British Journal of Experimental Pathology* **1929**, *10*, 226-236.
24. Wise, E.M.; Park, J.T. *Proceedings of the National Academy of Sciences of the United States of America* **1965**, *54*, 75-81.
25. Tipper, D.J.; Stroming.Jl. *Proceedings of the National Academy of Sciences of the United States of America* **1965**, *54*, 1133-1141.
26. Josephine, H.R.; Kumar, I.; Pratt, R.F. *Journal of the American Chemical Society* **2004**, *126*, 8122-8123.
27. Wilke, M.S.; Lovering, A.L.; Strynadka, N.C.J. *Current Opinion in Microbiology* **2005**, *8*, 525-533.
28. Majiduddin, F.K.; Materon, I.C.; Palzkill, T.G. *International Journal of Medical Microbiology* **2002**, *292*, 127-137.
29. Livermore, D.M. *Clinical Microbiology Reviews* **1995**, *8*, 557-584.
30. Nagai, K.; Davies, T.A.; Jacobs, M.R.; Appelbaum, P.C. *Antimicrobial Agents and Chemotherapy* **2002**, *46*, 1273-1280.
31. Rybkine, T.; Mainardi, J.L.; Sougakoff, W.; Collatz, E.; Gutmann, L. *Journal of Infectious Diseases* **1998**, *178*, 159-163.
32. Berger-Bachi, B.; Rohrer, S. *Archives of Microbiology* **2002**, *178*, 165-171.

33. du Plessis, M.; Bingen, E.; Klugman, K.P. *Antimicrobial Agents and Chemotherapy* **2002**, *46*, 2349-2357.
34. Weindorf, H.; Schmidt, H.; Martin, H.H. *Journal of Antimicrobial Chemotherapy* **1998**, *41*, 189-195.
35. Yigit, H.; Anderson, G.J.; Biddle, J.W.; Steward, C.D.; Rasheed, J.K.; Valera, L.L.; McGowan, J.E.; Tenover, F.C. *Antimicrobial Agents and Chemotherapy* **2002**, *46*, 3817-3822.
36. Poole, K. *Clinical Microbiology and Infection* **2004**, *10*, 12-26.
37. Masuda, N.; Sakagawa, E.; Ohya, S.; Gotoh, N.; Tsujimoto, H.; Nishino, T. *Antimicrobial Agents and Chemotherapy* **2000**, *44*, 3322-3327.
38. Hancock, R.E.W.; Diamond, G. *Trends in Microbiology* **2000**, *8*, 402-410.
39. Zasloff, M. *Nature* **2002**, *415*, 389-395.
40. Yamaguchi, S.; Huster, D.; Waring, A.; Lehrer, R.I.; Kearney, W.; Tack, B.F.; Hong, M. *Biophysical Journal* **2001**, *81*, 2203-2214.
41. Sawai, M.V.; Waring, A.J.; Kearney, W.R.; McCray, P.B.; Forsyth, W.R.; Lehrer, R.I.; Tack, B.F. *Protein Engineering* **2002**, *15*, 225-232.
42. Bhunia, A.; Ramamoorthy, A.; Bhattacharjya, S. *Chemistry-a European Journal* **2009**, *15*, 2036-2040.
43. Ramamoorthy, A.; Thennarasu, S.; Lee, D.K.; Tan, A.; Maloy, L. *Biophys J* **2006**, *91*, 206-216.
44. Bhunia, A.; Domadia, P.N.; Bhattacharjya, S. *Biochim Biophys Acta* **2007**, *1768*, 3282-3291.
45. Naito, A.; Nagao, T.; Norisada, K.; Mizuno, T.; Tuzi, S.; Saito, H. *Biophysical Journal* **2000**, *78*, 2405-2417.
46. Strandberg, E.; Zerweck, J.; Wadhwani, P.; Ulrich, A.S. *Biophysical Journal* **2013**, *104*, L09-L11.
47. Kim, C.; Spano, J.; Park, E.K.; Wi, S. *Biochim Biophys Acta* **2009**, *1788*, 1482-1496.
48. Morgera, F.; Vaccari, L.; Antcheva, N.; Scaini, D.; Pacor, S.; Tossi, A. *Biochem J* **2009**, *417*, 727-735.
49. Vigano, C.; Manciu, L.; Buyse, F.; Goormaghtigh, E.; Ruysschaert, J.M. *Biopolymers* **2000**, *55*, 373-380.
50. Ding, F.X.; Xie, H.B.; Arshava, B.; Becker, J.M.; Naider, F. *Biochemistry* **2001**, *40*, 8945-8954.
51. Tamm, L.K.; Han, X.; Li, Y.L.; Lai, A.L. *Biopolymers* **2002**, *66*, 249-260.
52. Martin, I.; Goormaghtigh, E.; Ruysschaert, J.M. *Biochimica Et Biophysica Acta-Biomembranes* **2003**, *1614*, 97-103.
53. Shai, Y. *Biochimica Et Biophysica Acta-Biomembranes* **2013**, *1828*, 2306-2313.
54. Nguyen, K.T.; Le Clair, S.V.; Ye, S.J.; Chen, Z. *Journal of Physical Chemistry B* **2009**, *113*, 12358-12363.
55. Ding, B.; Glukhova, A.; Sobczyk-Kojiro, K.; Mosberg, H.I.; Tesmer, J.J.G.; Chen, Z. *Langmuir* **2014**, *30*, 823-831.
56. Yang, P.; Wu, F.G.; Chen, Z. *J Phys Chem C Nanomater Interfaces* **2013**, *117*, 3358-3365.
57. Ding, B.; Soblosky, L.; Nguyen, K.; Geng, J.Q.; Yu, X.L.; Ramamoorthy, A.; Chen, Z. *Scientific Reports* **2013**. *3*, 1-8, DOI: 10.1038/srep01854.
58. Ding, B.; Chen, Z. *J Phys Chem B* **2012**, *116*, 2545-2552.

59. Yang, P.; Ramamoorthy, A.; Chen, Z. *Langmuir* **2011**, *27*, 7760-7767.
60. Boughton, A.P.; Yang, P.; Tesmer, V.M.; Ding, B.; Tesmer, J.J.G.; Chen, Z. *Proceedings of the National Academy of Sciences of the United States of America* **2011**, *108*, E667-E673.
61. Boughton, A.P.; Nguyen, K.; Andricioaei, I.; Chen, Z. *Langmuir* **2011**, *27*, 14343-14351.
62. Nguyen, K.T.; King, J.T.; Chen, Z. *Journal of Physical Chemistry B* **2010**, *114*, 8291-8300.
63. Nguyen, K.T.; Le Clair, S.V.; Ye, S.J.; Chen, Z. *Journal of Physical Chemistry B* **2009**, *113*, 12169-12180.
64. Shen, Y.R., *The principles of nonlinear optics*. 1984, New York: Wiley.
65. Bain, C.D. *Journal of the Chemical Society-Faraday Transactions* **1995**, *91*, 1281-1296.
66. Eisenthal, K.B. *Chemical Reviews* **1996**, *96*, 1343-1360.
67. Lambert, A.G.; Davies, P.B.; Neivandt, D.J. *Applied Spectroscopy Reviews* **2005**, *40*, 103-145.
68. Buck, M.; Himmelhaus, M. *Journal of Vacuum Science & Technology A: Vacuum, Surfaces, and Films* **2001**, *19*, 2717-2736.
69. Wang, J.; Woodcock, S.E.; Buck, S.M.; Chen, C.Y.; Chen, Z. *Journal of the American Chemical Society* **2001**, *123*, 9470-9471.
70. Chen, Z.; Shen, Y.R.; Somorjai, G.A. *Annual Review of Physical Chemistry* **2002**, *53*, 437-465.
71. Chen, C.; Wang, J.; Woodcock, S.E.; Chen, Z. *Langmuir* **2002**, *18*, 1302-1309.
72. Wilson, P.T.; Briggman, K.A.; Wallace, W.E.; Stephenson, J.C.; Richter, L.J. *Applied Physics Letters* **2002**, *80*, 3084-3086.
73. Liu, Y.; Messmer, M.C. *Journal of Physical Chemistry B* **2003**, *107*, 9774-9779.
74. Hong, S.C.; Zhang, C.; Shen, Y.R. *Applied Physics Letters* **2003**, *82*, 3068-3070.
75. Rao, A.; Rangwalla, H.; Varshney, V.; Dhinojwala, A. *Langmuir* **2004**, *20*, 7183-7188.
76. McGall, S.J.; Davies, P.B.; Neivandt, D.J. *Journal of Physical Chemistry B* **2004**, *108*, 16030-16039.
77. Sung, J.; Kim, D.; Whang, C.N.; Oh-e, M.; Yokoyama, H. *Journal of Physical Chemistry B* **2004**, *108*, 10991-10996.
78. Ohe, C.; Sasaki, T.; Noi, M.; Goto, Y.; Itoh, K. *Anal Bioanal Chem* **2007**, *388*, 73-79.
79. Kett, P.J.; Casford, M.T.; Davies, P.B. *J Phys Chem B* **2011**, *115*, 6465-6473.
80. Bonn, M.; Roke, S.; Berg, O.; Juurlink, L.B.F.; Stamouli, A.; Muller, M. *Journal of Physical Chemistry B* **2004**, *108*, 19083-19085.
81. Boughton, A.P.; Andricioaei, I.; Chen, Z. *Langmuir* **2010**, *26*, 16031-16036.
82. Chen, X.; Chen, Z. *Biochim Biophys Acta* **2006**, *1758*, 1257-1273.
83. Chen, X.; Wang, J.; Kristalyn, C.B.; Chen, Z. *Biophys J* **2007**, *93*, 866-875.
84. Chen, X.Y.; Wang, J.; Boughton, A.P.; Kristalyn, C.B.; Chen, Z. *Journal of the American Chemical Society* **2007**, *129*, 1420-1427.
85. Ye, S.; Nguyen, K.T.; Le Clair, S.V.; Chen, Z. *J Struct Biol* **2009**, *168*, 61-77.
86. Ye, S.J.; Nguyen, K.T.; Chen, Z. *Journal of Physical Chemistry B* **2010**, *114*, 3334-3340.
87. Boyd, R.W., *Nonlinear optics*. 3rd ed. 2008: Academic Press.
88. Zhuang, X.; Miranda, P.B.; Kim, D.; Shen, Y.R. *Physical Review B* **1999**, *59*, 12632-12640.
89. Moad, A.J.; Simpson, G.J. *Journal of Physical Chemistry B* **2004**, *108*, 3548-3562.
90. Superfine, R.; Huang, J.Y.; Shen, Y.R. *Chemical Physics Letters* **1990**, *172*, 303-306.

91. Woodcock, S.E., University of Michigan, 2005.

CHAPTER 2

EFFECT OF CHOLESTEROL IN MODEL MEMBRANES ON MEMBRANE-PEPTIDE INTERACTION

2.1 Introduction

Over time, the rise of antibiotic resistance in bacteria has caused complications in treating bacterial infections. One solution to this problem is the development of antimicrobial peptides (AMPs) which generally target the cell membrane and are thus harder for bacteria to develop resistances against [1-5]. In addition to the required antibiotic properties, it is important for any successful AMP or therapy to not be toxic to eukaryotic cells as well. In order to develop a molecule with good selectivity, it is important to study its activity and mechanism in both bacterial and eukaryotic cell environments. For the bacterial model cell membrane, we often use lipid bilayers prepared using 1-palmitoyl-2-oleoyl-*sn*-glycero-3-phospho-(1'-*rac*-glycerol) (POPG), 1,2-dipalmitoyl-*sn*-glycero-3-phospho-(1'-*rac*-glycerol) (DPPG), or a mixture of POPG and a zwitterionic phospholipid [6-10]. For the eukaryotic model cell membrane, a lipid bilayer consisting of pure POPC or DPPC molecules is generally used [10-12]. However, there are many other components of a eukaryotic cell membrane. The outer leaflet contains PC lipids, glycosphingolipids and sphingolipids such as sphingomyelin, while the inner leaflet contains phosphatidylserine (PS), phosphatidylethanolamine (PE), phosphatidylinositol (PI), and other minor lipids [13, 14]. There is also cholesterol (CHO) and various membrane proteins [13, 15].

The amount of cholesterol seems to vary depending on the cell type [16]. Human erythrocytes are reported to have approximately a CHO/phospholipid ratio of ~0.8 [17, 18]. Lange and coworkers [16] found that the ratio for erythrocytes was 0.82, but cited 0.36 for fibroblasts and 0.084 for liver cells. Another study reported cholesterol to be ~54% of the total lipid in the erythrocyte ghost cell membranes [18]. However, there is controversy in these percentages due to the difficulty of the lipid extraction methods [14].

Even though a cell membrane or membrane mimic with all of the components would exhibit the most accurate membrane properties, using a complex model cell membrane with all of the components to study their interactions with AMPs would be extremely difficult. Although our goal is to form a more complex model membrane, we decided to start with a more simple system of 1-palmitoyl-2-oleoyl-*sn*-glycero-3-phosphocholine (POPC) and cholesterol to understand the effect of cholesterol on cell membrane-AMP interaction. Cholesterol is an amphipathic molecule composed of a four-ring structure with a hydrocarbon tail on one end and a hydroxyl group on the other (Figure 1). The ring structure is described as having two faces, the α planar face and the rougher β face [19, 20]. The hydroxyl group is hydrophilic and can form hydrogen bonds with neighboring lipids or proteins [19].

Cholesterol is known to influence the lipid membrane phase. It has a tendency to make gel phase bilayers more fluid and fluid liquid disordered phase more ordered [21]. Several studies have shown that cholesterol causes a more condensed bilayer when interacting with phospholipids [22, 23], but actually interacts more favorably with sphingomyelin [24]. Although there is some discrepancy on their existence, size and structure, cholesterol is believed by many to form condensed phases called “lipid rafts” with sphingomyelin [25-28].

The interaction between bilayers containing cholesterol and membrane active peptides has been studied by many groups. Evidence from McGee and coworkers suggests that cholesterol helps *H. pylori* to be more resistant to the AMP LL-37 and certain antibiotics [29]. Another study reported that the incorporation of cholesterol caused increased lipid packing and decreased the ability of the α-helical peptide Modelin-5 to associate to the bilayer [30]. A study comparing normal erythrocytes and ones with a naturally occurring higher cholesterol content found that the higher cholesterol content decreased hemolysis due to Gramicidin-S [31]. These examples show that cholesterol is capable of increasing a membrane's resistance to disruption.

This chapter will apply sum frequency generation vibrational spectroscopy (SFG) to study the effect of cholesterol on the membrane–AMP interactions, using LL-37 as an example. LL-37 is a 37 amino acid α-helical human cathelicidin peptide [32, 33]. It is described as having a helix-break-helix motif and a dynamic N terminus region in dodecylphosphocholine (DPC) [34] and bent structure in sodium dodecyl sulfate (SDS) [35]. LL-37 has been shown to disrupt anionic DPPG, but not DPPE or DPPC lipids [36]. It has also been shown to induce leakage in vesicles containing POPG lipids, but not in pure POPC vesicles [37]. LL-37 has been suggested to act through the toroidal pore mechanism [38].

As stated in Chapter 1, SFG is a surface and interface sensitive technique [39-41]. It has been successfully used to study the membrane association and orientation of peptides and proteins [7, 8, 10, 42]. In this work, we use SFG to study the interaction of the α-helical peptide, LL-37, with model cell membranes containing cholesterol and compare them to bilayers without cholesterol. We find that cholesterol decreases the amount of peptide association on POPC:CHO (1:1) and POPC:POPG:CHO (0.7:0.3:1) bilayers compared to pure POPC and POPC:POPG (7:3) bilayers.

This chapter is an adaptation of Ding, B., et al. (2013). "Physiologically-Relevant Modes of Membrane Interactions by the Human Antimicrobial Peptide, LL-37, Revealed by SFG Experiments." Scientific Reports **3**: 8. Figures 2.1, 2.2, and 2.3 are from Ding, B., et al. *Scientific Reports*, 2013. **3**: 8. The work shown in Figure 2.1 and Figure 2.3 (1-4) was done by Bei Ding.

2.2 Experiment Methods

2.2.1 Materials

Phospholipids in this study, including 1-palmitoyl-2-oleoyl-sn-glycero-3-phospho-(1'-rac-glycerol) (POPG) and 1-palmitoyl-2-oleoyl-sn-glycero-3-phosphocholine (POPC) were purchased from Avanti Polar Lipids, Inc. (Alabaster, AL). Cholesterol (CHO) (≥99%) was purchased from Sigma-Aldrich (St. Louis, MO). LL-37 was purchased from AnaSpec, Inc. (Fremont, CA).

2.2.2 SFG Experimental Setup

The SFG theory was reviewed in Chapter 1 and will not be repeated here. The symmetric bilayers were formed via the Langmuir Blodgett/Langmuir Schaefer method and were submerged in 1.6 mL water in a sample reservoir. Appropriate volumes of 0.5 mg/ml LL-37 stock solution were injected into the subphase with a magnetic micro stir bar to ensure the most homogeneous mixing possible. During and for approximately 1.5 h after the injection, time dependent spectra at 1655 cm^{-1} and 2880 cm^{-1} were recorded to monitor the interaction progress. Amide I range spectra were taken in ssp and ppp polarizations after approximately 1.5 h and the time dependent spectra were stable.

2.3 Results and Discussion

Figure 2.1 shows the results from the interaction of 0.46 μM and 1.6 μM LL-37 and symmetric bilayers of POPC, POPG, and mixed POPC/POPG. These results are important as they serve as a comparison for our POPC/CHO and POPC/POPG/CHO results. Figure 2.1a shows the SFG spectra collected in the amide I frequency region for a POPC/POPC lipid bilayer in contact with subphase with a LL-37 concentration of 0.46 μM (top) or 1.6 μM (bottom). There is a peak at approximately 1647 cm^{-1} in both ppp and ssp polarizations for each concentration. This suggests that LL-37 molecules are bilayer in an α-helical conformation when associated with the POPC/POPC bilayer. The spectral intensities and ppp/ssp signal intensity ratios for the two subphase LL-37 concentrations are similar, showing that the associated LL-37 number and orientation with the POPC/POPC bilayer are independent of the subphase LL-37 concentration. It was determined from the fitting that the LL-37 was approximately lying down on the bilayer surface for both cases, which agrees with NMR literature [33, 38].

Figure 2.1b (top) shows the SFG spectra collected in the 3000-3600 cm^{-1} range before and after LL-37 addition to the subphase in contact with a POPC/POPC bilayer. POPC lipids have a zwitterionic head group and thus water molecules are not well ordered at the bilayer surface. Because SFG signal is dependent on molecular ordering, there is no water signal evident before peptide injection into the subphase. However, after peptide injection, a strong and broad signal with peaks approximately at 3200 cm^{-1} and 3500 cm^{-1} is detected. This signal is most likely due to the water O-H stretch at ~3200 cm^{-1} and 3500 cm^{-1} as well as the N-H stretch of LL-37 at ~3280 cm^{-1}. LL-37 is positively charged and its association with the bilayer likely causes the previously unordered interfacial water molecules to assume an ordered orientation,

resulting in strong SFG signal. This confirms that LL-37 molecules are associated with the POPC/POPC bilayer.

For a pure POPG bilayer (Figure 1b (bottom) and Figure 1c), the amide I signal detected from the LL-37 associated with the bilayer in contact with the 0.46 μM LL-37 solution is similar to the amide I signal in both of our POPC/POPC bilayer cases. The SFG amide I signal of LL-37 in contact with a subphase with 1.6 μM LL-37 is higher than that associated with the POPC/POPC bilayer at the same LL-37 subphase concentration. It was shown from amide I region spectral fitting that LL-37 inserts into the bilayer at the low subphase concentration and is lying parallel to the bilayer surface at the higher concentration. There is some difference in the 3000-3600 cm^{-1} region spectrum for a bilayer that incorporates anionic POPG lipids. PG is a negatively charged head group which allows the associated water molecules to become ordered which results in strong O-H stretch signal. However, after adding LL-37 to the subphase, this signal decreases significantly and there is only an N-H stretch peak at approximately 3300 cm^{-1}. This signal decrease is expected as the positively charged peptide associates with the negatively charged bilayer and neutralizes some of the surface charge. With the strong negative charge partially negated, the previously well-ordered water molecules may become less ordered which results in a decrease of water signal.

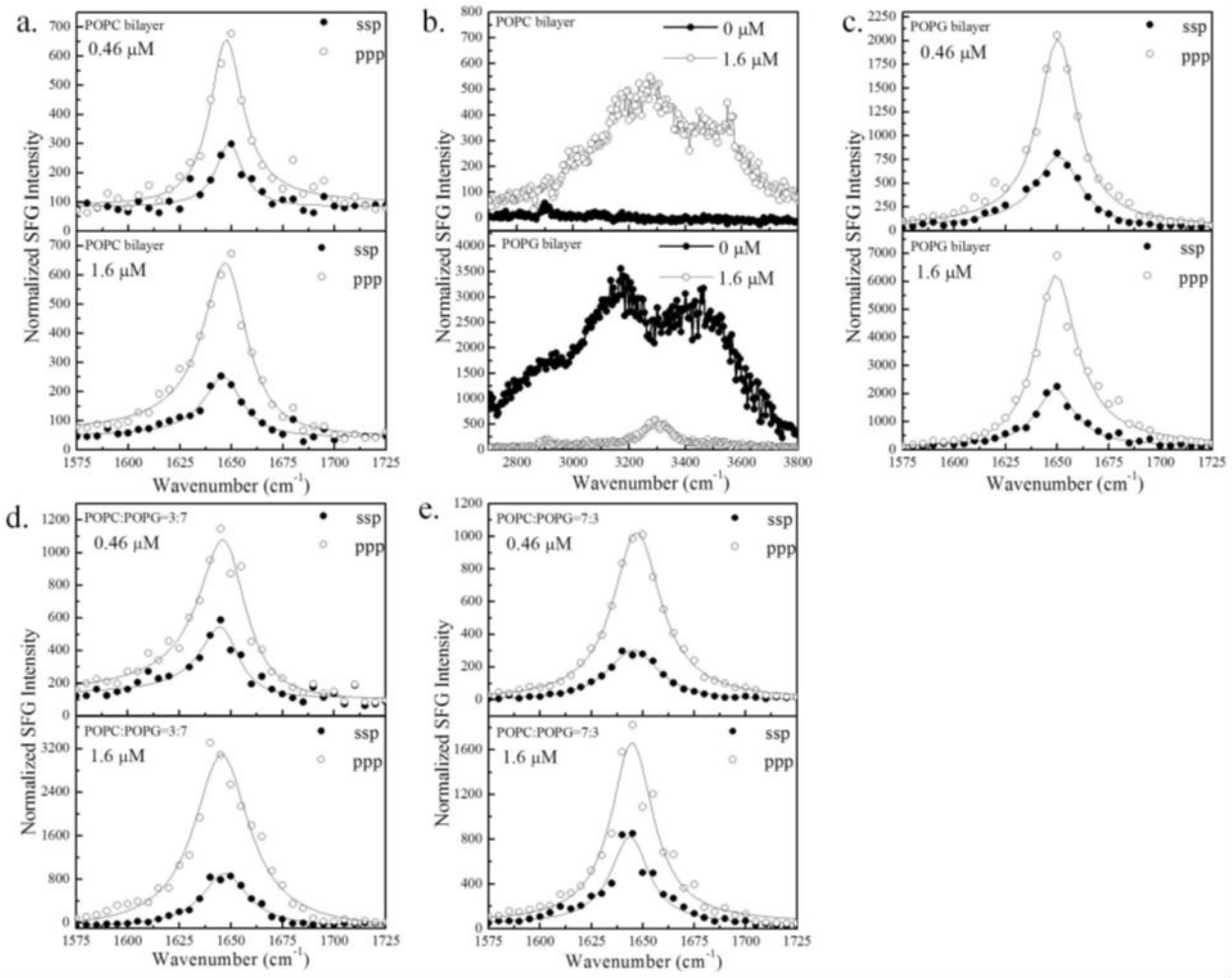

Figure 2.1: (a) Amide I spectra of LL-37 on POPC/POPC bilayer; (b) O-H/N-H stretching signals from the POPC (top) and POPG (bottom) bilayers in contact with LL-37 solution; (c) Amide I spectra of LL-37 on POPG/POPG bilayer, (d) Amide I spectra of LL-37 on POPC:POPG (3:7) (e) Amide I spectra of LL-37 on POPC:POPG (7:3) lipid bilayers.

In addition to the pure POPC/POPC and POPG/POPG lipid bilayers, we also studied molecular interactions between LL-37 and mixed POPC:POPG bilayers. Figure 2.1 (d) and (e) show SFG amide I signals from LL-37 associated with POPC:POPG (3:7) bilayer and POPC:POPG (7:3) bilayer respectively. For the mixed lipid bilayer of POPC:POPG (7:3), the LL-37 interaction is concentration dependent (Figure 1e). At 0.46 μM, the peptide molecules lay down like they do on a pure POPC bilayer. At 1.6 μM, however, they insert at 0-15 degrees

versus the bilayer normal, like they do in the low concentration case on a pure POPG bilayer. At higher concentrations, they are lying down on the bilayer surface again.

We then added CHO to POPC to investigate if the presence of CHO affected the interactions between LL-37 and lipid bilayers. Figure 2.2 shows the SFG spectra collected in the 3000-3600 cm^{-1} region and amide I frequency region from the mixed POPC:CHO (1:1) bilayer before and after addition of LL-37 into the subphase. The 3000-3600 cm^{-1} spectrum in the top panel of Figure 2.2a shows that there is little water signal before peptide is injected, but the signal increases after the peptide addition to the subphase, although not as much as it did in the pure POPC case. This increase in O-H stretching signal is due to the water molecules becoming ordered because of the associated cationic peptide molecules. The lower water signal for the POPC:CHO bilayer case, compared to the pure POPC case, after LL-37 adsorption is due to fewer peptide molecules being adsorbed to the CHO containing bilayer. In addition to this, there is no peak apparent at 3300 cm^{-1} (N-H stretching from LL-37) in this CHO containing system. Furthermore, there is no amide I signal detected from the peptides associated with the POPC:CHO 1:1 lipid bilayer. From the above observations, we can conclude that there are peptides on the surface, but there are not enough to cause a large water signal, peptide N-H stretching signal at 3300 cm^{-1} peak, or peptide amide I signal. As a result, we could not determine the orientation of these peptides. Our above results show that the incorporation of CHO in the POPC lipid bilayer can resist LL-37 adsorption.

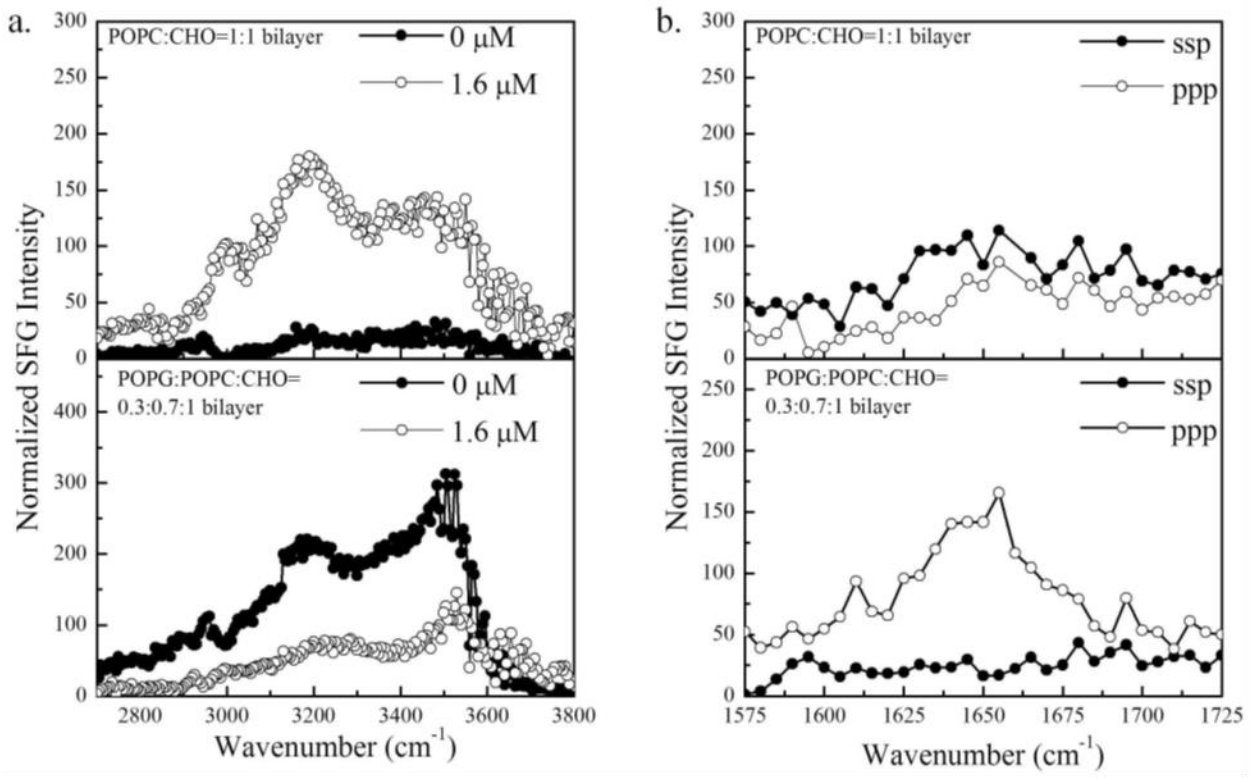

Figure 2.2: (a) SFG O-H/N-H stretching signals from the POPC:CHO (1:1) bilayer (top) and POPG:POPC:CHO (0.3:0.7:1) bilayer (bottom) bilayers in contact with subphase before and after addition of LL-37 to reach 1.6 μM. (b) SFG amide I spectra of LL-37 associated with POPC:CHO (1:1) (top) and POPG:POPC:CHO (0.3:0.7:1) (bottom) bilayers in contact with 1.6 μM LL-37 solution.

Figure 2.2 a and b (bottom) show the SFG spectra in the 3000-3600 cm^{-1} and amide I frequency regions for the POPG:POPC:CHO (0.3:0.7:1) bilayer. Because of the anionic PG lipids, there was some SFG signal from the O-H stretch before the LL-37 injection into the subphase. After the injection, the water O-H stretching signal decreased but there was not any signal for the N-H stretch at 3300 cm^{-1}. Also the amide I region showed a small signal at ~1650 cm^{-1} in the ppp polarization but nothing in the ssp polarization. The emergence of the ppp amide I signal means that there are more LL-37 molecules at the POPG:POPC:CHO bilayer, likely because of the addition of the anionic POPG head group. However, the amount of associated LL-

37 is still lower than on the POPG:POPC (3:7) bilayer, which showed significantly higher amide I signal in both polarizations. Again, this suggests that the addition of CHO to the bilayer decreases the ability of LL-37 to associate with lipid bilayer. This is in agreement with literature [38, 43].

In this work we showed the interaction of an α-helical peptide, LL-37, with cholesterol containing bilayers and compared those results to both pure and mixed phospholipid bilayers. We found that the addition of CHO to POPC bilayers results in lower LL-37 association, evident from the lower O-H stretching signal compared to pure POPC bilayers in contact with peptide solution of the same concentration as well as the absence of a peptide 3300 cm^{-1} N-H peak and amide I region signal. This is in agreement with literature. One study found that the best conditions for attenuating LL-37 and temporin L interaction with a SOPC bilayer is at X_{sterol} = 0.5 with cholesterol, compared to other percentages and other sterols [44]. Another study found that *H. pylori* bacteria that incorporate host cholesterol into their membranes are more resistant to LL-37 than those without cholesterol [29]. Dennison et al.[30] found that the addition of cholesterol to a DMPC bilayer resulted in inhibition of the binding of the α-helical peptide Modelin-5. Another study saw 30% cholesterol in DPPC liposomes inhibits the binding and insertion of melittin [45].

There could be a few explanations as to why cholesterol has this inhibiting effect on peptide association/insertion. One is the condensation effect, in which cholesterol causes the increased order of acyl chains and the decrease in area per molecule [46, 47]. It is thought that the small polar OH head group is unable to cover its bulky hydrophobic region, so it orients such that the larger head groups of adjacent phospholipids shield those hydrophobic portions [46, 47]. The bulky hydrophobic portion of cholesterol is in the same region as the acyl chains of

phospholipids, which causes a “condensation” effect [47]. This is just one explanation for the condensation effect, however. There is also a condensed complex model and the superlattice model. The condensed complex model is a thermodynamic model that is based on the idea that the cholesterol and phospholipid form a different, reversible phase through a cooperative “chemical reaction” [48]. The superlattice model says that at certain concentrations, cholesterol is regularly distributed into hexagonal superlattices [49]. There is still debate on which model is the correct one [50]. It has been suggested that as the area/molecule decreases and the packing becomes tighter, the hydrophobic area becomes less accessible and thus the hydrophobic interactions weaken [45]. Hydrophobic interactions were mentioned earlier in this work as a possibility as to how LL-37 interacts with zwitterionic POPC bilayers. If the access to the hydrophobic region is inhibited, it is reasonable to expect the association of LL-37 to decrease, which is what we observed.

Additionally, it has been observed that cholesterol interacts preferentially with saturated versus unsaturated phospholipids [51-53]. This interaction preference is often seen in cholesterol’s affinity for sphingomyelin (SM), which has saturated acyl chains [51, 53]. It is thought that this interaction facilitates the formation of “lipid rafts”, although this theory is still debatable [25, 27, 28]. Many groups are interested in investigating the other properties of sphingomyelin which may influence its interactions with cholesterol and other phospholipids [53-55]. It has even been shown that melittin interacts with a zwitterionic bilayer differently depending on the composition, POPC, POPC/SM, and POPC/SM/CHO [56].

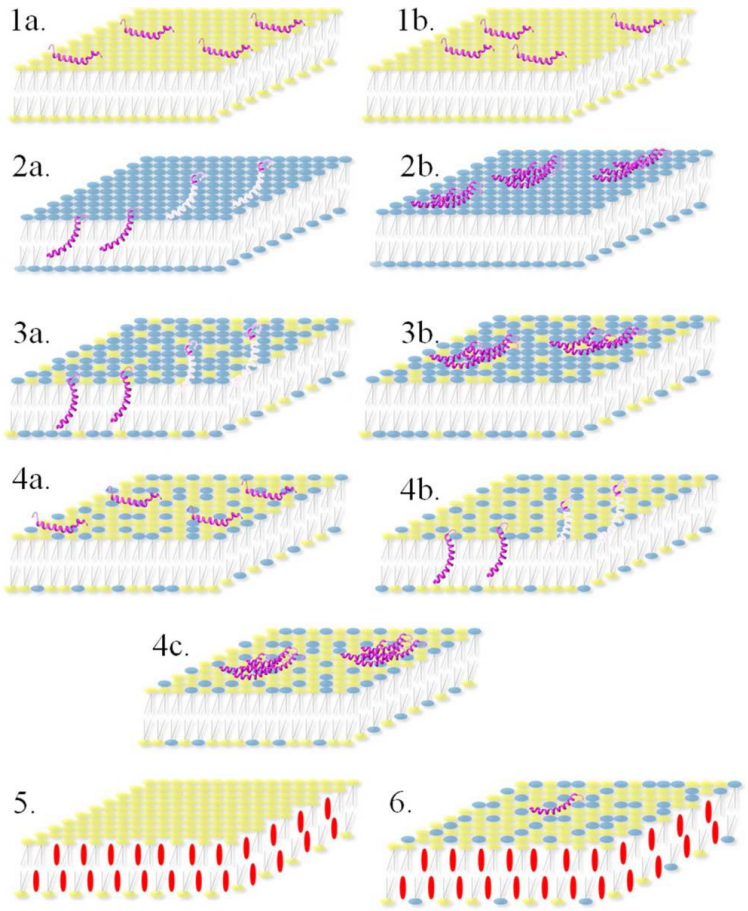

Figure 2.3: Schematics showing interactions between LL-37 and different lipid bilayers. (1) POPC bilayer 0.46 µM (left, 1a) and 1.6 µM (right, 1b); (2) POPG bilayer 0.46 µM (left, 2a) and 1.6 µM (right, 2b); (3) POPC:POPG (3:7) lipid bilayer at 0.46 µM (left, 3a) 1.6 µM (right, 3b); (4) POPC:POPG (7:3) lipid bilayer at 0.46 µM (left, 4a) and 1.6 µM (right, 4b) and 4.8 µM, 6.4 µM, 7.9 µM (bottom, 4c); (5) POPC:CHO (1:1) lipid bilayer at 1.6 µM; (6) POPG:POPC:CHO (0.3:0.7:1) lipid bilayer at 1.6 µM.

2.4 Conclusions

We have shown that the addition of cholesterol to POPC results in a decrease in the amount of LL-37 molecules associated with the lipid bilayer. Adding cholesterol to POPG:POPC bilayers results in more LL-37 associated than with POPC:CHO, but fewer than with POPG:POPC (3:7). This clearly shows that cholesterol disrupts LL-37's ability to associate with lipid bilayers, even if anionic PG lipids are present. Figure 2.3 shows cartoons representing the different interactions between LL-37 and the studied lipid bilayers. Figure 2.3 part (5) and (6)

shows the cholesterol cases discussed in this work. Our results agree with previous studies that the presence or absence of CHO in cell membranes contribute to AMP selectivity [29-31]. This is likely because the addition of CHO causes the bilayer to become more gel-like. This gel-like phase could make it more energetically unfavorable for peptides to interact with the cholesterol containing bilayer compared to liquid-ordered bilayers without cholesterol. A similar effect was seen in a previous study with alamethicin where the peptide signal was significantly higher on fluid phase lipids compared to gel phase lipids with the same head group [57].

Cholesterol is known to preferentially interact with saturated acyl chains, such as those found on sphingomyelin. This offers an interesting possibility for further studies since it has been shown in literature that peptide interactions can be different depending on the presence or absence of sphingomyelin.

2.5 References

1. Zasloff, M. *Nature* **2002**, *415*, 389-395.
2. Matsuzaki, K. *Biochimica Et Biophysica Acta-Biomembranes* **1999**, *1462*, 1-10.
3. Hancock, R.E.W.; Scott, M.G. *Proceedings of the National Academy of Sciences of the United States of America* **2000**, *97*, 8856-8861.
4. Hancock, R.E.W.; Diamond, G. *Trends in Microbiology* **2000**, *8*, 402-410.
5. Epand, R.M.; Vogel, H.J. *Biochimica Et Biophysica Acta-Biomembranes* **1999**, *1462*, 11-28.
6. Chen, X.; Chen, Z. *Biochim Biophys Acta* **2006**, *1758*, 1257-1273.
7. Chen, X.; Wang, J.; Kristalyn, C.B.; Chen, Z. *Biophys J* **2007**, *93*, 866-875.
8. Ding, B.; Chen, Z. *J Phys Chem B* **2012**, *116*, 2545-2552.
9. Ding, B.; Soblosky, L.; Nguyen, K.; Geng, J.Q.; Yu, X.L.; Ramamoorthy, A.; Chen, Z. *Scientific Reports* **2013**. *3*, 1-8, DOI: 10.1038/srep01854.
10. Nguyen, K.T.; Le Clair, S.V.; Ye, S.J.; Chen, Z. *Journal of Physical Chemistry B* **2009**, *113*, 12358-12363.
11. Yang, P.; Wu, F.G.; Chen, Z. *J Phys Chem C Nanomater Interfaces* **2013**, *117*, 3358-3365.
12. Yang, P.; Ramamoorthy, A.; Chen, Z. *Langmuir* **2011**, *27*, 7760-7767.
13. Ikeda, M.; Kihara, A.; Igarashi, Y. *Biological & Pharmaceutical Bulletin* **2006**, *29*, 1542-1546.

14. Liscum, L.; Munn, N.J. *Biochimica Et Biophysica Acta-Molecular and Cell Biology of Lipids* **1999**, *1438*, 19-37.
15. Holthuis, J.C.; Levine, T.P. *Nat Rev Mol Cell Biol* **2005**, *6*, 209-220.
16. Lange, Y.; Swaisgood, M.H.; Ramos, B.V.; Steck, T.L. *Journal of Biological Chemistry* **1989**, *264*, 3786-3793.
17. Spector, A.A.; Yorek, M.A. *Journal of Lipid Research* **1985**, *26*, 1015-1035.
18. Locher, R.; Neyses, L.; Stimpel, M.; Kuffer, B.; Vetter, W. *Biochemical and Biophysical Research Communications* **1984**, *124*, 822-828.
19. Fantini, J.; Barrantes, F.J. *Front Physiol* **2013**. *4*, 1-9, DOI: 10.3389/fphys.2013.00031.
20. Rose, I.A.; Hanson, K.R.; Wilkinson, K.D.; Wimmer, M.J. *Proceedings of the National Academy of Sciences of the United States of America-Biological Sciences* **1980**, *77*, 2439-2441.
21. Henriksen, J.; Rowat, A.C.; Brief, E.; Hsueh, Y.W.; Thewalt, J.L.; Zuckermann, M.J.; Ipsen, J.H. *Biophys J* **2006**, *90*, 1639-1649.
22. Alwarawrah, M.; Dai, J.A.; Huang, J.Y. *Journal of Physical Chemistry B* **2010**, *114*, 7516-7523.
23. Bonn, M.; Roke, S.; Berg, O.; Juurlink, L.B.F.; Stamouli, A.; Muller, M. *Journal of Physical Chemistry B* **2004**, *108*, 19083-19085.
24. Mattjus, P.; Slotte, J.P. *Chemistry and Physics of Lipids* **1996**, *81*, 69-80.
25. Simons, K.; Ikonen, E. *Nature* **1997**, *387*, 569-572.
26. El Kirat, K.; Morandat, S. *Biochim Biophys Acta* **2007**, *1768*, 2300-2309.
27. Veatch, S.L.; Keller, S.L. *Biochim Biophys Acta* **2005**, *1746*, 172-185.
28. Munro, S. *Cell* **2003**, *115*, 377-388.
29. McGee, D.J.; George, A.E.; Trainor, E.A.; Horton, K.E.; Hildebrandt, E.; Testerman, T.L. *Antimicrob Agents Chemother* **2011**, *55*, 2897-2904.
30. Dennison, S.R.; Phoenix, D.A. *Biochemistry* **2011**, *50*, 10898-10909.
31. Hackl, E.V.; Berest, V.P.; Gatash, S.V. *International Journal of Peptide Research and Therapeutics* **2012**, *18*, 163-170.
32. Burton, M.F.; Steel, P.G. *Natural Product Reports* **2009**, *26*, 1572-1584.
33. Durr, U.H.; Sudheendra, U.S.; Ramamoorthy, A. *Biochim Biophys Acta* **2006**, *1758*, 1408-1425.
34. Porcelli, F.; Verardi, R.; Shi, L.; Henzler-Wildman, K.A.; Ramamoorthy, A.; Veglia, G. *Biochemistry* **2008**, *47*, 5565-5572.
35. Wang, G.S. *Journal of Biological Chemistry* **2008**, *283*, 32637-32643.
36. Neville, F.; Cahuzac, M.; Konovalov, O.; Ishitsuka, Y.; Lee, K.Y.C.; Kuzmenko, I.; Kale, G.M.; Gidalevitz, D. *Biophysical Journal* **2006**, *90*, 1275-1287.
37. Zhang, X.; Oglecka, K.; Sandgren, S.; Belting, M.; Esbjorner, E.K.; Norden, B.; Graslund, A. *Biochim Biophys Acta* **2010**, *1798*, 2201-2208.
38. Wildman, K.A.H.; Lee, D.K.; Ramamoorthy, A. *Biochemistry* **2003**, *42*, 6545-6558.
39. Zhuang, X.; Miranda, P.B.; Kim, D.; Shen, Y.R. *Physical Review B* **1999**, *59*, 12632-12640.
40. Shen, Y.R. *Nature* **1989**, *337*, 519-525.
41. Moad, A.J.; Simpson, G.J. *Journal of Physical Chemistry B* **2004**, *108*, 3548-3562.
42. Boughton, A.P.; Yang, P.; Tesmer, V.M.; Ding, B.; Tesmer, J.J.G.; Chen, Z. *Proceedings of the National Academy of Sciences of the United States of America* **2011**, *108*, E667-E673.

43. Ramamoorthy, A.; Lee, D.K.; Narasimhaswamy, T.; Nanga, R.P. *Biochim Biophys Acta* **2010**, *1798*, 223-227.
44. Sood, R.; Kinnunen, P.K. *Biochim Biophys Acta* **2008**, *1778*, 1460-1466.
45. Lin, J.J.; Cheng, C.W.; Lin, J.J.; Chen, W.Y. *Analytical Biochemistry* **2007**, *367*, 49-55.
46. Huang, J.Y.; Feigenson, G.W. *Biophysical Journal* **1999**, *76*, 2142-2157.
47. Dai, J.; Alwarawrah, M.; Huang, J.Y. *Journal of Physical Chemistry B* **2010**, *114*, 840-848.
48. Radhakrishnan, A.; McConnell, H.M. *Biophysical Journal* **1999**, *77*, 1507-1517.
49. Chong, P.L.G. *Proceedings of the National Academy of Sciences of the United States of America* **1994**, *91*, 10069-10073.
50. de Meyer, F.; Smit, B. *Proceedings of the National Academy of Sciences of the United States of America* **2009**, *106*, 3654-3658.
51. Halling, K.K.; Ramstedt, B.; Nystrom, J.H.; Slotte, J.P.; Nyholm, T.K. *Biophys J* **2008**, *95*, 3861-3871.
52. Pan, J.; Tristram-Nagle, S.; Nagle, J. *Physical Review E* **2009**. *80*, 021931, DOI: 10.1103/PhysRevE.80.021931.
53. Bjorkbom, A.; Rog, T.; Kaszuba, K.; Kurita, M.; Yamaguchi, S.; Lonnfors, M.; Nyholm, T.K.; Vattulainen, I.; Katsumura, S.; Slotte, J.P. *Biophys J* **2010**, *99*, 3300-3308.
54. Jaikishan, S.; Bjorkbom, A.; Slotte, J.P. *Biochim Biophys Acta* **2010**, *1798*, 1987-1994.
55. Janosi, L.; Gorfe, A. *Biophys J* **2010**, *99*, 2957-2966.
56. Gómara, M. *Biochimica et Biophysica Acta (BBA) - Biomembranes* **2003**, *1612*, 83-89.
57. Ye, S.J.; Nguyen, K.T.; Chen, Z. *Journal of Physical Chemistry B* **2010**, *114*, 3334-3340.

CHAPTER 3

INTERACTION BETWEEN PEPTIDES AND LIPID BILAYERS PREPARED USING *E. COLI* POLAR LIPID EXTRACT

3.1 Introduction

The emergence of antibiotic resistance is a well-known problem that has occurred due to the wide use of antibiotics. As a result, many bacterial infections that were relatively easy to treat in the past have become difficult and expensive to combat and cure. This problem can affect everyone from the patient to the family, school or workplace, resulting in loss of productivity due to extended time away and the potential to spread such an infection. Because of these issues, there has been an effort to find new and better alternatives to conventional antibiotics, including antimicrobial peptides [1].

Many antimicrobial peptides (AMPs) have been shown to have broad spectrum effectiveness, often due to the fact that they target the cell membrane rather than specific receptors or membrane proteins. It is thought that it is much more difficult for the bacteria to change the fundamental bilayer lipid composition than to change these other targets [1-3]. Therefore, it is of great interest to study how AMPs interact with bacterial cell membranes and how they function so we can develop therapies based on their natural mode of action and effectiveness.

Studying the peptides interacting with live bacteria would be ideal for learning more about the interaction of AMPs with bacterial cell membranes. However, working with live bacteria for the purpose of investigating peptide interaction would be complex, and time consuming. As a result, using model membranes of various mixtures of lipids and other membrane constituents is considered an acceptable alternative. The complexity of these model bilayers can be customized based on the study. Many studies in the past have used the phospholipid 1-palmitoyl-2-oleoyl-*sn*-glycero-3-phospho-(1'-*rac*-glycerol) (POPG) or a mixture of POPG and a zwitterionic lipid such as 1-palmitoyl-2-oleoyl-*sn*-glycero-3-phosphocholine (POPC) or 1-palmitoyl-2-oleoyl-*sn*-glycero-3-phosphoethanolamine (POPE) as a model for the bacterial lipid membrane. This is because the bacterial membrane is known to be composed of negatively charged and zwitterionic lipids, but eukaryotic outer membranes are generally zwitterionic.

However, not all bacterial membranes are the same. For example, the cell walls in gram negative and gram positive bacteria have different compositions. *E. coli* membranes contain PE, PG and cardiolipin as the majority of their lipid composition and the removal of any of these could impact peptide-bilayer interaction. One study showed that a peptide, aurein 1.2, could heavily disrupt DMPC/DMPG bilayers but there was almost no association or disruption on DMPE/DMPG or *E. coli* lipid extract bilayers [4]. Another study showed evidence that a particular peptide interacted very similarly with DOPG and DOPE monolayers even though, between two bacterial strains with one having more PG lipids, it was less effective against the bacteria with more PG lipids [5]. This shows that one must use care when choosing the composition of some of the simple models, as subtle differences can lead to changes in how the

peptides interact with a membrane and may not be the best predictor of how these peptides might interact with an actual bacterial membrane.

Our lab has used sum frequency generation vibrational spectroscopy (SFG) to study the interaction of various membrane active peptides with substrate supported model cell membranes. We have shown that SFG can help deduce interaction mechanisms and, often, orientation [6] for peptides such as Tachyplesin [7], MSI-78 [8], magainin 2 [9], alamethicin [10], pep-1 [11], melittin [12, 13], and ovispirin-1 [14]. However, in almost all of these studies, the bilayer for modeling the bacterial cell membrane was composed of either POPG or DPPG, with one case of mixed POPG/POPC. This is mainly because using one type of lipid makes the sample preparation, data analysis, and data interpretation easier. Although important information can be obtained regarding the AMP-cell membrane interaction, based on the previous studies, it can be seen that using just PG lipids are not the most accurate way to determine peptide-bilayer interaction.

In this study, we evaluated multiple well-studied peptides at solid supported model cell membranes, composed of either POPG or *E. coli* polar lipid extract in the outer leaflet, and determined whether POPG alone could be considered an appropriate model for a bacterial cell membrane. In theory, the cell membrane should be better modeled by the *E. coli* polar lipid extract containing bilayer. The peptides investigated include MSI-594, LL-37, ovispirin-1, magainin 2, and melittin. MSI-594 is a 24 amino acid peptide with a charge of +6 and the sequence: LLGDFFRKSKEKIGKEFKRIVQRIKDFLRNLVPRTES. It is a hybrid of MSI-78 and melittin and acts through the carpet mechanism for both PC and PG lipids [15]. As discussed in the previous chapter, LL-37 is a human cathelicidin peptide with a charge of +6 and the sequence: LLGDFFRKSKEKIGKEFKRIVQRIKDFLRNLVPRTES. It is generally thought to be

more disruptive of anionic lipids rather than zwitterionic ones and acts through the toroidal pore mechanism [16-18], although there is some dispute over selectivity based on surface charge [19]. Ovispirin-1 is another α-helical peptide with a charge of +7 and the sequence: KNLRRIIRKIIHIIKKYG. It is known to generally lie parallel to the bilayer [20, 21]. Magainin 2 is an α-helical peptide with broad spectrum activity with a charge of +4 and the sequence: GIGKFLHSAKKFGKAFVGEIMNS. Magainin 2 is well studied and is largely thought to act through the toroidal pore mechanism; being significantly more active towards anionic versus zwitterionic lipids [9, 22-24]. Melittin is a membrane active peptide that is thought to be non-cell specific, but some think it to be hemolytic. The N-terminus of melittin is hydrophobic and the C-terminus is hydrophilic with the sequence: GIGAVLKVLTTGLPALISWIKRKRQQX. It interacts preferentially with negatively charged lipids, potentially acting through the mechanism different mechanisms depending on the lipid [12, 25]. It is also known, however, that anionic charged lipids inhibit its lytic activity [26].

3.2 Experiment Methods

3.2.1 Materials

All lipids in this study, including 1-palmitoyl-2-oleoyl-*sn*-glycero-3-phospho-(1'-*rac*-glycerol) (POPG), 1,2-dipalmitoyl-d62-*sn*-glycero-3-[phospho-*rac*-(1-glycerol)] (dDPPG), and *E. coli* polar lipid extract, were purchased from Avanti Polar Lipids, Inc. (Alabaster, AL). Ovispirin-1 (with the sequence H_2N-KNLRRIIRKIIHIIKKYGCOOH) G18 was synthesized by Peptide 2.0, Inc. (Chantilly, VA). Magainin 2 was purchased from AnaSpec (Fremont, CA). Melittin was purchased from Sigma-Aldrich (Saint Louis, MO). LL-37 was purchased from Bachem (Bubendorf, Switzerland).

3.2.2 Bilayer Preparation

Bilayers were deposited on CaF_2 right angle prisms via the Langmuir-Blodgett and Langmuir-Schaefer (LB/LS) methods for the proximal and distal leaflets, respectively. SFG spectra of the C-H and C-D regions, including the 2880 cm^{-1} and 2070 cm^{-1} bands, were taken to ensure bilayer quality.

3.2.3 SFG Experimental Setup

In depth detail on the theory of SFG, the instrument set up, and data analysis methods have been covered extensively in previous publications and discussed in Chapter 1. Therefore, they will not be repeated here [9, 27-33]. During the experiment, a 532 nm visible beam and a frequency tunable (1300-4300 cm^{-1}) IR beam are overlapped spatially and temporally on the bottom of the right angle CaF_2 prism which is supporting the lipid bilayer. The experiments were carried out at room temperature (~ 20 °C). The inner leaflet for all experiments was dDPPG, which is in the gel phase at room temperature and was used to minimize the lipid bilayer flip-flop and keep the bilayer asymmetrical. The outer leaflet was either POPG or *E. coli* polar extract. The bilayer is formed and constantly submerged in a 1.6 mL reservoir to which the peptide is added during the experiment. The peptide concentration in the reservoir was kept constant and homogeneous by using a magnetic micro-stirrer at 100 rpm.

SFG spectra were collected in the C-D stretching frequency range (2000-2300 cm^{-1}) to assess the deuterated inner leaflet and in the C-H/O-H stretching frequency range (2700-4000 cm^{-1}) to assess the hydrogenated outer leaflet before and after peptide addition to the subphase. Additionally, time dependent spectra in this region were taken to monitor the bilayer integrity during the experiment. SFG spectra were also taken in the amide I frequency range (1500-1800

cm^{-1}) in the ppp (SFG, visible, IR) and/or ssp polarizations to help monitor the peptide while interacting with the bilayer. The optical set up was purged with nitrogen during amide I signal collection to reduce the dips in the spectrum resulting from a loss in IR intensity due to water vapor absorbing IR along the optical pathway.

3.3 Results and Discussion

3.3.1 MSI-594

We used SFG spectra in different frequency ranges to monitor or examine different parts of the peptide-lipid bilayer interaction system. The 2000-2300 cm^{-1} frequency range has a peak of interest for the CD_3 symmetric stretch (2070 cm^{-1}) which is used to monitor the deuterated bilayer leaflet containing terminal CD_3 groups on the acyl chains. The frequency range from 2700-4000 cm^{-1} is the C-H/N-H/O-H stretching frequency region which has peaks of interest for the CH_3 symmetric stretch (2880 cm^{-1}), the N-H symmetric stretch (3300 cm^{-1}), and water O-H stretches (3200 and 3400 cm^{-1}). There are also peaks at 2940 cm^{-1} (CH_3 Fermi resonance), 2850 cm^{-1} (CH_2 symmetric stretch), and 2920 cm^{-1} (CH_2 asymmetric stretch) in this region.

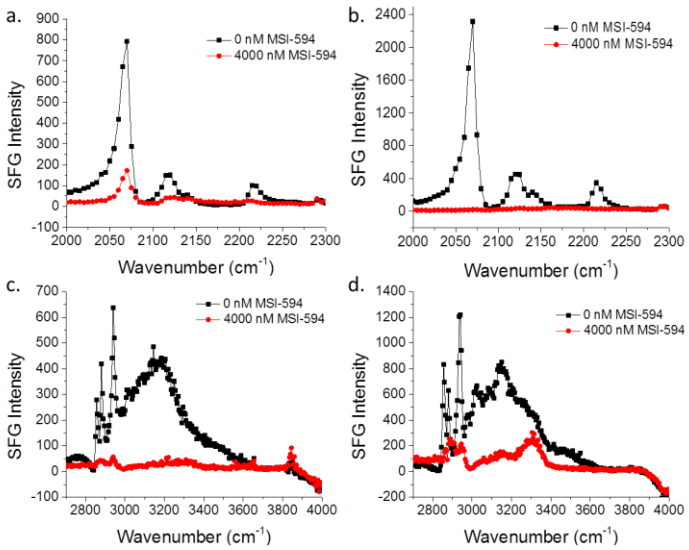

Figure 3.1: SFG spectra collected before (black) and after (red) the addition of MSI-594 to the subphase of (a) dDPPG/POPG bilayer in the C-D stretching frequency range; (b) dDPPG/*E. coli* polar extract bilayer in the C-D stretching frequency range; (c) dDPPG/ POPG in the C-H stretching frequency range; (d) dDPPG/*E. coli* polar extract bilayer in the C-H stretching frequency range.

In Figure 3.1, for both bilayers, we can see that there is a significant decrease in the peaks at ~3200, ~2070 cm^{-1} and 2880 cm^{-1} after the addition of MSI-594 to the subphase to reach a concentration of 4000 nM. The peak at ~3200 cm^{-1} is due to ordered water O-H stretching at the bilayer surface. The peak at 2070 cm^{-1} is from the terminal CD_3 groups of the acyl chain on the inner leaflet while the 2880 cm^{-1} peak is from the terminal CH_3 on the acyl chains of the outer leaflet. The decrease of the ~3200 cm^{-1} peak is due to the charge neutralization at the bilayer interface. Before the addition of the peptides to the subphase, the negatively charged lipid bilayers (for both dDPPG/POPG and dDPPG/*E. coli* extract) induced order in the water molecules at the interface which generates strong O-H stretching signals. After the addition of peptides, the positively charged peptides adsorb to the bilayer and neutralize the charge. As a result, the interfacial water molecules become disordered and the O-H stretching signal decreases. The decreases at 2070 cm^{-1} and 2880 cm^{-1} suggest that there was significant bilayer

disruption caused by the addition of the peptide. Overall, although it is somewhat different for the two bilayers, the spectra in Figure 3.1 show that this aspect of the interaction is similar for the MSI-594 and the bilayers with POPG and *E. coli* outer leaflets. Both leaflets of the two bilayers were seriously disrupted. However, the interaction dynamics are quite different, as can be seen in Figures 3.2 and 3.3.

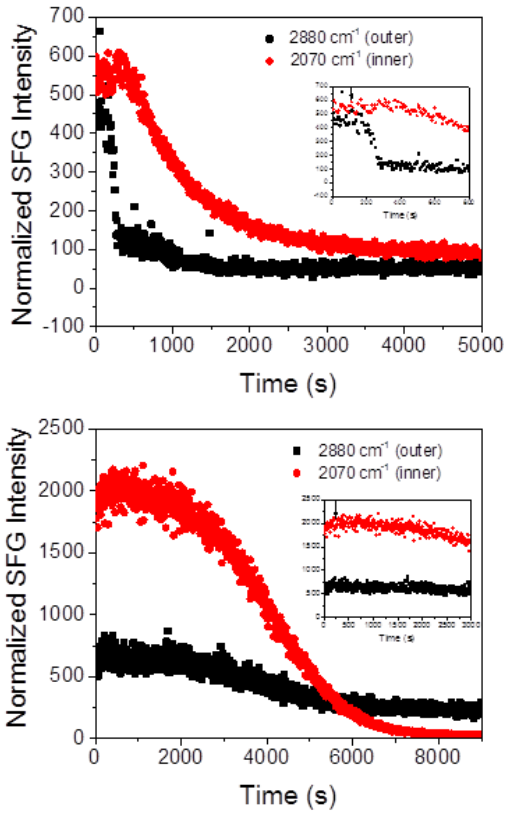

Figure 3.2: Time-dependent SFG signal observed from the dDPPG-POPG bilayer (top) and the dDPPG-*E. coli* polar extract bilayer (bottom). The arrow in the insert shows the time when the MSI-594 was added to the lipid bilayer subphase.

Figure 3.2 shows the time-dependent interactions of the MSI-594 with the dDPPG-POPG lipid bilayer (top) and dDPPG-*E. coli* polar extract lipid bilayer (bottom). These SFG spectra show that the time from injection, indicated by an arrow on the spectrum inset, to the time that both of the signals decrease is significantly different for the two different model bilayers. For the

dDPPG-POPG system, the 2880 cm^{-1} signal starts to decrease after about 100 s and then decreased very quickly. After the 2880 cm^{-1} signal for the outer leaflet begins to equilibrate, the 2070 cm^{-1} signal starts to decrease at a much slower rate. This can be interpreted as the peptide quickly associating to the bilayer and disrupting the outer leaflet before moving to the inner leaflet and causing disruption. Since the SFG signals from the two leaflets exhibit different decreasing kinetics, we believe that the signal decrease is not due to lipid flip-flop. The final signal is sufficiently low that it can be considered bilayer destruction. We also see bilayer destruction for the dDPPG-*E. coli* polar lipid bilayer, but the time dependent interaction is different. The time from injection to a noticeable decrease in the 2880 cm^{-1} or 2070 cm^{-1} signal is in the range of 500-1000 s and is very gradual.

A possible explanation for the difference in interaction kinetics is the overall net charge of the bilayer. POPG is a negatively charged lipid that is frequently used to model bacterial membranes because the PG head group is very common in bacterial cell membranes. However, the bilayer is composed only of PG while real cell membranes, like that of *E. coli*, are composed of other lipids as well. In particular, the *E. coli* polar lipid mixture is 67.0 wt/wt% PE, 23.2 wt/wt% PG, and 9.8 wt/wt% cardiolipin, which means that the *E. coli* polar lipid leaflet is potentially only approximately 1/3 the charge of a POPG leaflet. Due to the discrepancy in the overall charge of the leaflet, we could expect to see a stronger interaction between the positively charged peptide MSI-594 with the POPG leaflet, evident in a quicker interaction and disruption time. However, this difference in charge did not protect the dDPPG-*E. coli* polar lipid bilayer from destruction. This is to be expected, since it has been shown that *E. coli* is susceptible to MSI-594, as well as other MSI peptides [15, 34-36]. It was reported by Ramamoorthy et al. that the MIC for MSI-594 against *E. coli* was ~2 μg/ml, which is ~817 nM [15]. They performed

leakage assays that showed at 1.4 µM, almost 90% of the dye had leaked out of POPC:POPG (3:1) vesicles by 5 min. There was significant interaction leading to lysis in a very short time after peptide addition which is similar in behavior to our case involving POPG outer leaflet experiment, but not the *E. coli* lipid extract. Our *E. coli* extract did eventually experience destruction, but it took closer to 20 min, rather than the 5 min stated in the paper. Additionally, it is not stated how much disruption had occurred in their case as the bilayer wouldn't need to be destroyed to leak dye.

It was reported from NMR experiments that on POPC lipids, MSI-594 likely acted through the "carpet mechanism" [15]. On POPG lipids at low concentrations, it was proposed that MSI-594 induced some acyl chain disorder, but that most of the lipids were aligned, as opposed to high concentrations where non-bilayer lipid structures were formed, such as hexagonal phases [15]. It is worth noting that the concentration used in our experiment was more than four times the MIC and almost three times the concentration of their dye leakage experiments.

It is possible that the difference in interaction/disruption time is related to the mechanism that took place on the POPG bilayer, which was possibly the formation of non-bilayer lipid structures. These non-bilayer structures would have occurred quickly after the MSI-594 interacted with the dDPPG/POPG bilayer. In contrast, the *E. coli* polar leaflet was lower in anionic charge and behaved more like a POPC leaflet would. It has been seen before with other peptides that a mixed bilayer could foster behavior in-between what was observed when in environments composed of only one of the two components [17]. This could be further investigated with other methods such as ATR-FTIR, which is a vibrational spectroscopy that can provide further insight to peptide-membrane interactions.

Furthermore, it has been shown that other MSI peptides have the ability to induce a "charge cluster mechanism" which causes the lipids in the membrane to rearrange such that defects could occur and potentially aid in cell lysis [35]. It is possible that MSI-594 could act through this mechanism as well, and the interaction could take a different amount of time to reorganize the lipids. This could cause the time dependent spectrum/activity to differ between *E. coli* polar lipid and pure POPG.

MSI-594 has been reported as having a bend at the GIG region, causing a "kink" in the peptide in the presence of zwitterionic dodecylphosphocholine micelles, but a helical hairpin in an environment of lipopolysaccharide [37-39]. Both of the environments we use in this study are negatively charged, we assume that the peptide is in a hairpin for our experiments. However, we do not have structural data to confirm this.

We can see further evidence of similar peptide adsorption to the dDPPG-POPG bilayer relative to the dDPPG-*E. coli* polar lipid bilayer by the intensity of the peak at ~1655 cm^{-1} in Figure 3.3. This peak is the peptide amide I peak and is indicative of the ordered peptide on the bilayer surface. The MSI-584 amide I peak intensities in the ssp and ppp polarized spectra are similar for both lipid bilayers. Furthermore, the ppp/ssp intensity ratios for the two cases are similar. SFG signal intensity is proportional to the square of the number of peptides and is related to the peptide orientation while the ppp/ssp signal intensity ratio is primarily related to the peptide orientation. For this reason, we believe that MSI-594 molecules associated with two types of lipid bilayers are similar in number and in structure.

Figure 3.1a shows that the CD region spectrum has a small peak at 2070 cm^{-1} while Figure 3.1b shows no CD signal. This might be due to the two bilayers being disrupted different

amounts at the time of the spectrum collection. Figure 3.1a was collected after 5000 seconds where the signal looked to be almost equilibrated, while Figure 3.2 was detected after 8000 seconds where it looked equilibrated. If given enough time, the 2070 cm^{-1} signal in Figure 3.1a may have decreased further, but at a very slow rate.

In summary, we believe that MSI-594 can disrupt both dDPPG-POPG bilayer and dDPPG-*E. coli* polar extract bilayers. Given a long enough interaction time, both lipid bilayers can be completely disrupted. The amount of peptide associated and the peptide orientation are not significantly different between the two bilayers. However, the disruption kinetics for the dDPPG-POPG bilayer is much faster, perhaps due to the larger negative change of the bilayer compared to the dDPPG-*E. coli* polar extract bilayer. Other possibilities are two different disruption methods: lying down and causing disorder on zwitterionic lipids and leading to the formation of non-bilayer phases when associated with anionic lipids; or there is charge cluster mechanism interaction in which the peptide induces the lipid reorganization. Perhaps in the charge cluster mechanism case, the peptide does not start causing disorder in the bilayer until the clusters of anionic and zwitterionic lipids form, resulting in a slower interaction time. Therefore, the POPG lipid can be used as a model for bacterial cell membranes to understand a certain degree of interaction with MSI-594, such as peptide-bilayer association, bilayer order before and after peptide addition and peptide orientation. However, other aspects, such as kinetics, are not as well modeled.

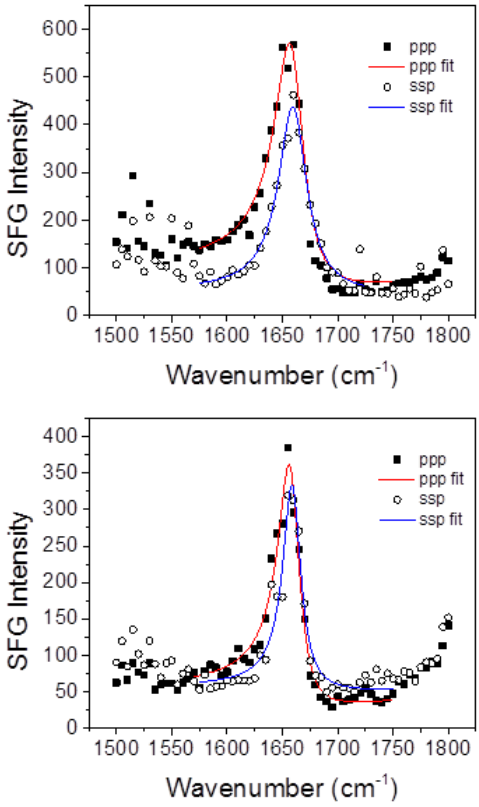

Figure 3.3: SFG signal of Amide I signal from the MSI-594 associated with (top) dDPPG-POPG bilayer and (bottom) dDPPG-*E. coli* polar extract bilayer.

3.3.2 Ovispirin-1 G18

Ovispirin-1 G18 is an alpha helical peptide with an isotope label $^{13}C=O$ at G18. Figure 3.4 shows SFG spectra collected from the CD and CH stretching frequency regions of dDPPG-POPG and dDPPG-*E .coli* polar systems before and after addition of peptide stock solution to achieve 7.5 µM Ovispirin-1 G18. It can be seen that after the addition of peptide to the subphase, the inner and outer leaflets of the dDPPG-POPG system are significantly disrupted as evident from the decrease in the CD signal at 2070 cm^{-1} and the CH_3 symmetric stretching signal at 2880 cm^{-1}. For the dDPPG-*E. coli* polar extract bilayer system, the 2880 cm^{-1} peak from the outer leaflet in contact with the peptide solution only slightly decreased, but the signal at 2070 cm^{-1}

from the inner leaflet is nearly the same before and after peptide addition, which suggests that the peptide may only slightly disrupt the outer leaflet and does not interact with the inner leaflet of the bilayer. However, because of the decrease in the water signal at ~3200 cm^{-1}, we can conclude that the peptide is present at the bilayer surface and the absence of change in the CH_3 and CD_3 signals is not due to the peptide not interacting with the dDPPG-*E. coli* polar extract bilayer.

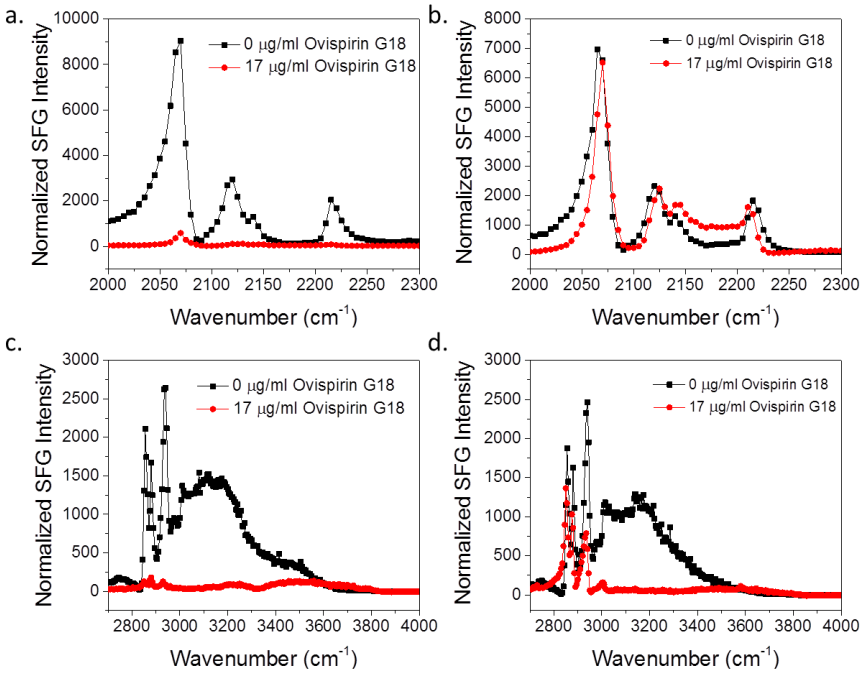

Figure 3.4: SFG spectra collected before (black) and after (red) the addition of ovispirin-1 G18 to the subphase of (a) dDPPG/POPG bilayer in the C-D stretching frequency range; (b) dDPPG/*E. coli* polar extract bilayer in the C-D stretching frequency range; (c) dDPPG/ POPG in the C-H stretching frequency range; (d) dDPPG/*E. coli* polar extract bilayer in the C-H stretching frequency range.

From Figure 3.4 we can see that ovispirin-1 G18 does not have the same interaction with the dDPPG-POPG bilayer and the dDPPG-*E. coli* polar extract bilayers. As with the previous study on MSI-594, we also studied the interaction kinetics between the two lipid bilayers and the

peptide. Figure 3.5 shows the time-dependent SFG signal for the 2070 cm^{-1} and 2880 cm^{-1} frequencies which monitor the signal change of the two lipid bilayers after the addition of ovispirin-1 G18 to the subphase. We can see that the change in the time-dependent SFG signal is very different for the two bilayer systems. After the injection of ovispirin-1 to the subphase to reach a concentration of 7.5 μM for the dDPPG-POPG bilayer, the 2880 cm^{-1} signal of the POPG outer leaflet drops sharply after ~ 100 s, and then decreases more gradually. The 2070 cm^{-1} signal starts dropping after the initial drop of 2880 cm^{-1} and decreases at a similar rate as the gradual rate of 2880 cm^{-1}. This suggests that the peptide quickly associates with the bilayer, indicated by the quick drop of 2880 cm^{-1}, followed by a gradual disruption of the bilayer. The rate of CH and CD signal decrease is not significantly different, but are not identical either, which suggests that this could be the bilayer disruption/destruction and possibly a degree of bilayer flip-flop activity. If the rate was the same, flip-flop would be suspected since lipids from both leaflets would be moving to the opposing leaflet causing both to become more symmetric as a result. This mechanism would show up during the time dependent monitoring as the signal dropping at the same rate for both leaflets. The possibility of flip-flop can be further investigated by doing experiments with AFR-FTIR, which is not sensitive to molecule order and would shed light on whether the lipids are still present or removed.

The bilayer interaction of ovispirin-1 with the dDPPG-*E. coli* lipid system is different than with the dDPPG-POPG system. Although the peptide concentration is the same, there is no sharp drop in the 2880 cm^{-1} signal after the addition of the peptide to the subphase and the signal decreases very slowly over the course of hundreds of seconds. Both the 2880 cm^{-1} and 2070 cm^{-1} signals drop so slowly, that after 1.5 h they are still similar to before peptide injection. Since the water signal shown in Figure 3.4 d decreased substantially, we believe that ovispirin-1 molecules

were associated with the dDPPG-*E. coli* polar extract bilayer, but they do so much more slowly than on dDPPG-POPG and do not cause bilayer disruption. Figure 3.4b shows the inner leaflet spectra are similar before and after peptide addition, but the time-dependent CD stretching signals shown in Figure 3.5b decrease. Perhaps this is because the peak center of the ~2070 cm^{-1} signal shifted slightly, therefore the signal intensity observed at this wavenumber exhibits some time-dependent changes.

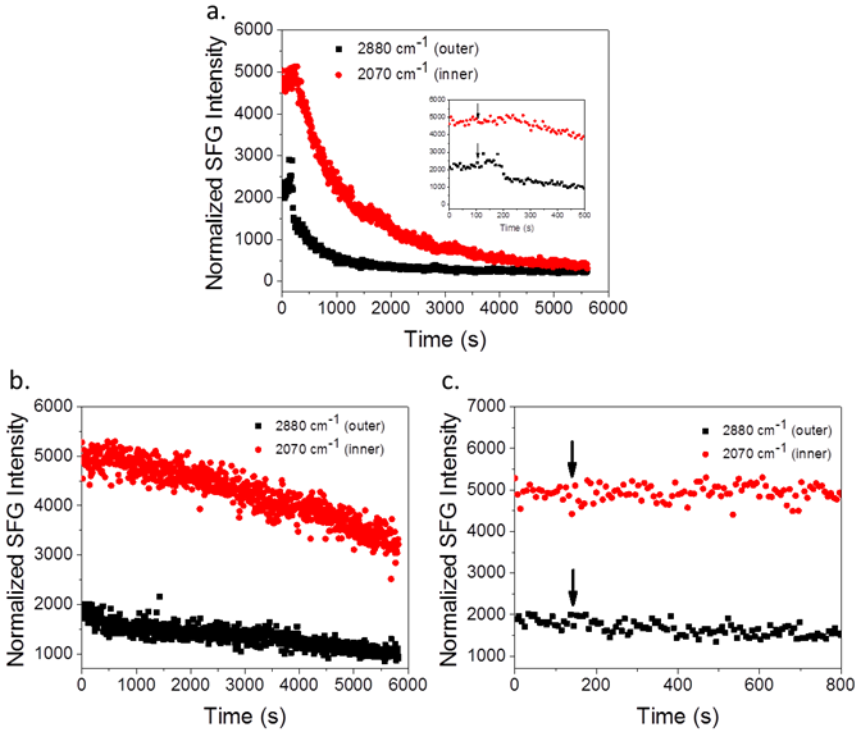

Figure 3.5: SFG time-dependent signal detected from (a) dDPPG-POPG bilayer, inset is zoomed; (b) dDPPG-*E. coli* polar extract bilayer; (c) dDPPG-*E. coli* polar extract bilayer zoomed in before and after the injection of ovispirin-1 G18 to the subphase. Peptide injection is indicated by arrow.

We also monitored the ovispirin-1 during interacting with the bilayers. Figure 3.6 shows the amide I peak at ~1655 cm^{-1} which is associated with the peptide backbone. The overall intensity of the amide I signals associated with the two lipid bilayers and the ppp/ssp intensity ratios are similar. This suggests that the number of peptides/peptide order is potentially similar in

both cases. This could mean that while the same number of peptides associated to both bilayers, the leaflet with fewer negative charges (*E. coli* polar extract) might require more ovispirin-1 peptides to disrupt the bilayer quickly.

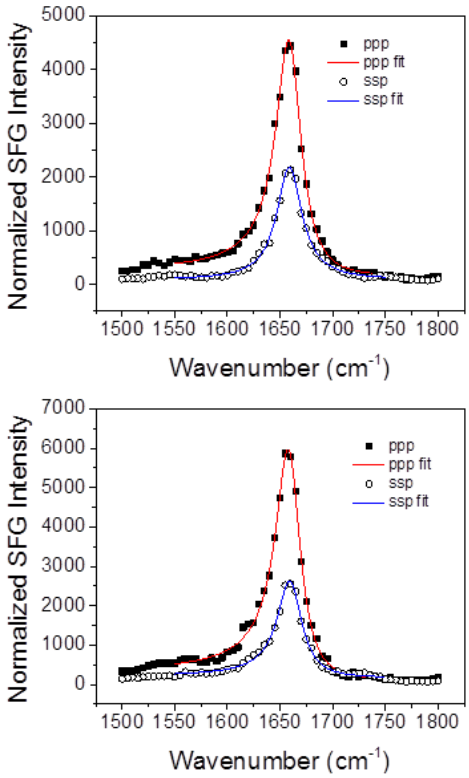

Figure 3.6: SFG signal of Amide I signal from the ovispirin-1 associated with (top) dDPPG-POPG bilayer and (bottom) dDPPG-*E. coli* polar extract bilayer.

Ovispirin-1 is well known to be potent as an antimicrobial, but is also hemolytic and cytotoxic to the point that it is not able to be used for any therapeutics. Even with this being the case, the MIC for several bacteria is much lower than the concentration used for cell lysis [40, 41]. Therefore, it seems as though ovispirin-1 still is more toxic to bacteria which contain a higher fraction of anionic lipids. From this information, it could be reasonable to suggest that even from that data, we would expect that ovispirin-1 would associate less with a more neutral

lipid bilayer. However, the MIC for several bacteria are very low (< 10 µg/ml) and given that our concentration used was 17 µg/ml, we had hoped to see more disruption activity at the *E. coli* polar extract leaflet. Additionally, my experimental conditions are not necessarily a true model of a bacterium in its environment and it is possible that we might have seen a different response if we had raised or lowered the concentration. There have been several molecular dynamics simulations projects studying ovispirin-1 that have more generally focused on zwitterionic systems with the goal of finding an analogue that would be suitable for therapeutic use [42-44]. Additionally, solution and solid state NMR experiments have elucidated the structure of ovisprin-1 in environments of trifluoroethanol (TFE) and POPC:POPG (3:1) lipids [21, 40], and with 2D IR characterizing the structure and location of ovispirin-1 in a POPC:POPG (3:1) environment [20]. All agree that the peptide is alpha-helical, but other specifics of the structure seem to be dependent on the environment. In lipid environments, it is generally agreed on that the peptide is residing near the lipid head groups in the bilayer and lying down, parallel to the bilayer and perpendicular to the surface normal [20, 21].

Yamaguchi and coworkers mention that ovispirin-1 also maintains an orientation parallel to the bilayer surface, even at high peptide/lipid ratios and does not exhibit a "two stage orientation" that is sometime seen in other peptides where they insert into the bilayer at high concentrations [17, 45]. Their result suggests that we probably would not see an increased disruption from the peptides inserting into the bilayer, but it is possible that they require more peptides to quickly disrupt the outer leaflet from a non-pore forming mechanism. Alternatively, it is possible that the peptide could have two different modes of action depending the lipid content, like in the case of the α-helical peptide VP1, which acts via the carpet model on membranes higher in cardiolipin and PG lipids while entering the membrane at an oblique angle

and solubilizing/lysing the membrane on *E. coli* lipids [46]. They observed that fewer peptides associated to an *E. coli* membrane, but the membrane eventually lysed. However, in our case, the leaflet was at best slowly affected. If this concentration dependent interaction is what is happening in our system, maybe it is possible that it would take more peptide to eventually see a strong disruption effect.

The amide I spectra suggest that there are possibly slightly more peptides on the *E. coli* leaflet vs. the POPG leaflet and we did see some decrease in the signal but it was not nearly as fast as the more charged POPG environment. It is a possibility that a higher concentration would result in a faster interaction time.

In summary, ovispirin-1 molecules associate with dDPPG-POPG and dDPPG-*E. coli* polar extract lipid bilayers. The number and orientation of the associated peptides for the two types of the bilayers are similar, showing that POPG can model this aspect of the interaction. However, ovispirin-1 disrupted both leaflets of the dDPPG-POPG bilayer quickly, but could not disrupt the dDPPG inner leaflet and only slightly disrupted the outer leaflet of the dDPPG-*E. coli* polar lipid extract bilayer. It is possible that the ovispirin-1 could disrupt the latter bilayer, but at a much slower speed. Based on these results, it is clear that the POPG can model some aspects of the ovispirin-1 interaction with *E. coli* lipids, but there are still important aspects of the interaction, such as the interaction kinetics, that cannot be accurately modeled with the simple system. This is probably at least partly due to the difference in the overall net charge of the bilayers. The maximum number of peptides might be associated with both bilayers at this concentration. However, at a bilayer with a lower net charge, a higher number of peptide molecules would be needed to induce disorder similar to the pure PG system.

3.3.3 Magainin 2

Figure 3.7 shows the CD and CH stretching frequency ranges for 800 nM magainin 2 interacting with the two bilayer systems. It is shown that at this concentration, the magainin 2 clearly associates with both systems, evident by the drop in the water signal at ~3200 cm^{-1}. As discussed above, the O-H water signal decrease is due to the charge neutralization. The positively charged bilayer associated peptides neutralize the negative charge on the PG lipids. However, the outer leaflet is only disrupted in the POPG case, as indicated by the decrease in the 2880 cm^{-1} CH_3 symmetric peak. For the *E. coli* case, there is no change in the 2880 cm^{-1} peak before and after peptide addition to the subphase, so we believe that there is no disruption of the outer leaflet by magainin 2. The inner leaflet was unaffected in both systems, evident by the unchanged 2070 cm^{-1} peak intensity. Since magainin 2 molecules are antimicrobial, they should also disrupt the inner leaflet when reaching a certain concentration. It is likely that the concentration is not high enough to disrupt the inner leaflet.

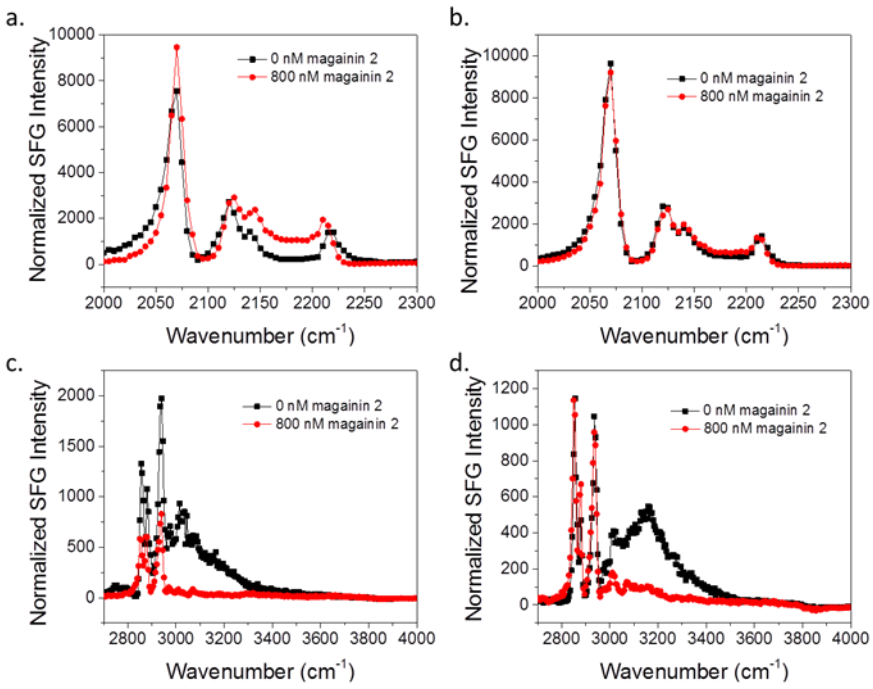

Figure 3.7: SFG spectra collected before (black) and after (red) the addition of magainin 2 to the subphase of (a) dDPPG-POPG bilayer in the C-D stretching frequency range; (b) dDPPG-*E. coli* polar extract bilayer in the C-D stretching frequency range; (c) dDPPG-POPG in the C-H stretching frequency range; (d) dDPPG-*E. coli* polar extract bilayer in the C-H stretching frequency range. The magainin subphase concentration is 800 nM.

Figure 3.8 shows the time dependent SFG signals of the two lipid bilayer systems interacting with magainin 2. For the dDPPG-POPG bilayer case, the 2880 cm^{-1} signal increases quickly before a more slow decrease and eventual equilibration while the 2880 cm^{-1} signal for *E. coli* polar lipid extract seems to increase a small amount and then is equilibrates without a signal decrease. From this time-dependent observation and the data from the CD and CH spectra, it is possible that the initial increase in 2880 cm^{-1} signal is due to the peptide association with the bilayer. It could be that the peptides induce a sort of order in the outer leaflet before causing disruption. Figure 3.9 shows the amide I signal detected from magainin 2 when the bilayers were in contact with the 800 nM magainin 2 solution. The overall intensity of the ~1655 cm^{-1} peptide

signal on the dDPPG-POPG bilayer is approximately four times more intense than the signal of magainin 2 associated with the dDPPG-*E. coli* polar extract lipid leaflet containing system, suggesting that there are more peptides on the POPG bilayer. This agrees with the CH signal being lower for POPG vs *E. coli* polar since it was seen that the CH_3 signal decreased, which could occur because a certain threshold was reached and allowed the peptide to disrupt the bilayer. Because fewer magainin 2 molecules were adsorbed onto the *E. coli* polar lipid extract leaflet, no disruption was observed.

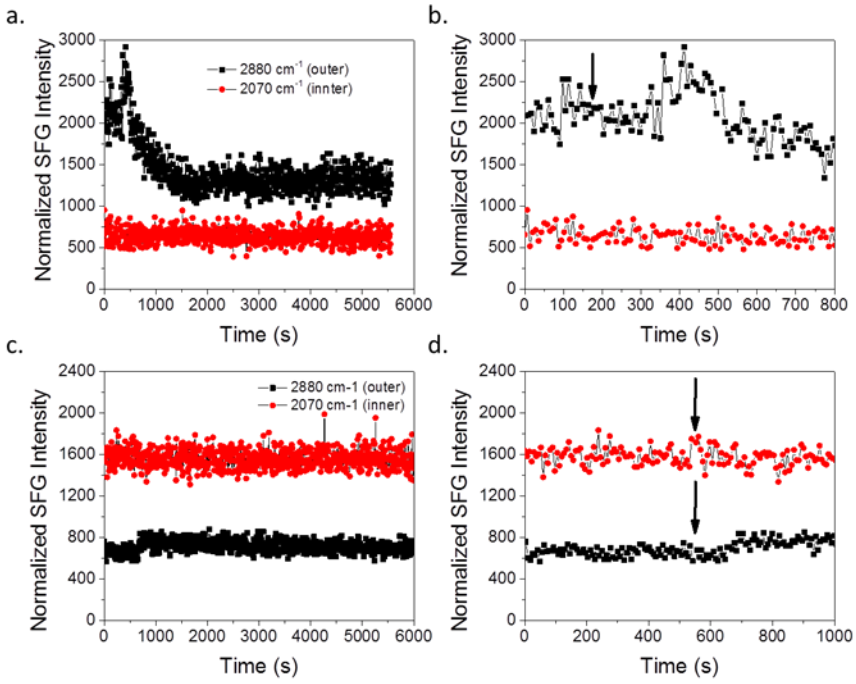

Figure 3.8: SFG time-dependent signal detected from (a) dDPPG-POPG bilayer, (b) dDPPG-POPG bilayer in the first 800 seconds, (c) dDPPG-*E. coli* polar extract bilayer; (c) d-DPPG-*E. coli* polar extract bilayer zoomed in the first 1000 seconds, before and after the injection of magainin 2 to the subphase to reach 800 nM. Peptide injection is indicated by arrow.

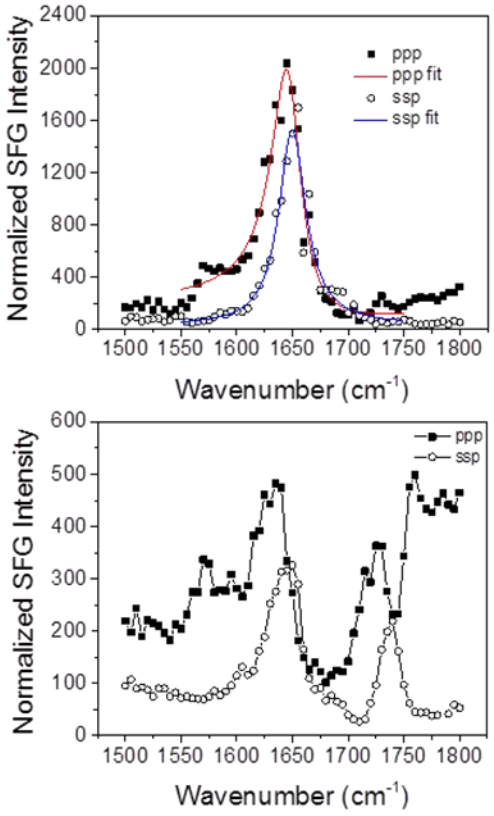

Figure 3.9: SFG signal of Amide I signal from the magainin 2 associated with (top) dDPPG-POPG bilayer and (bottom) dDPPG-*E. coli* polar extract bilayer. The magainin 2 subphase concentration is 800 nM

We then increased the magainin 2 concentration in the subphase in anticipation that a higher concentration would enable magainin 2 to disrupt both leaflets in the lipid bilayer. Figure 3.10 shows the SFG signals detected in the CD and CH stretching frequency regions for dDPPG-POPG and dDPPG-*E. coli* polar extract bilayers when in contact with 2 μM magainin 2. At this higher concentration, there is a similar amount of disruption for the POPG leaflet as was seen at 800 nM. However, there is some minor disruption in the *E. coli* extract leaflet as well. The deuterated leaflet was still unaffected in both high concentration cases. This could be because a minimum concentration of peptide needs to be reached before disruption can begin. Since it

seems to be more difficult for magainin 2 to associate on dDPPG-*E. coli* polar extract bilayers, either due to electrostatic differences or because of a difference in other bilayer properties, the solution concentration may need to be higher before enough peptide is present on the surface to cause a disturbance.

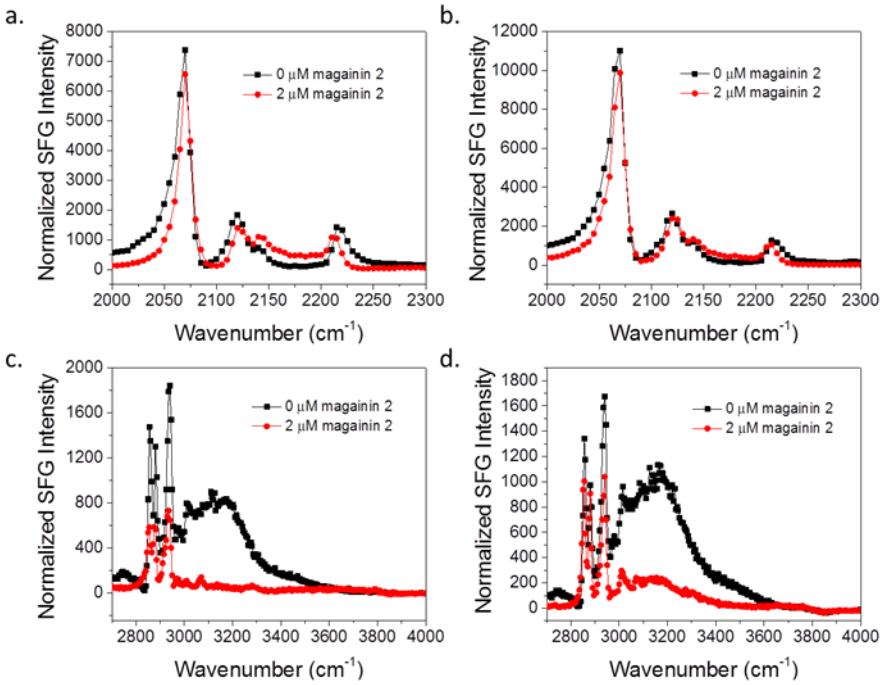

Figure 3.10: SFG spectra collected before (black) and after (red) the addition of magainin 2 to the subphase of (a) dDPPG-POPG bilayer in the C-D stretching frequency range; (b) dDPPG-*E. coli* polar extract bilayer in the C-D stretching frequency range; (c) dDPPG-POPG in the C-H stretching frequency range; (d) dDPPG-*E. coli* polar extract bilayer in the C-H stretching frequency range. The magainin subphase concentration is 2.0 μM.

Figure 3.11 shows the time dependent injection spectra for 2 μM magainin 2. The 2880 cm^{-1} signal for the dDPPG-POPG system looks very similar for 2 μM compared that of 800 nM, with the exception that the delay time before interaction seems to be much shorter, less than half the time as before. This is to be expected with a much higher concentration of peptide. The 2880 cm^{-1} signal for the dDPPG-*E. coli* polar extract system appeared to take much longer to respond

to the peptide addition, but ultimately was not significantly different than the 800 nM case, although it did slightly decrease over time.

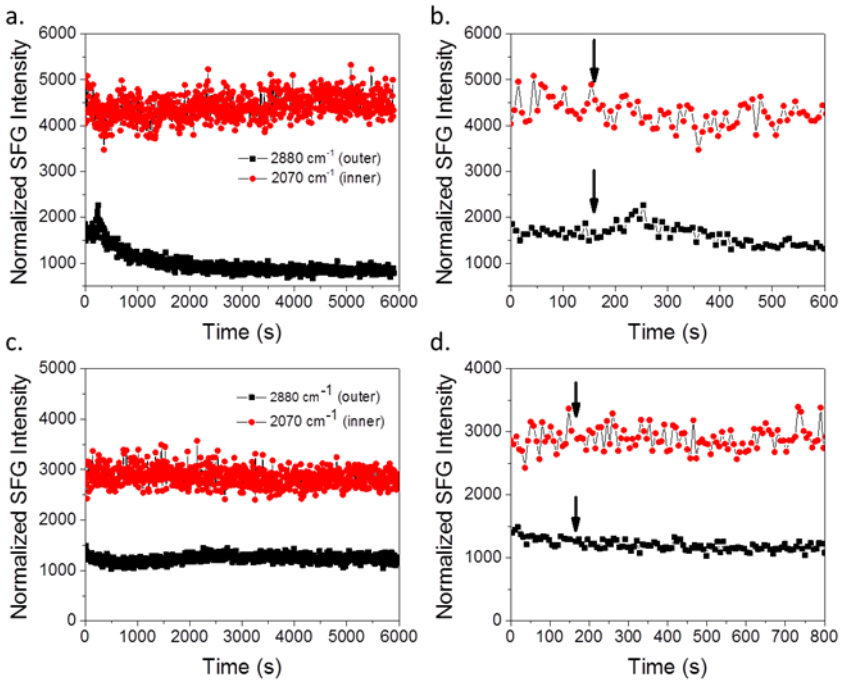

Figure 3.11: SFG time-dependent signal detected from (a) dDPPG-POPG bilayer, (b) dDPPG-POPG bilayer in the first 600 seconds, (c) dDPPG-*E. coli* polar extract bilayer; (c) d-DPPG-*E. coli* polar extract bilayer zoomed in the first 800 seconds, before and after the injection of magainin 2 to the subphase to reach 2.0 µM. Peptide injection is indicated by arrow.

The amide I region signal at ~1655 cm^{-1} for 2 µM on the POPG system was comparable to that on the 800 nM system (Figure 3.12). This is consistent with the similar looking CH, CD, and time dependent spectra between the two concentrations. For the *E. coli* polar extract case, the ~1655 cm^{-1} signal was slightly higher at 2 µM than it was at 800 nM. This apparent slight increase in adsorbed peptide can be the cause of the slightly disrupted outer leaflet that was observed in Figure 3.8. Again, this effect could be due to the higher charged density on the POPG leaflet relative to the *E. coli* polar extract leaflet.

The fact that we do not see very much acyl chain disruption is not completely surprising. The MIC for magainin 2 against *E. coli* seems to vary with different strains; 55.5 μM for ATCC strain 8739, ~3 μM for ATCC 25922, and 20 μM for ATCC 25922 with F5W-magainin 2, an equipotent analogue of magainin 2 [22, 47, 48]. A previous study in our lab observed amide I signal on POPG/POPG bilayers using 800 nM magainin 2 and on POPC/POPC bilayer with 2 μM magainin 2 and determined that the peptide was in a transmembrane orientation in POPG and generally laying down on POPC [9]. Because of this success, we started at a concentration of 800 nM in our study. This relatively low concentration was used in the original study because the bilayer was a purely anionic POPG bilayer and peptides should have associated at a lower concentration compared to what was considered a toxic concentration to *E. coli*.

We do see peptide association at 800 nM for both systems, which is lower than all of the listed MICs. We saw minimal disruption and the amide I χ_{ppp}/χ_{ssp} ratios, which are orientation and polarization dependent measurements, were different from a previous study in our lab (indicating a different peptide orientation – perhaps related to the different inner leaflet – see the discussion below), so we increased the concentration. At 2 μM we saw the same case for the POPG system and slightly higher adsorption for the *E. coli* system, indicated by the amide I intensity. The 2 μM concentration is still approximately close to the lowest of the MIC values and it would be prudent to try higher magainin 2 concentrations for future work.

We see some chain disruption on the POPG leaflet and on the *E. coli* leaflet at 2 μM. We believe that this is reasonable since this peptide is thought by many to operate via associating with membranes until instability causes toroidal pores to form resulting in leakage and cell death [23, 49, 50]. However, there is some dispute about this mode of action being correct [24]. In these toroidal pores, there is not a large amount of acyl chain disruption. This agrees with most

of the previous studies, which cited that they saw very little acyl chain disruption and that the peptide had extensive interaction with the lipid head groups [47, 51, 52]. However, if there were pores forming we would expect to see some disturbance to both leaflets. Evidence that lipid flip flop was taking place and was facilitated by these pores would be observing the 2880 $cm^{-1}$and 2070 cm^{-1} signals decreasing at approximately the same rate [50]. However, we do not observe this for either system at either concentration. This suggests that we might not be seeing toroidal pores, but just association near the lipid head groups. This is likely due to the lower concentration of magainin 2 we used in the study.

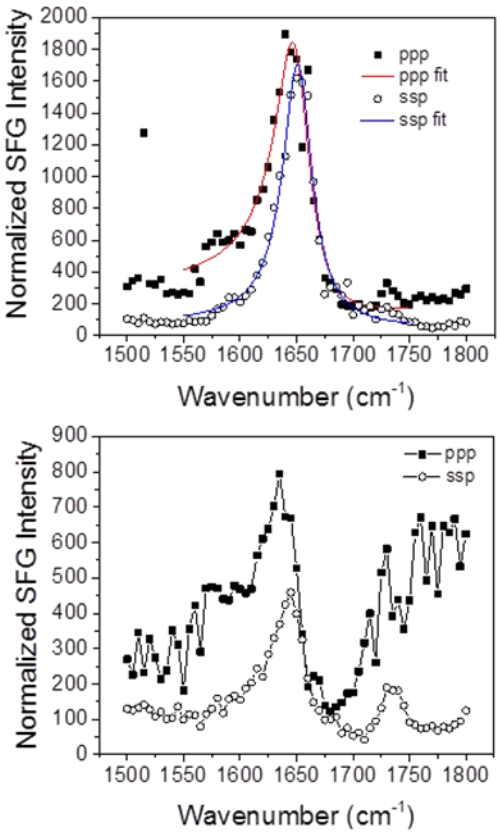

Figure 3.12: SFG signal of Amide I signal from the magainin 2 associated with (top) dDPPG-POPG bilayer and (bottom) dDPPG-*E. coli* polar extract bilayer. The magainin 2 subphase concentration is 2.0 µM.

Also of note is that most of the studies used POPC and POPG (transition temperature -2 °C) or DMPC and DMPG (transition temperature 24 °C). Because 24 °C is very close to room temperature, the lipid might be in gel or fluid phase depending on the experimental conditions. The one study that used DPPG observed that the peptide did not insert into the bilayer and stayed associated with the head groups (this could be a misinterpretation since the toroidal pore theory was not yet known) [51]. Without more studies in the gel phase, it isn't currently known if magainin 2 cannot insert into gel phase DPPG or if the lack of activity is due to low concentration or misinterpretation, but this phenomenon has been observed before [53]. However, the possibility exists that the fact that since we employ a gel phase inner leaflet which may stabilize the outer fluid phase's leaflet, this could make it difficult for the peptide to enter and create a pore. Additionally, the *E. coli* lipid extract used for the outer leaflet contains ~60% PE lipids. It has been shown that the addition of PE lipids decreases the incidence of magainin 2 induced pores in PG lipids [54]. This is explained by the PE causing negative curvature of the bilayer which opposes apparent positive curvature strain caused by the magainin 2 and results in a possibly unfavorable environment for pore formation [54-56].

The low magainin 2 concentration and the lack of signal change in the 2070 cm^{-1} time dependent spectrum make toroidal pore formation a less likely possibility than the case where the peptide is inserting into the outer leaflet and participating in transient pore formation as stated in early papers. Increasing the concentration, however, might result in a more defined pore and stronger evidence of the toroidal pore mechanism.

In summary, magainin 2 adsorbed to both lipid bilayer systems at both concentrations used in this study, but there was significantly more association on POPG containing bilayers. Magainin 2 can disrupt the outer leaflet of the dDPPG-POPG bilayers at both 800 nM and 2.0

μM, and can slightly disrupt the outer leaflet of the dDPPG-*E.coli* polar extract lipid bilayer at 2.0 μM. The difference in interaction is likely partially due to the difference in bilayer surface charge and it has been observed that magainin 2 interacts differently with anionic and zwitterionic lipid bilayers. The lack of inner leaflet disruption for the POPG containing system might be due to the inner leaflet being gel phase and the bilayer thus being more resistant to flip flop and potentially toroidal pore formation. Additionally, the combination of lower surface charge and the PE lipids' tendency to oppose positive curvature induced by magainin 2 could explain why the *E. coli* lipids were less disrupted compared to the POPG lipids. Therefore this study again demonstrated that POPG can serve as a simple model for bacteria cell membrane association, but the results are not comparable for the lipid dynamics/interactions and one should be aware of the potential differences in results when choosing a model cell membrane system.

3.3.4 Melittin

In addition to the AMPs we have discussed so far, we also studied melittin. As was discussed above, melittin can disrupt both bacterial and mammalian cell membranes. Figure 3.13 shows the SFG signals detected from the C-H and C-D stretching signals of the dDPPG-POPG and dDPPG-*E. coli* polar extract bilayer systems before and after addition of melittin to the subphase to reach a concentration of 0.78 μM. At this concentration, both the inner and outer leaflets of the dDPPG-POPG system are disrupted, evident by the decrease in 2880 cm^{-1} and 2070 cm^{-1} signal. The O-H stretching signal decrease also indicates the association of the melittin molecules with the dDPPG-POPG bilayer. There is also a negative peak at ~3300 cm^{-1}, which is contributed by the N-H stretch from the peptide backbone, and indicates again that the peptide is at the bilayer surface. For the dDPPG-*E. coli* polar extract system, the SFG signal decrease in both C-H and C-D stretching frequency regions was observed. Interestingly, there

seemed to be a slightly larger decrease in the 2880 cm^{-1} and 2070 cm^{-1} peaks here compared to the POPG system. It is possible that there is more disruption of the inner and outer layers of the dDPPG-*E. coli* polar extract lipid bilayer.

Figure 3.14 shows the time dependent SFG signal intensities observed at 2880 cm^{-1} and 2070 cm^{-1} from both the dDPPG-POPG bilayer and the dDPPG-*E. coli* polar extract bilayer before and after the addition of melittin to the subphase to reach 0.78 μM. The overall features of the time dependent signal intensities are similar, showing a drop in the outer 2880 cm^{-1} signal and the inner 2070 cm^{-1} signal as a function of time. It is important to note that while the inner leaflets were disrupted in both bilayers, the time dependent shows that the inner leaflet of the *E. coli* containing bilayer was disrupted more than the POPG containing one. This shows that melittin can gradually disrupt both lipid bilayers. The signal decreases in the two leaflets of each bilayer are different, showing that the signal decrease is not due to the lipid flip-flop. Interestingly, there was first a signal increase on the POPG leaflet, perhaps due to the POPG lipid order change or CH signal that may have been contributed by melittin.

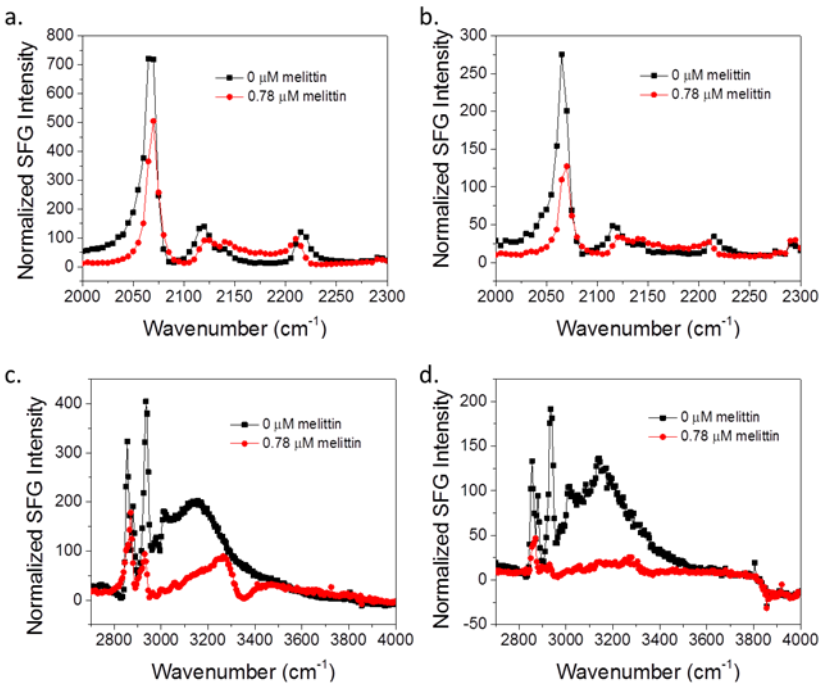

Figure 3.13: SFG spectra collected before (black) and after (red) the addition of melittin to the subphase of (a) dDPPG-POPG bilayer in the C-D stretching frequency range; (b) dDPPG-*E. coli* polar extract bilayer in the C-D stretching frequency range; (c) dDPPG/ POPG in the C-H stretching frequency range; (d) dDPPG-*E. coli* polar extract bilayer in the C-H stretching frequency range. The melittin subphase concentration is 0.78 μM.

Figure 3.15 shows the amide I signal detected from melittin associated with the two types of lipid bilayer at a sample concentration of 0.78 μM. The intensity of the 1655 cm^{-1} peak of melittin interacting with the POPG leaflet was slightly higher than that on *E. coli* polar extract leaflet, but they are relatively close, which is a little surprising since the disorder in the *E. coli* polar extract system was slightly higher. However, it is possible that the intensity discrepancy is due to peptide order, rather than peptide number. For example, even if there were more peptides in a system, the intensity could be lower if those peptides were not all sharing the same orientation.

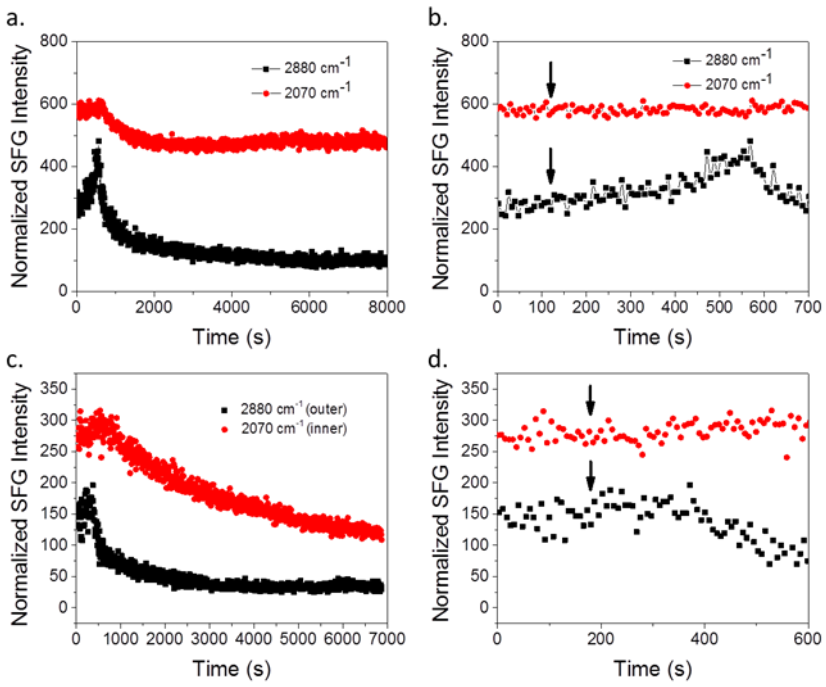

Figure 3.14: SFG time-dependent signal detected from (a) dDPPG-POPG bilayer, (b) dDPPG-POPG bilayer in the first 700 seconds, (c) dDPPG-*E. coli* polar extract bilayer; (c) d-DPPG-*E.coli* polar extract bilayer zoomed in the first 600 seconds, before and after the injection of melittin to the subphase to reach 0.78 µM. Peptide injection is indicated by arrow.

Figure 3.16 shows the CD and CH spectra detected from the dDPPG-POPG bilayer and the dDPPG-E. coli polar lipid extract bilayer before and after the addition of melittin to the subphase to reach 2 µM. Similar to the results obtained for the 0.78 µM melittin case, the 2880 cm^{-1} and 2070 cm^{-1} signal intensities decreased for both the lipid bilayer systems. The POPG leaflet signal decreased slightly more at the 2.0 µM case compared to the 0.78 µM case, but the difference is not large. The peak for the *E. coli* system is approximately the same at both concentrations. Overall, the disruptions for the two bilayer systems are not significantly different at this higher concentration. Figure 3.17 shows the amide I signal from melittin interacting with

the two lipid bilayer systems after the addition of 2 µM melittin. Again we see lower 1655 cm^{-1} signal for the peptide on *E. coli* extract compared to POPG.

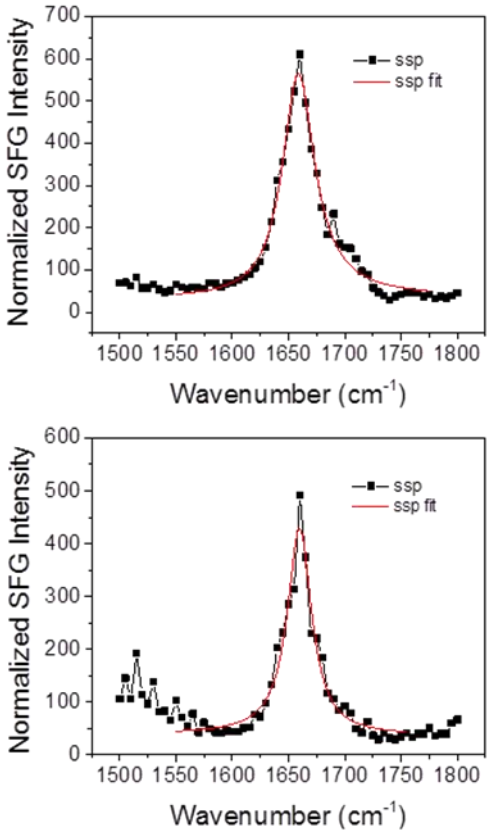

Figure 3.15: SFG signal of Amide I signal from the melittin associated with (top) dDPPG-POPG bilayer and (bottom) dDPPG-*E. coli* polar extract bilayer. The melittin subphase concentration is 0.78 µM.

Melittin has been shown to associate and adsorb more strongly to negatively charged bilayers vs. less charged or zwitterionic ones [57-61]. This is not unexpected. However, because of this strong association, melittin has generally been generally found to not insert into negatively charged bilayers [25, 61]. The most commonly proposed mode of action is a carpet/detergent-like interaction [25, 62]. Therefore, it makes sense that melittin associated with negatively charged lipids has a generally weaker SFG amide I signal (due to the lying down

orientation). However, it has been reported that melittin forms pores in PC membranes. While the pore theory is widely held, there is some discrepancy whether it is a barrel stave [25, 63], or the more popular toroidal pore which is correct [64-68]. In fact, one calcein leakage assay showed that adding PG lipids to PC LUVs inhibited melittin ability to lyse the vesicle [57]. Given this information, it is not necessarily surprising to see that at 0.78 µM melittin there is more disorder in the *E. coli* polar extract containing bilayer. It has less of a charge compared to the POPG containing bilayer and according to the above information, that charge difference likely allows the peptide to interact more with the hydrophobic bilayer core rather than being tightly associated with the PG headgroups.

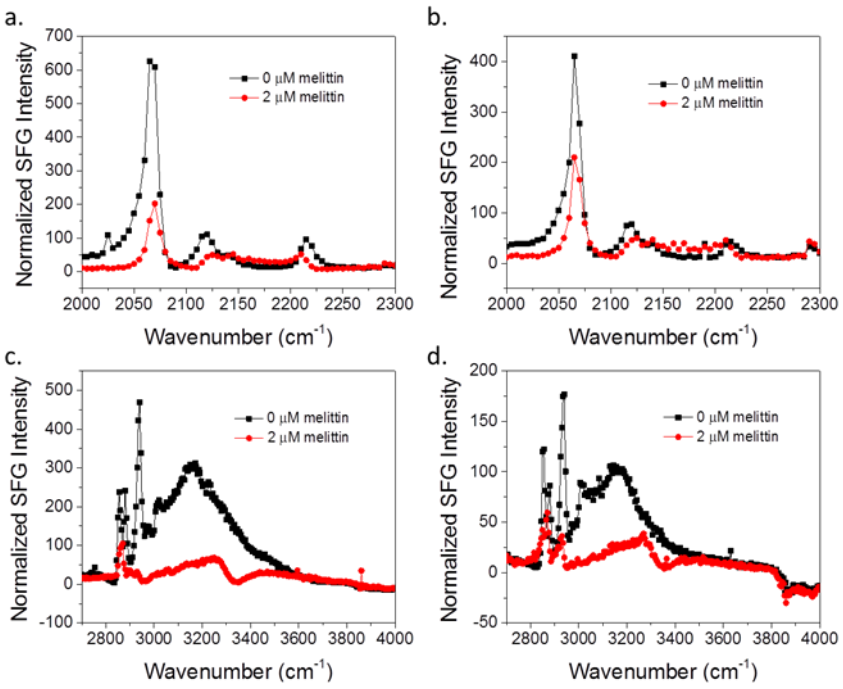

Figure 3.16: SFG spectra collected before (black) and after (red) the addition of melittin to the subphase of (a) dDPPG-POPG bilayer in the C-D stretching frequency range; (b) dDPPG-*E. coli* polar extract bilayer in the C-D stretching frequency range; (c) dDPPG-POPG in the C-H stretching frequency range; (d) dDPPG-*E. coli* polar extract bilayer in the C-H stretching frequency range. The melittin subphase concentration is 2.0 µM.

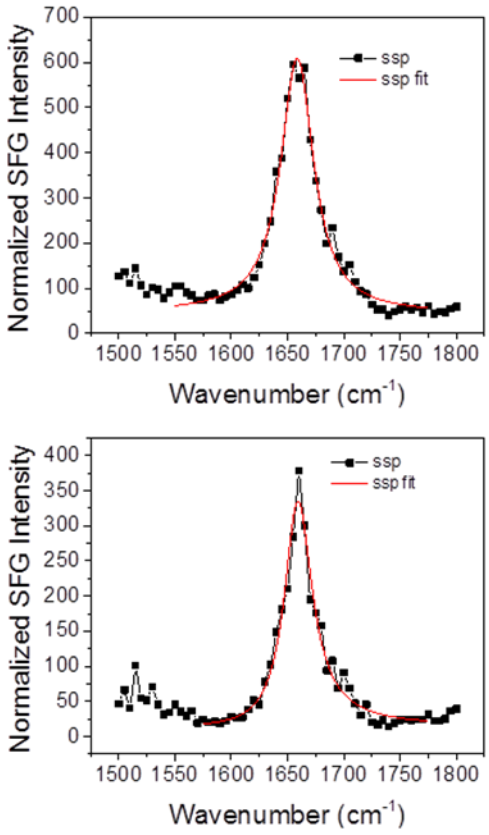

Figure 3.17: SFG signal of Amide I signal from the melittin associated with (top) dDPPG-POPG bilayer and (bottom) dDPPG-*E. coli* polar extract bilayer. The melittin subphase concentration is 2.0 µM.

However, this could not explain why the amide I 1655 cm^{-1} signal is slightly higher for the POPG containing bilayer vs. the *E. coli* extract containing one, assuming the same number of peptides are associated with each lipid bilayer. The peptides associating on a POPG leaflet are likely oriented approximately parallel to the bilayer and held near the headgroups instead of being allowed to penetrate into the bilayer. This orientation should lead to weaker SFG amide I signal. However, if the number of peptides associating on the POPG containing bilayer is actually higher than on the *E. coli* polar lipid containing bilayer there could be signal differences. If there are many more peptides on the POPG containing bilayer (due to the strong electrostatic

interactions), the amide I signal intensity could be higher because of the higher number of peptide molecules. In this case, the *E. coli* containing bilayer would have fewer peptides associated, but they would be inserted into the bilayer to some degree, which would explain why the inner leaflet is more disordered for the *E. coli* containing bilayer system. This has been investigated using wavelength dependence fluorescence polarization and circular dichroism [26, 59], dye leakage experiments [69], SPR biosensor experiments [62], and cryo-transmission electron microscopy [70]. Therefore, we believe the stronger signal for the POPG case is due to the fact that more melittin molecules are adsorbed to the dDPPG-POPG bilayer compared to the dDPPG-*E. coli* extract bilayer.

After increasing the concentration to 2 μM, the CH_3 and CD_3 peaks for the POPG containing bilayer further decreased and those for the *E. coli* extract containing bilayer remained the same as the lower concentration. Additionally, the 1655 cm^{-1} peak was approximately twice as big for the POPG bilayer as compared to the *E. coli* polar lipid containing bilayer. This difference in peak intensity could be due to the increased concentration of peptide providing more peptide to associate at the bilayer which only happens for POPG because of its high negative charge density. According to this theory, the *E. coli* extract containing bilayer is not attracting much more peptide, opposed to the POPG one. This interpretation fits the observation that it takes a higher concentration of peptide to disrupt highly negative bilayers vs. a less negatively charged bilayer that has been reported previously [69].

An interesting point about these interactions is that it has been found in several studies that the initial association and the disruption are two different processes [26, 61, 62, 64, 69, 71-73]. It is generally accepted that the initial association is governed by electrostatic interactions while the disruption step is governed by several processes and depends on multiple factors

including the hydrophobic effects, lipid phase, head group charge, head group size and peptide properties [74, 75]. Also, it seems as though there is a critical peptide association concentration, P/L*, at which the peptide can switch from its associated orientation to pore formation [63, 66, 67, 75]. These variables show that the interactions between peptides and model bilayers are not as easy and straightforward as simply considering the bilayer charge.

Several of the studies mentioned previously reported that the PG membranes were eventually solubilized or destroyed through a carpet or detergent-like mechanism [25, 61, 62]. The detergent-like mechanism usually involves peptide covering the bilayer like a carpet and then peptide-lipid structures, like micelles, being removed from the bilayer [25]. We are unable to determine by SFG if the drop in the 2070 cm^{-1} and 2880 cm^{-1} signals is due to the loss of lipids because the signal can also decrease due to the peptide flip-flop or disorder. However, a method such as ATR-FTIR, which is order independent, can give us this information. According to our ATR-FTIR spectrum of the CH region of dDPPG-*E. coli* extract, there is no drop in lipid signal after the addition of melittin. Therefore, we do not believe that there is a loss of lipid material at this concentration. Because of this observation, we do not think that a normal detergent-like mode takes place on *E. coli* extract. A more likely mechanism to explain the signal decrease is disorder or flip-flop due to a disturbance in bilayer structure in the form of defects or possibly pores induced by melittin, as was mentioned as a possibility in Ladokhin et al., 2001 [25].

In summary, the interactions between melittin and two types of the lipid bilayers at two peptide concentrations are different. POPG can serve as a model system for the bacterial cell membrane for certain criteria, such as peptide-bilayer association. However, the time dependent interaction spectra and the lipid spectra which relate the interaction dynamics were not

effectively modeled by pure POPG. It was demonstrated that melittin exhibits more disruption on the dDPPG-*E. coli* polar extract bilayer than the dDPPG-POPG bilayer at 0.78 μM melittin. This might be due to the fact that melittin is known to disrupt both bacterial and mammalian cell membranes. In contrast to the MSI-594, ovispirin-1, and magainin-2, which only disrupts the PG and not PC bilayers, melittin interacts strongly with both PG and PC bilayers. Melittin likely becomes "trapped" in the anionic POPG headgroups which inhibits the peptide's ability to disorder the inner bilayer leaflet. For *E. coli* lipid extract, there is less anionic charge on the bilayer surface so the peptide can engage in hydrophobic interactions with the acyl chain groups of the lipids which results in increased inner leaflet disorder. At a higher concentration, the interactions of the peptide with the two bilayer systems are similar – showing that higher peptide concentrations are needed to achieve the same amount of disorder in anionic bilayers compared to those with a lower net charge. Assuming we are only considering the surface charge interactions, this was well modeled with the POPG containing system. However, we again see that the simple system falls short in being able to model some significant peptide-lipid interactions.

3.3.5 LL-37

We then studied the interactions between another AMP, LL-37, with the two types of the lipid bilayers. Figure 3.18 shows the CD and CH stretching signals from the two lipid bilayer systems before and after the addition of LL-37 to the subphase of the dDPPG-POPG and dDPPG-*E. coli* polar extract model lipid bilayers to reach a concentration of 1.6 μM. In both cases, the decrease of the water signal ~3200 cm^{-1} indicates that the peptide interacts with the bilayer. In both cases, the C-D stretching signal does not change, showing that LL-37 does not disrupt the inner leaflet. It is difficult to see whether the C-H signal changed or not because the

O-H signal interferes with the C-H signal, and the O-H signal is very different before and after the addition of LL-37. This means that both the inner and outer leaflets for both systems are left undisrupted by the LL-37 even though the LL-37 molecules were associated with the both lipid bilayers.

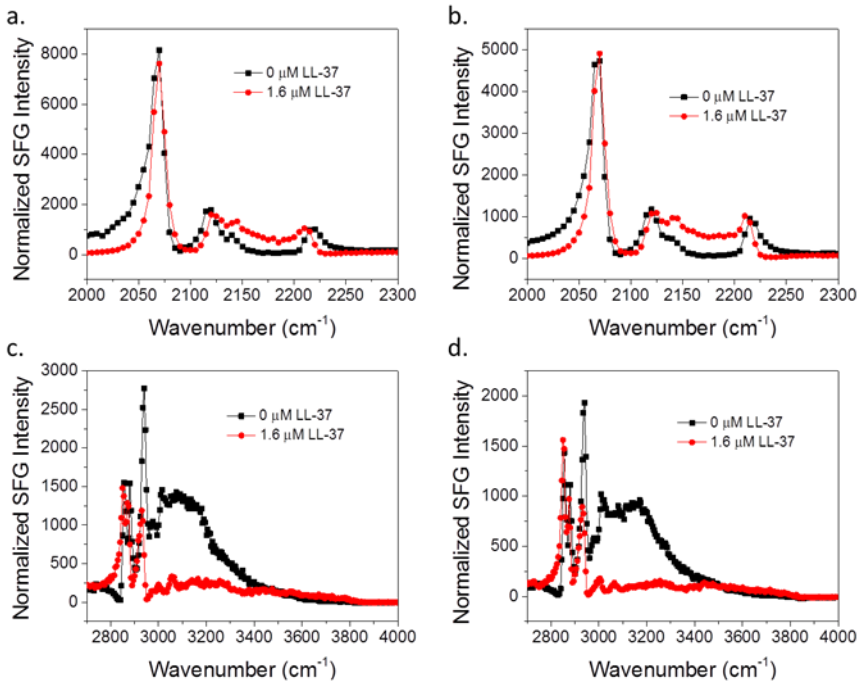

Figure 3.18: SFG spectra collected before (black) and after (red) the addition of LL-37 to the subphase of (a) dDPPG-POPG bilayer in the C-D stretching frequency range; (b) dDPPG-*E. coli* polar extract bilayer in the C-D stretching frequency range; (c) dDPPG-POPG in the C-H stretching frequency range; (d) dDPPG-*E. coli* polar extract bilayer in the C-H stretching frequency range. The LL-37 subphase concentration is 1.6 μM.

Figure 3.19 shows the time dependent CD and CH stretching SFG signals of the two bilayer systems after injection of the peptide to the subphase. There is no change in the CD signal, but a slight decrease in the C-H signal may be due to the water signal change. The C-H signal does not change after the slight, sharp decrease. This decrease happened faster for the

POPG system after the addition of LL-37 to the subphase, which is likely due to the fact that it has a higher charge density compared to the *E. coli* extract leaflet.

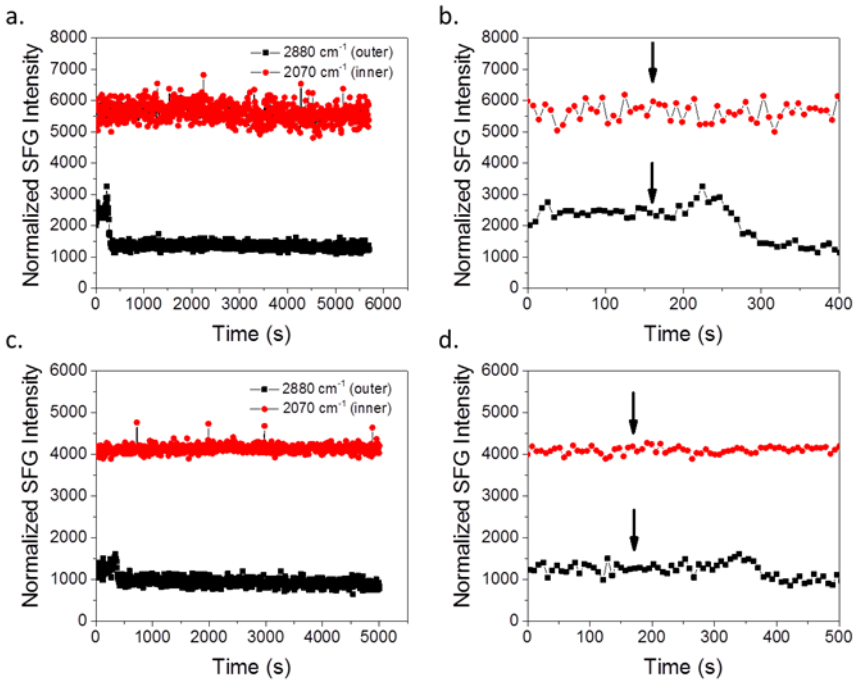

Figure 3.19: SFG time-dependent signal detected from (a) dDPPG-POPG bilayer, (b) dDPPG-POPG bilayer in the first 400 seconds, (c) dDPPG/-*E. coli* polar extract bilayer; (c) d-DPPG-*E.coli* polar extract bilayer zoomed in the first 500 seconds, before and after the injection of LL-37 to the subphase to reach 1.6 μM. Peptide injection is indicated by arrow.

Figure 3.20 shows the amide I signal detected from LL-37 associated with both lipid bilayer systems. The amide I spectral features look very similar, indicating the formation of α-helical conformation. The intensity of the 1655 cm^{-1} amide I peak is much stronger (~2000 vs. ~450) on the POPG system vs. the *E. coli* extract system. Again, this is not unexpected since the higher charge density on POPG could cause more positively charged peptides to adsorb to the bilayer surface.

The presented data suggests that at this concentration, the LL-37 has associated with the bilayer surface in a manner that reflects the outer leaflet charge. However, for some reason, it is unable to either insert into the bilayer or bury far enough into the outer leaflet to induce enough chain disorder to cause the drop in the CH_3 or CD_3 signals. The amide I data presented is only in ssp polarization, and thus cannot give us orientation information. Unidentified spectral features made the ppp peaks unable to be fitted so just the ssp, which can still give us information about the population, is presented. However, SFG signal is also dependent on order so that could also be a factor in the intensity difference. Given the drastic difference in surface charge and the fact that it has been established that LL-37 associates more readily with anionic lipids, we feel that the difference in intensity is highly likely related to the number of peptides at the surface [17-19, 76]. The concentration we used, 1.6 μM, is approximately 7 μg/ml which fits into the MIC for *E. coli* under most conditions [77]. Also, our group showed that LL-37 was laying down on POPG/POPG bilayers at the same concentration, but inserted into the bilayer at a lower concentration [17]. In this study, because no lipid bilayers were disrupted, we believe that for both lipid bilayers the associated LL-37 is generally oriented parallel to the bilayer.

It has been shown that just a difference in lipid head groups can change the way LL-37 interacts with membranes[19]. Sevcsik, et al. observed that adding LL-37 to DPPC/DPPG, DPPE/DPPG, and DPPS/DPPC resulted in different interactions even though the overall charge for each bilayer is the same and all have the same hydrophobic acyl chains. This is attributed to the fact that the head groups have different physical properties. For example, PC and PG are cylindrical in shape while the smaller head group of PE causes it to have an inverted cone shape, which can influence lipid packing [78]. The ability for PE to induce negative curvature and be more likely to produce non-bilayer phases such as hexagonal phases has been mentioned in other

literature as well [55, 75, 79]. Sevcsik, et al. reported that the packing density for PC/PG is lower than that for PE/PG and PC/PS which is likely due to the hydrogen bonding in the PE and PS head groups that is absent in PG. Additionally, they observed that for PC/PG the bilayers behave closer to pure PG and the PC/PS behave more like PC and mentioned that this could be because the hydrophobic effects are stronger than the electrostatic ones in that case.

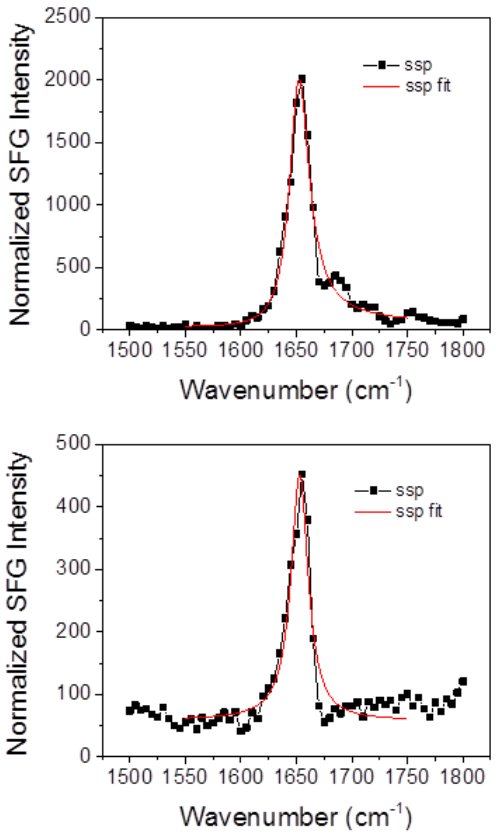

Figure 3.20: SFG signal of Amide I signal from the LL-37 associated with (top) dDPPG-POPG bilayer and (bottom) dDPPG-*E. coli* polar extract bilayer. The LL-37 subphase concentration is 1.6 µM.

In this work, our experiments showed that the interactions between LL-37 and dDPPG/POPG bilayers as well as a dDPPG-*E. coli* extract (PE, PG, CL) bilayers are similar. At the LL-37 concentration we investigated, both inner and outer leaflets were not disrupted. LL-37

molecules were associated with both lipid bilayers; however, there were more peptide molecules associated on the more negatively charged POPG containing bilayer. Although the previous discussion shows that different lipids interact with LL-37 in different ways, perhaps here the PG lipids in *E. coli* polar extract dominantly interact with LL-37.

It was briefly discussed in Chapter 2 how LL-37 interacts differently with bilayers of different compositions, including mixtures of PC and PG. From the previous discussion, it was seen that LL-37 does interact with POPG lipids and we did not see that in these experiments. Because of this lack of interaction, it is difficult to decide whether POPG or *E. coli* lipids would be a better model. The gel phase of the inner leaflet should not pose a problem, as it might have with other peptides, because LL-37 has interacted with gel phase lipids in literature [76]. It is possible that we observe LL-37 lying down on the POPG containing bilayer surface at the 1.6 μM concentration, similar to prior studies in our lab [17]. For the *E. coli* lipids, the effective negative charge is much lower compared to POPG lipids. A lower net negative bilayer charge resulted in peptide insertion in a mixed POPG:POPC bilayer in that study. However, it is possible that the inclusion of PE lipids in the *E. coli* extract induces negative curvature which opposed the positive curvature associated with toroidal pore formation. This effect was discussed earlier for magainin 2. As a result, we might be observing the LL-37 lying down on the E. coli extract containing bilayer due to the effect of PE lipid shape.

Considering these possibilities, it is apparent that POPG is not a good model for bacterial membranes since the suspected explanations for the observed signals are different; even if the resulting lipid signals are similar. Using more complex lipid mixtures, such as *E. coli* polar extract lipids, should be a more accurate representation of a cell membrane and yield more relevant results.

3.4 Conclusions

In this study we investigated the interactions between several membrane active peptides and bilayers consisting of dDPPG-POPG and dDPPG-*E. coli* polar lipid extract. Because *E. coli* lipids include ~60% PE as well as other components, there can be big differences in how a peptide might interact with a membrane of POPG or POPG/POPC vs. *E. coli* lipids [4, 46, 80]. Some of these concerns come from the fact that *E. coli* lipids contain PE, which has a small head group that is more rigid, more ordered, and is able to form a hydrogen bond, unlike the PC head group [78, 81-83]. Its size and packing geometry causes it to be cone shaped and it has a tendency to form non lamellar structures [78, 84]. As a result, some peptides can experience differences in potency when in an environment with PE lipids [19, 79, 85].

Our studies indicate that the interaction between various peptides and the two model bilayer, dDPPG-POPG and dDPPG-*E. coli* polar lipid extract, are different. However, the degree to which the interactions are different and what aspects are different depend on the peptide. MSI-594 can disrupt both types of the lipid bilayers, although not at the same rate, and the bilayer associated MSI-594 molecules have similar number and orientation. The peptide associates with the POPG containing bilayer much more quickly than with the *E. coli* lipid containing bilayer. This difference in interaction rate is important because one would want to ensure that a drug will be effective as quickly as possible and that time is influenced by the model system used.

Ovispirin-1 associates with both types of lipid bilayers. The number and orientation of the bilayer-associated ovispirin-1 molecules on the two bilayer systems are also similar. However, ovispirin-1 disrupted both leaflets of the dDPPG-POPG system while it barely disrupted the outer leaflet of the dDPPG-*E. coli* polar extract system. It too has a much slower

interaction time with the dDPPG-*E. coli* polar lipid system. Magainin 2 molecules also associated with both types of the lipid bilayers. At a low concentration of 800 nM, magainin 2 can disrupt the POPG leaflet, but cannot disrupt the *E. coli polar* extract leaflet. At 2.0 μM, magainin 2 can disrupt the outer leaflet for both POPG and *E. coli* polar lipid extract, but cannot disrupt the inner leaflet dDPPG for either bilayer. Melittin can disrupt both leaflets for both lipid bilayers but disrupted the dDPPG-*E. coli* extract bilayer slightly more. The difference in inner leaflet disruption suggests the possibility of a different orientation for the peptide on the two different systems. LL-37 did not disrupt either of the leaflets of the two types of the bilayers, even though more LL-37 associated with the dDPPG-POPG system over the dDPPG-*E. coli* polar extract system.

All of the peptides in this study favored interacting with anionic PG lipids over zwitterionic ones. However, the spectra and interpreted interactions for the peptides on the two systems were not always similar. In fact, even the type of spectra that were the same between the two systems differed depending on the peptide. For example, both MSI-594 and ovispirin-1 exhibited extremely fast interaction and disruption times on dDPPG-POPG but either interacted very slowly with or did not disrupt dDPPG-*E. coli* polar extract. The other peptides often interacted with POPG faster, but not to the same degree as those two peptides. Also, the inner leaflet was never disrupted for melittin, magainin 2 or LL-37 like it was for MSI-594 and ovispirin-1. Some potential reasons for this were discussed earlier, but one is that these peptides operate at least part of the time through toroidal pores while MSI-594 and ovispirin-1 operate through the carpet/detergent mode. The formation of toroidal pores does not destroy a bilayer, but it does induce disruption. The interaction time differences can possibly be described by a difference in peptide charge density. If one looks at the charge on all of the peptides, they do not

differ substantially (MSI-594 at +6, ovispirin-1 at +7, magainin 2 at +4, melittin at +5 and LL-37 at +6). However, if we consider the charge to the number of residues, a larger difference is seen. The charge/residue for MSI-594 is 0.25/residue, ovispirin 1 is 0.39/residue, magainin 2 is 0.17/residue, melittin is 0.19/residue and LL-37 is 0.16/residue. It can be seen that the two quick associating carpet/detergent peptides have relatively high charge/residue values. This is likely the cause of their quick association and it may also explain why they stay associated with the charged anionic headgroups rather than forming pores. Of the three remaining peptides, only magainin 2 seems to generally operate through a pore mechanism. Both melittin and LL-37 seem to depend on the charge of the environment to determine whether they insert or lay on the surface. Regardless, all of the peptides with any pore forming character have a lower charge/residue value. This lower charge density probably allows the peptide to more easily engage in hydrophobic interactions that are required for pore formation.

Through these studies, it has been seen that to more accurately examine peptide-bacterial cell membrane interactions, including the electrostatic interactions and disruption mechanism, more complicated model lipid bilayers such as bilayers prepared using *E. coli* lipid extract are needed. These studies utilized SFG to monitor the bilayer integrity, peptide association and time dependent interaction of the peptide with the bilayer. This time dependent monitoring is a unique feature of the SFG method that allows us to study the kinetics of the interaction and proved to be vital in the determination that pure POPG is not sufficient to model cell membranes. This ability is especially valuable because the time to interact with a cell is an important quality to consider when designing new antibiotic molecules. Thus, in addition to showing that the proper model system is required to collect accurate interaction information, we displayed a SFG method that is able to easily show the interaction kinetic differences. Hopefully,

this information can be utilized in order to properly design environments in which to test future antibacterial therapies.

3.5 References

1. Zasloff, M. *Nature* **2002**, *415*, 389-395.
2. Matsuzaki, K. *Biochimica Et Biophysica Acta-Biomembranes* **1999**, *1462*, 1-10.
3. Hancock, R.E.W.; Diamond, G. *Trends in Microbiology* **2000**, *8*, 402-410.
4. Lee, T.H.; Heng, C.; Swann, M.J.; Gehman, J.D.; Separovic, F.; Aguilar, M.I. *Biochimica Et Biophysica Acta-Biomembranes* **2010**, *1798*, 1977-1986.
5. Dennison, S.R.; Kim, Y.S.; Cha, H.J.; Phoenix, D.A. *European Biophysics Journal with Biophysics Letters* **2008**, *38*, 37-43.
6. Nguyen, K.T.; Le Clair, S.V.; Ye, S.J.; Chen, Z. *Journal of Physical Chemistry B* **2009**, *113*, 12169-12180.
7. Boughton, A.P.; Nguyen, K.; Andricioaei, I.; Chen, Z. *Langmuir* **2011**, *27*, 14343-14351.
8. Yang, P.; Ramamoorthy, A.; Chen, Z. *Langmuir* **2011**, *27*, 7760-7767.
9. Nguyen, K.T.; Le Clair, S.V.; Ye, S.J.; Chen, Z. *Journal of Physical Chemistry B* **2009**, *113*, 12358-12363.
10. Yang, P.; Wu, F.G.; Chen, Z. *J Phys Chem C Nanomater Interfaces* **2013**, *117*, 3358-3365.
11. Ding, B.; Chen, Z. *J Phys Chem B* **2012**, *116*, 2545-2552.
12. Chen, X.; Wang, J.; Kristalyn, C.B.; Chen, Z. *Biophys J* **2007**, *93*, 866-875.
13. Chen, X.Y.; Wang, J.; Boughton, A.P.; Kristalyn, C.B.; Chen, Z. *Journal of the American Chemical Society* **2007**, *129*, 1420-1427.
14. Ding, B.; Chen, Z. *Abstracts of Papers of the American Chemical Society* **2013**, *246*, 14625-14634.
15. Ramamoorthy, A.; Thennarasu, S.; Lee, D.K.; Tan, A.; Maloy, L. *Biophys J* **2006**, *91*, 206-216.
16. Wildman, K.A.H.; Lee, D.K.; Ramamoorthy, A. *Biochemistry* **2003**, *42*, 6545-6558.
17. Ding, B.; Soblosky, L.; Nguyen, K.; Geng, J.Q.; Yu, X.L.; Ramamoorthy, A.; Chen, Z. *Scientific Reports* **2013**. *3*, 1-8, DOI: 10.1038/srep01854.
18. Zhang, X.; Oglecka, K.; Sandgren, S.; Belting, M.; Esbjorner, E.K.; Norden, B.; Graslund, A. *Biochim Biophys Acta* **2010**, *1798*, 2201-2208.
19. Sevcsik, E.; Pabst, G.; Richter, W.; Danner, S.; Amenitsch, H.; Lohner, K. *Biophys J* **2008**, *94*, 4688-4699.
20. Woys, A.M.; Lin, Y.S.; Reddy, A.S.; Xiong, W.; de Pablo, J.J.; Skinner, J.L.; Zanni, M.T. *Journal of the American Chemical Society* **2010**, *132*, 2832-2838.
21. Yamaguchi, S.; Huster, D.; Waring, A.; Lehrer, R.I.; Kearney, W.; Tack, B.F.; Hong, M. *Biophysical Journal* **2001**, *81*, 2203-2214.
22. Zasloff, M.; Martin, B.; Chen, H.C. *Proceedings of the National Academy of Sciences of the United States of America* **1988**, *85*, 910-913.
23. Matsuzaki, K. *Biochimica Et Biophysica Acta-Reviews on Biomembranes* **1998**, *1376*, 391-400.
24. Wieprecht, T.; Beyermann, M.; Seelig, J. *Biochemistry* **1999**, *38*, 10377-10387.

25. Ladokhin, A.S.; White, S.H. *Biochimica Et Biophysica Acta-Biomembranes* **2001**, *1514*, 253-260.
26. Ghosh, A.K.; Rukmini, R.; Chattopadhyay, A. *Biochemistry* **1997**, *36*, 14291-14305.
27. Chen, Z.; Shen, Y.R.; Somorjai, G.A. *Annual Review of Physical Chemistry* **2002**, *53*, 437-465.
28. Shen, Y.R. *Nature* **1989**, *337*, 519-525.
29. Zhuang, X.; Miranda, P.B.; Kim, D.; Shen, Y.R. *Physical Review B* **1999**, *59*, 12632-12640.
30. Eisenthal, K.B. *Chemical Reviews* **1996**, *96*, 1343-1360.
31. Voges, A.B.; Al-Abadleh, H.A.; Musorrariti, M.J.; Bertin, P.A.; Nguyen, S.T.; Geiger, F.M. *Journal of Physical Chemistry B* **2004**, *108*, 18675-18682.
32. Moad, A.J.; Simpson, G.J. *Journal of Physical Chemistry B* **2004**, *108*, 3548-3562.
33. Paszti, Z.; Guczi, L. *Vibrational Spectroscopy* **2009**, *50*, 48-56.
34. Giacometti, A.; Cirioni, O.; Kamysz, W.; D'Amato, G.; Silvestri, C.; Licci, A.; Nadolski, P.; Riva, A.; Lukasiak, J.; Scalise, G. *Int J Antimicrob Agents* **2005**, *26*, 235-240.
35. Epand, R.F.; Maloy, W.L.; Ramamoorthy, A.; Epand, R.M. *Biochemistry* **2010**, *49*, 4076-4084.
36. Buer, B.C.; Chugh, J.; Al-Hashimi, H.M.; Marsh, E.N. *Biochemistry* **2010**, *49*, 5760-5765.
37. Porcelli, F.; Buck-Koehntop, B.A.; Thennarasu, S.; Ramamoorthy, A.; Veglia, G. *Biochemistry* **2006**, *45*, 5793-5799.
38. Bhattacharjya, S.; Ramamoorthy, A. *Febs Journal* **2009**, *276*, 6465-6473.
39. Bhunia, A.; Ramamoorthy, A.; Bhattacharjya, S. *Chemistry* **2009**, *15*, 2036-2040.
40. Sawai, M.V.; Waring, A.J.; Kearney, W.R.; McCray, P.B.; Forsyth, W.R.; Lehrer, R.I.; Tack, B.F. *Protein Engineering* **2002**, *15*, 225-232.
41. Kalfa, V.C.; Jia, H.P.; Kunkle, R.A.; McCray, P.B.; Tack, B.F.; Brogden, K.A. *Antimicrobial Agents and Chemotherapy* **2001**, *45*, 3256-3261.
42. Khandelia, H.; Kaznessis, Y.N. *Journal of Physical Chemistry B* **2005**, *109*, 12990-12996.
43. Khandelia, H.; Kaznessis, Y.N. *Peptides* **2005**, *26*, 2037-2049.
44. Khandelia, H.; Kaznessis, Y.N. *Peptides* **2006**, *27*, 1192-1200.
45. Huang, H.W. *Biochemistry* **2000**, *39*, 8347-8352.
46. Dennison, S.R.; Morton, L.H.; Harris, F.; Phoenix, D.A. *Chem Phys Lipids* **2008**, *151*, 92-102.
47. Matsuzaki, K.; Murase, O.; Tokuda, H.; Funakoshi, S.; Fujii, N.; Miyajima, K. *Biochemistry* **1994**, *33*, 3342-3349.
48. Imura, Y.; Nishida, M.; Matsuzaki, K. *Biochimica Et Biophysica Acta-Biomembranes* **2007**, *1768*, 2578-2585.
49. Ludtke, S.J.; He, K.; Heller, W.T.; Harroun, T.A.; Yang, L.; Huang, H.W. *Biochemistry* **1996**, *35*, 13723-13728.
50. Matsuzaki, K.; Murase, O.; Fujii, N.; Miyajima, K. *Biochemistry* **1996**, *35*, 11361-11368.
51. Hirsh, D.J.; Hammer, J.; Maloy, W.L.; Blazyk, J.; Schaefer, J. *Biochemistry* **1996**, *35*, 12733-12741.
52. Matsuzaki, K.; Murase, O.; Miyajima, K. *Biochemistry* **1995**, *34*, 12553-12559.
53. Ye, S.J.; Nguyen, K.T.; Chen, Z. *Journal of Physical Chemistry B* **2010**, *114*, 3334-3340.

54. Matsuzaki, K.; Sugishita, K.; Ishibe, N.; Ueha, M.; Nakata, S.; Miyajima, K.; Epand, R.M. *Biochemistry* **1998**, *37*, 11856-11863.
55. Heller, W.T.; He, K.; Ludtke, S.J.; Harroun, T.A.; Huang, H.W. *Biophysical Journal* **1997**, *73*, 239-244.
56. Ludtke, S.; He, K.; Huang, H. *Biochemistry* **1995**, *34*, 16764-16769.
57. Benachir, T.; Lafleur, M. *Biochimica Et Biophysica Acta-Biomembranes* **1995**, *1235*, 452-460.
58. Beschiaschvili, G.; Seelig, J. *Biochemistry* **1990**, *29*, 52-58.
59. Dathe, M.; Meyer, J.; Beyermann, M.; Maul, B.; Hoischen, C.; Bienert, M. *Biochimica Et Biophysica Acta-Biomembranes* **2002**, *1558*, 171-186.
60. Kleinschmidt, J.H.; Mahaney, J.E.; Thomas, D.D.; Marsh, D. *Biophysical Journal* **1997**, *72*, 767-778.
61. Lad, M.D.; Birembaut, F.; Clifton, L.A.; Frazier, R.A.; Webster, J.R.P.; Green, R.J. *Biophysical Journal* **2007**, *92*, 3575-3586.
62. Papo, N.; Shai, Y. *Biochemistry* **2003**, *42*, 458-466.
63. Ladokhin, A.S.; Selsted, M.E.; White, S.H. *Biophysical Journal* **1997**, *72*, 1762-1766.
64. Allende, D.; Simon, S.A.; McIntosh, T.J. *Biophysical Journal* **2005**, *88*, 1828-1837.
65. Chen, F.Y.; Lee, M.T.; Huang, H.W. *Biophysical Journal* **2003**, *84*, 3751-3758.
66. Huang, H.W. *Biophysical Journal* **2009**, *96*, 3263-3272.
67. Lee, M.T.; Chen, F.Y.; Huang, H.W. *Biochemistry* **2004**, *43*, 3590-3599.
68. Lee, M.T.; Sun, T.L.; Hung, W.C.; Huang, H.W. *Proceedings of the National Academy of Sciences of the United States of America* **2013**, *110*, 14243-14248.
69. Ohki, S.; Marcus, E.; Sukumaran, D.K.; Arnold, K. *Biochimica Et Biophysica Acta-Biomembranes* **1994**, *1194*, 223-232.
70. Wessman, P.; Morin, M.; Reijmar, K.; Edwards, K. *J Colloid Interface Sci* **2010**, *346*, 127-135.
71. Stromstedt, A.A.; Wessman, P.; Ringstad, L.; Edwards, K.; Malmsten, M. *Journal of Colloid and Interface Science* **2007**, *311*, 59-69.
72. Yang, L.; Harroun, T.A.; Weiss, T.M.; Ding, L.; Huang, H.W. *Biophysical Journal* **2001**, *81*, 1475-1485.
73. Constantinescu, I.; Lafleur, M. *Biochimica Et Biophysica Acta-Biomembranes* **2004**, *1667*, 26-37.
74. Batenburg, A.M.; Vanesch, J.H.; Dekruijff, B. *Biochemistry* **1988**, *27*, 2324-2331.
75. Lee, M.T.; Hung, W.C.; Chen, F.Y.; Huang, H.W. *Biophysical Journal* **2005**, *89*, 4006-4016.
76. Neville, F.; Cahuzac, M.; Konovalov, O.; Ishitsuka, Y.; Lee, K.Y.C.; Kuzmenko, I.; Kale, G.M.; Gidalevitz, D. *Biophysical Journal* **2006**, *90*, 1275-1287.
77. Turner, J.; Cho, Y.; Dinh, N.N.; Waring, A.J.; Lehrer, R.I. *Antimicrobial Agents and Chemotherapy* **1998**, *42*, 2206-2214.
78. McIntosh, T.J.; Simon, S.A. *Biochemistry* **1986**, *25*, 4948-4952.
79. Zweytick, D.; Turner, S.; Blondelle, S.E.; Lohner, K. *Biochemical and Biophysical Research Communications* **2008**, *369*, 395-400.
80. Hristova, K.; Selsted, M.E.; White, S.H. *Journal of Biological Chemistry* **1997**, *272*, 24224-24233.
81. Thurmond, R.L.; Dodd, S.W.; Brown, M.F. *Biophysical Journal* **1991**, *59*, 108-113.
82. McIntosh, T.J. *Biophysical Journal* **1980**, *29*, 237-245.

83. Hauser, H.; Pascher, I.; Pearson, R.H.; Sundell, S. *Biochimica Et Biophysica Acta* **1981**, *650*, 21-51.
84. Seddon, J.M.; Templer, R.H., *Polymorphism of lipid-water systems*. Handbook of biological physics, vol. 1; structure and dynamics of membranes: From cells to vesicles, ed. R. LipowskyE. Sackmann. 1995: Elsevier Science Publishers B.V., PO Box 211, Sara Burgerhartstraat 25, 1000 AE Amsterdam, Netherlands P.O. Box 882, Madison Square Station, New York, New York 10159-2101, USA.
85. Prenner, E.J.; Lewis, R.; Neuman, K.C.; Gruner, S.M.; Kondejewski, L.H.; Hodges, R.S.; McElhaney, R.N. *Biochemistry* **1997**, *36*, 7906-7916.

CHAPTER 4

ANTIMICROBIAL PEPTIDE-OUTER CELL MEMBRANE STUDIES

4.1 Introduction

Bacteria come in two classes, gram negative and gram positive. Gram positive bacteria have a plasma cell membrane and a cell wall consisting of a thick peptidoglycan layer which is composed of a repeating disaccharide, *N*-acetylmuramic acid-(β1-4)-*N*-acetylglucosamine, and other accessory proteins [1]. Gram negative bacteria, however, have a much thinner peptidoglycan layer and an outer membrane in addition to its plasma membrane [2]. The outer membrane is asymmetric with the inner leaflet containing phospholipids and resembling the plasma membrane and the outer leaflet is composed of mainly lipopolysaccharide (LPS), also known as endotoxin, but also proteins such as porins and lipoproteins [3]. LPS has been shown to induce immune responses such as sepsis and septic shock [4-6]. As a result, there has been a great deal of research into investigating peptides and other molecules that may be used to neutralize LPS [7-12].

LPS, which can be smooth or rough, has three main parts: lipid A, the core oligosaccharide (inner and outer core), and the variable O-antigen chain [13]. Lipid A is the hydrophobic anchor and is covalently linked to the core oligosaccharide. Lipid A is also the most

conserved portion of LPS in many bacteria and is composed of five or six fatty acids linked to diglucosamine phosphate [14-17]. The most general lipid A structure is bisphosphorylated β-(1-6)-linked glucosamine disaccharide substituted with fatty acids ester-linked at positions 3 and 3' and amide-linked at positions 2 and 2' [18]. There are other variations, though [18, 19]. Covalently attached to 6' of lipid A is the inner core of the core oligosaccharide which contains 3-deoxy-D-manno-oct-2-ulosonic acid (Kdo) and heptose [20]. The inner core and lipid A contain anionic groups, such as Kdo and phosphates [21]. The outer core is attached to Hep from the inner core and is an oligosaccharide that commonly contains Gal, Glc, or similar derivatives [18, 22]. The O-antigen chain is a variable chain of oligosaccharides that depends on the serotype of the bacteria [14, 18, 21, 22]. It is only found in smooth type LPS and is thought to contribute to bacterial resistance [23-25]. Rough mutant type LPS contain just lipid A and the core oligosaccharide regions. Additionally, the rough mutant type LPS can be categorized Ra, Rc, or Re depending on exactly where it terminates in the core region [26].

There have been a wide range of topics involving LPS that have been studied. LPS membrane dynamics have been studied by many groups [26-30]. The interactions between several membrane active peptides and LPS have been studied. For example, the anti-endotoxin abilities of LL-37 and BMAP-27 have been investigated [12, 31-33]. The insertion of LL-37, SMAP-29, and D2A22 into lipid A monolayers has been studied using surface X-ray scattering [34]. Melittin was shown to have a decreased effectiveness against LPS, similar to adding cholesterol to phospholipids [35]. It was also shown by NMR to be helical at the C terminus, while the N terminus is in an extended conformation [36]. Through NMR, MSI-594 was found to uniquely bind LPS micelles in a helical hairpin conformation [37, 38]. Protegrin-1 was shown to interact with lipid A, DPPC, and DPPG monolayers using grazing incidence X-ray diffraction

and X-ray reflectivity [39]. The structure of the LALF protein in LPS was determined by NMR [40]. A study involving magainin 2 interacting with LPS and LPS mutants determined that bacteriocidal activity was dependent on the O-polysaccharide length, while hydrophobic chain disruption was dependent on the LPS negative charge [41].

LPS's contribution to antimicrobial resistance is thought to come from several factors. The core region is thought to be responsible for hydrophilic molecule resistance [42]. Additionally, the membrane can also prevent small hydrophobic molecules from entering [3, 43]. Divalent cations, like Ca^{2+} and Mg^{2+} have been shown to bridge the negatively charged groups in neighboring LPS molecules, allowing for a more ordered lipid structure and increased resistance to permeability [43-49]. One X-ray reflectivity study determined that the presence of Ca^{2+} ions causes the O-polysaccharide chains to collapse onto the core oligosaccharide region and speculated that this is part of the AMP resistance mechanism [50].

As we discussed in the previous chapters, sum frequency generation vibrational spectroscopy (SFG) is a surface sensitive spectroscopy that has been successfully used to study several different surface active peptides and proteins including tachyplesin I [51], alamethicin [52, 53], MSI-78 [54], magainin 2 [55], LL-37 [56], Pep-1 [57], and melittin [58]. In particular, our lab has previously shown that SFG combined with isotope labeling an α-helical peptide, ovispirin-1, can reveal information about the membrane orientation of the peptide and the local environment the labeled residue is in [59]. Ovispirin-1 is a cytotoxic and hemolytic α-helical peptide that is generally found to act through the carpet mechanism regardless of the lipid bilayer environment [59-62].

In this study we investigated the interaction between different ovispririn-1 isotope labeled peptides and supported lipid bilayers with outer leaflets of phospholipids, Kdo2 lipid A and lipid A from *Salmonella minnesota* R595 using SFG. We want to understand the molecular interactions between ovispirin-1 and the outer membrane.

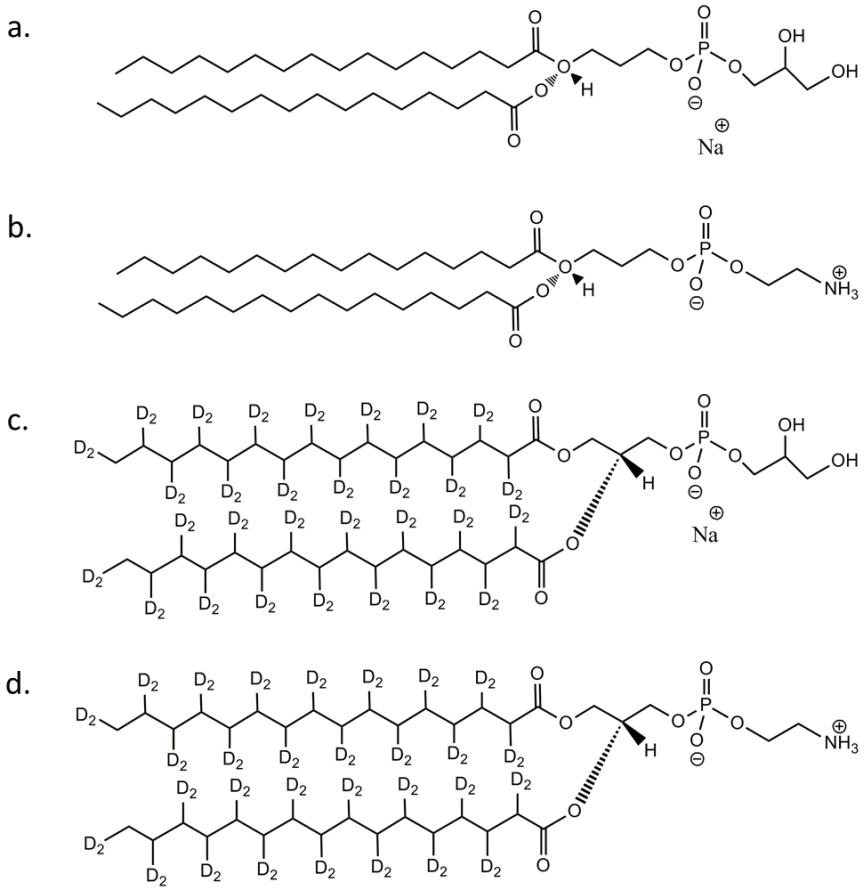

Figure 4.1: Phospholipids used in this study: (a) DPPG (b) DPPE (c) dDPPG (d) dDPPE

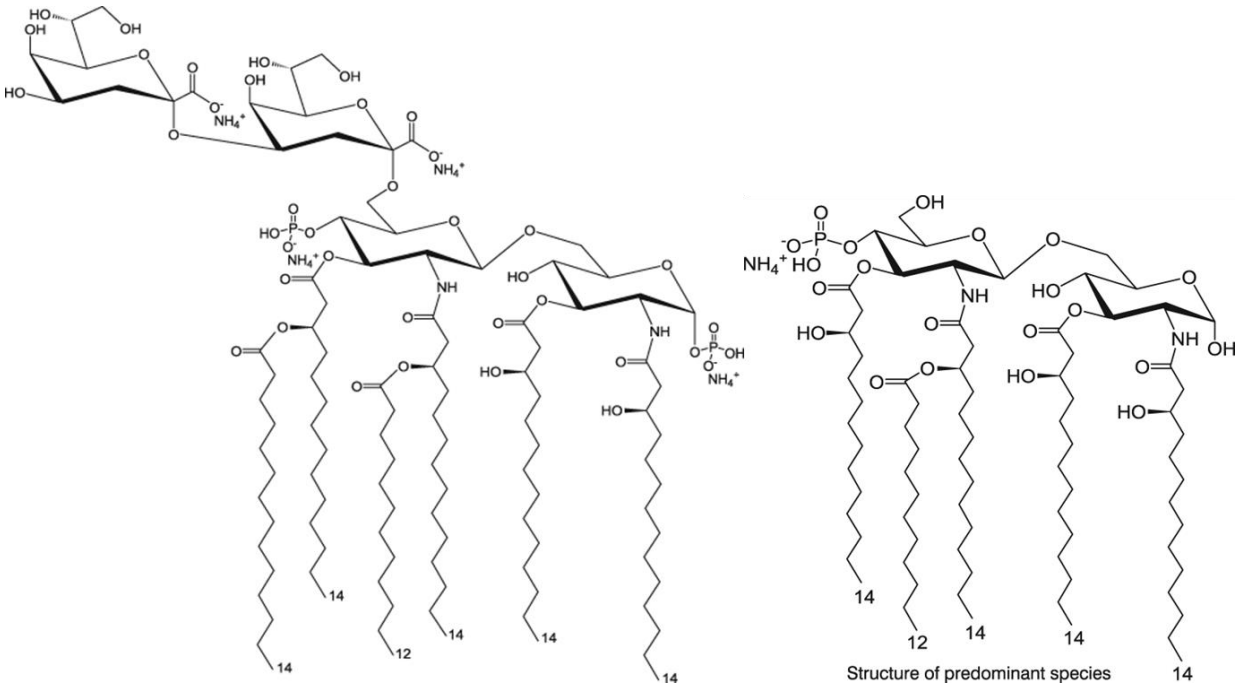

Figure 4.2: Outer cell membrane lipids used in this study: (a) Kdo2-Lipid A (b) Lipid A from *Salmonella minnesota* R595 [63, 64]

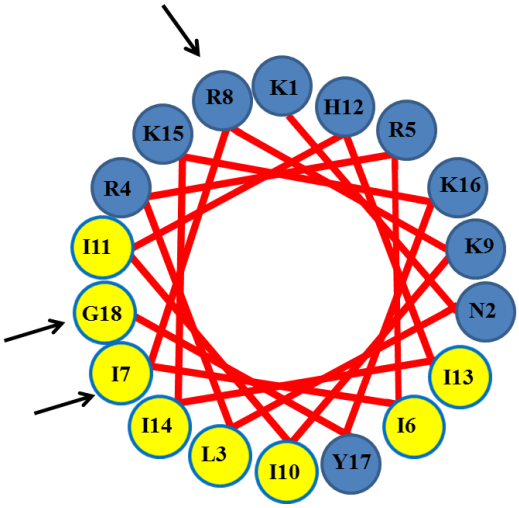

Figure 4.3: Helical wheel diagram of ovispirin-1. Hydrophilic residues are blue, hydrophobic residues are yellow. I7 is in the hydrophobic region, G8 is in the hydrophilic region. [61]

4.2 Experimental

4.2.1 Materials

Isotope labeled ovispirin-1 samples (unlabeled sequence H_2N-KNLRRIIRKIIHIIK KYGCOOH) were synthesized by Peptide 2.0, Inc. (Chantilly, VA). The ^{12}C=O of I7 was isotope labeled to ^{13}C=O. R8 and H12 were mutated into ^{13}C=O isotope labeled G8 and G18. 1,2-dipalmitoyl-*sn*-glycero-3-phosphoethanolamine (DPPE), 1,2-dipalmitoyl-d62-*sn*-glycero-3-phosphoethanolamine (dDPPE), 1,2-dipalmitoyl-*sn*-glycero-3-phospho-(1'-*rac*-glycerol) (DPPG), 1,2-dipalmitoyl-d62-*sn*-glycero-3-[phospho-*rac*-(1-glycerol)] (dDPPG), Di[3-deoxy-D-manno-octulosonyl]-lipid A (Kdo2-Lipid A), and Lipid A Detoxified (*Salmonella minnesota R595)* were purchased from Avanti Polar Lipids, Inc. (Alabaster, AL).

4.2.2 Lipid Bilayers

Surface supported lipid bilayers were deposited on right angle CaF_2 prisms via the Langmuir-Blodgett and Langmuir-Schaefer (LB/LS) methods for the proximal and distal leaflets, respectively. The bilayer is formed and submerged at the water-prism interface in a 1.6 mL reservoir. Appropriate volumes of 0.5 mg/ml ovispirin-1 were injected into the reservoir to reach the desired concentration. A magnetic micro stirring bar at 100 rpm was used to ensure that the concentration was homogeneous throughout the subphase. All water used for sample preparation and during the experiment was filtered through a Millipore system (EMD Millipore Corporation, Billerica, MA).

4.2.3 SFG

Details on SFG theory, our instrument set up, and data analysis have been published previously and will not be repeated here. SFG was generally explained in Chapter 1 [65-72]. During the experiment, a 532 nm visible beam and a frequency tunable IR beam (1300-4300 cm^{-1}) are overlapped spatially and temporally on the bottom of the right angle CaF_2 prism which is supporting the lipid bilayer. The experiments were carried out at room temperature (~ 20 °C). At this temperature, the lipids used are in the gel phase.

SFG spectra were taken in the 2000-2300 cm^{-1} range to assess the deuterated inner leaflet and in the 2700-4000 cm^{-1} range to assess the hydrogenated outer leaflet before and after peptide addition to the lipid bilayer subphase. SFG spectra were collected in the amide I frequency range (1500-1800 cm^{-1}) in the ppp (SFG, visible, IR) and ssp polarizations to help assess the peptide interaction with the bilayer. The optical set up was purged with nitrogen during amide I signal collection to reduce the dips in the spectrum resulting from a loss in IR intensity due to water vapor absorbing IR along the optical pathway.

4.3 Results and Discussion

4.3.1 dDPPG-DPPG and dDPPG-Kdo2 lipid A

SFG spectra were collected from the supported bilayer of dDPPG-Kdo2 Lipid A, intended to mimic the outer membrane of the bacterial cell and compared to those detected at a dDPPG-DPPG bilayer, which is commonly used as a model for bacterial cell membrane/inner membrane. To our knowledge, nobody has made supported bilayers with an outer lipid A leaflet so it was important to ensure that the bilayer would be structurally sound. Figure 4.4 shows that SFG spectra detected in both CD and CH stretching frequency regions are similar for dDPPG-

DPPG and dDPPG- lipid A bilayers, showing that both leaflets in the two bilayers are similar. Since it is well known that dDPPG-DPPG is a well ordered lipid bilayer, we therefore believe that the dDPPG-lipid A bilayer was well prepared and of good quality.

It has been shown previously that ovispirin-1 and the isotope labeled mutants do interact with DPPG bilayers [Ding, B.; Wang, Z.; Ho, J.; Laaser, J.E.; Zanni, M.T.; Chen, Z. Unique Site-specific Structural Information of a Biomolecule at Model Membrane Interface by Incorporating Isotope-labeled Sum Frequency Generation Probes, to be published]. Ovispirin-1 G18 is isotope labeled in a disordered area of the peptide and was used in that study. SFG spectra were collected from the two bilayers after addition of ovispirin-1 G18 to the bilayer subphase to reach a concentration of 50 μg/ml. Both C-H region spectra collected after the peptide addition have a negative peak at 3300 cm^{-1} which is more intense in the Kdo2 Lipid A case than for DPPG (Figure 4.5). This 3300 cm^{-1} peak is from the N-H stretching mode and its presence and intensity are likely an indicator of the relative amount of peptide associated to the bilayer. The higher intensity peak shows that there could be more peptide associating at the dDPPG-Kdo2 lipid bilayer compared to the dDPPG-DPPG bilayer, which is not what we initially expected. The broad peak at approximately 3200 cm^{-1} is attributed to water and its decrease is indicative that the peptide has displaced water at the bilayer surface. The peak at 2880 cm^{-1} (CH_3 symmetric stretch) is similar before and after peptide addition, and shows that the peptide did not destroy the bilayer. Therefore for both lipid bilayers, ovispirin-1 molecules are associated with the bilayers, but do not disrupt the bilayer.

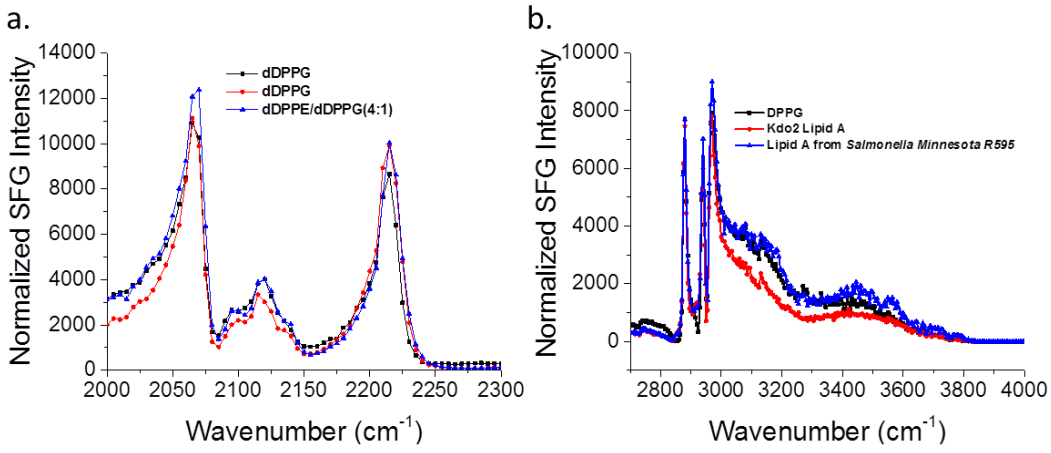

Figure 4.4: SFG spectra collected from the lipid bilayers before the addition of peptide to the subphase: (a) CD range spectra for inner leaflet of dDPPG-DPPG, dDPPG-Kdo2 lipid A, and dDPPE:dDPPG (4:1)-Lipid A from *Salmonella minnesota R595* (b) CH range spectra for the outer leaflet of dDPPG-DPPG, dDPPG-Kdo2 lipid A, and dDPPE:dDPPG (4:1)- Lipid A from *Salmonella minnesota* R595.

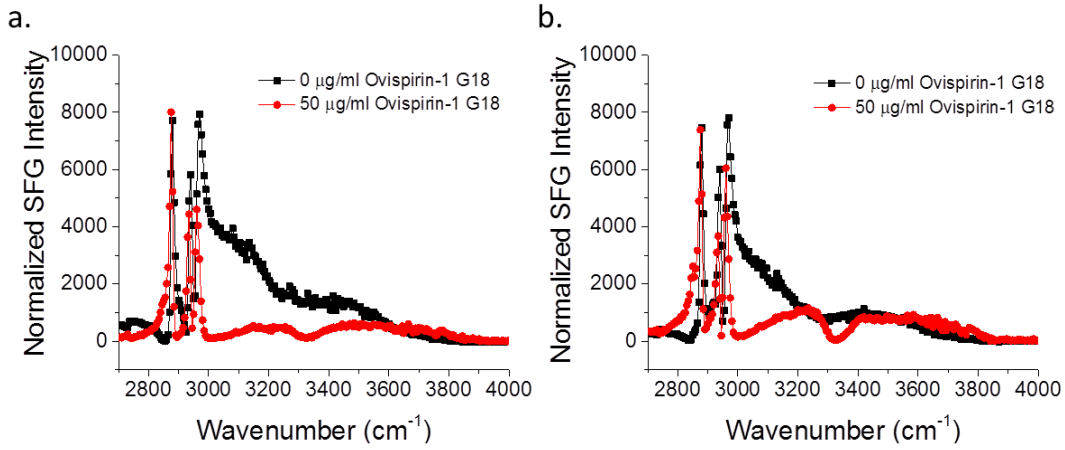

Figure 4.5: SFG C-H and O-H stretching signals detected before (black) and after (red) the addition of ovispirin-1 to the subphase of the (a) dDPPG-DPPG bilayer (b) dDPPG-Kdo2 Lipid A bilayer.

SFG spectra in the amide I range were also collected to study the peptide structure while interacting with the two bilayer systems. SFG signals centered between 1650 and 1660 cm^{-1} were detected, confirming that ovispirin-1 peptides were associated with both bilayers and have α-helical structure. In Figure 4.6, we can see that the amide I peak is considerably higher on the bilayer with a Kdo2 outer leaflet compared to the DPPG one. Figure 4.6 shows that the ppp/ssp

signal ratio for ovispirin-1 associated with the two lipid bilayers are similar, showing that the associated ovispirin-1 peptide molecules adopt a similar orientation on two bilayers. Therefore, the higher intensity suggests that there are more peptides on the surface of the Kdo2 containing bilayer. Results from the C-H, O-H and amide I regions, when considered together, confirm that the ovispririn-1 interacts with the model outer membrane, Kdo2 Lipid A, and that there is more interaction with that bilayer opposed to the dDPPG-DPPG bilayer. Because this is not what we expected, we decided to do further experiments with isotope labeled ovispirin-1 to gain more orientation information to possibly explain this behavior.

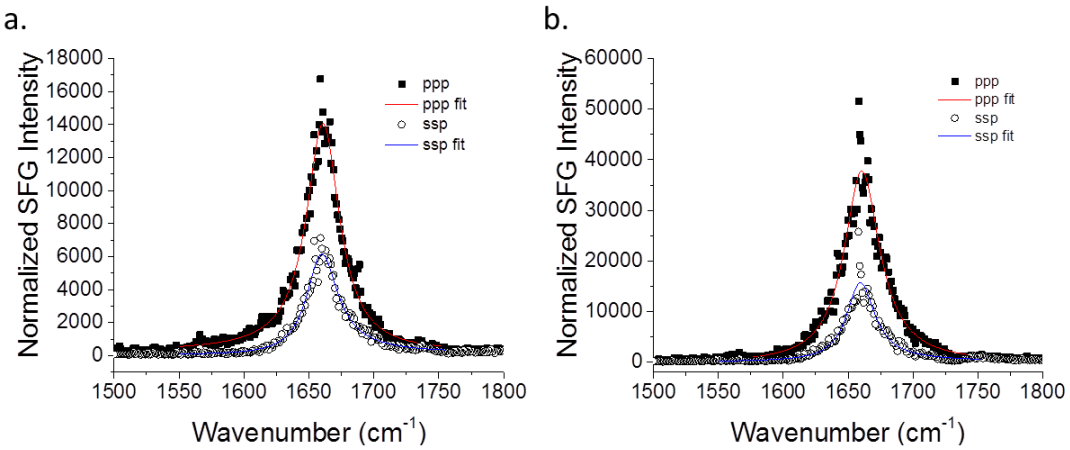

Figure 4.6: SFG spectra collected in the amide I region from ovispirin-1 associated with (a) dDPPG-DPPG bilayer (b) dDPPG-Kdo2 Lipid A bilayer

4.3.2 dDPPE:dDPPG (3:2)-Lipid A from *Salmonella minnesota* R595

We also used lipid A from *Salmonella minnesota* R595 as a model for outer lipid membranes. This lipid A is a somewhat different from the previously used Kdo2 lipid A in that it does not have the Kdo groups, only has five hydrocarbon tails, and only has one negative charge (vs. the four on Kdo2 lipid A). Because the charge density per acyl chain is much smaller than for the previous system, we used a mix of DPPE and DPPG to achieve a charge of -0.2/chain so

as to match that of lipid A from *Salmonella minnesota* and thus avoid interaction differences due to lipid charge effects. Therefore, we compared the interactions between ovispirin-1 G18 and dDPPE:dDPPG (3:2)-DPPE:DPPG(3:2) bilayers as well as dDPPE:dDPPG (3:2)-Lipid A (from *Salmonella minnesota* R595) bilayers. These two bilayers have the same overall charge.

SFG spectra were collected from both the lipid bilayer systems before and after the addition of 50 µg/ml ovispirin-1 G18 to the subphase. It can be seen in Figure 4.7 that the SFG C-H stretching signals are similar before and after the addition of ovispirin-1 G18 for both the mixed DPPE:DPPG and lipid A from Salmonella outer leaflet systems. This indicates that the bilayer, in both cases, is not being disrupted. However, the large water signals in the 3100-3200 cm^{-1} and 3400 cm^{-1} ranges do decrease after peptide addition, indicating that there is peptide association. Unlike the previous case, we do not see a peak at 3300 cm^{-1} (N-H stretch).

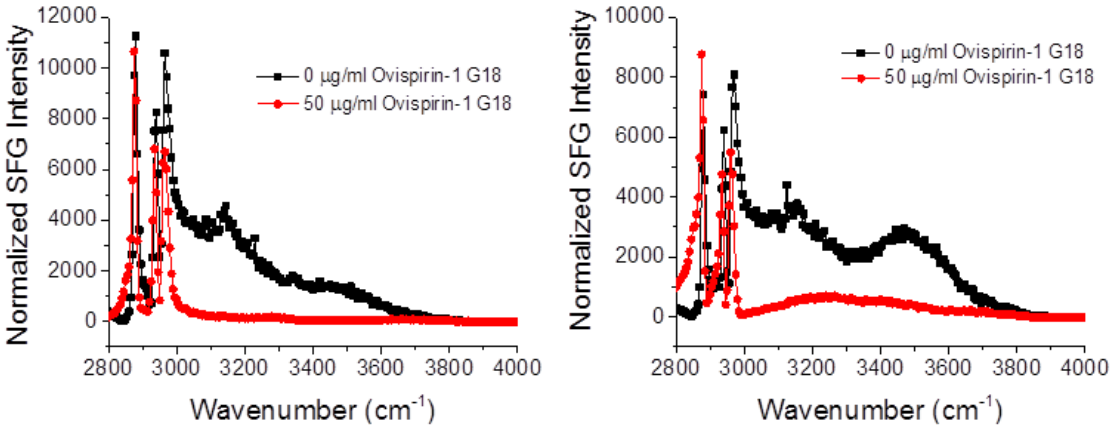

Figure 4.7: SFG spectra collected in the C-H and O-H stretching frequency region before (black) and after (ref) addition of ovispirin-1 G18 to the subphase (50 µg/ml) from the dDPPE:dDPPG (3:2)-DPPE:DPPG(3:2) bilayer (left) and the dDPPE:dDPPG (3:2)-Lipid A from *Salmonella minnesota* R595 bilayer (right).

SFG spectra were also detected from ovispirin-1 associated with the two lipid bilayer systems (Figure 4.8). It can be seen that the signals are centered between 1500 and 1660 cm^{-1},

indicating the formation of α-helical structure. The SFG amide I peak intensities and ppp/ssp intensity ratios for ovispirin-1 associated with two lipid systems are similar. This can indicate that there is a comparable amount of peptide at the surface of both of the lipid bilayers with a similar orientation. The peak at approximately 1715 cm^{-1} in the amide I spectrum for lipid A from *Salmonella minnesota* is from the CO bond in the lipid headgroups, and can be ignored for this study.

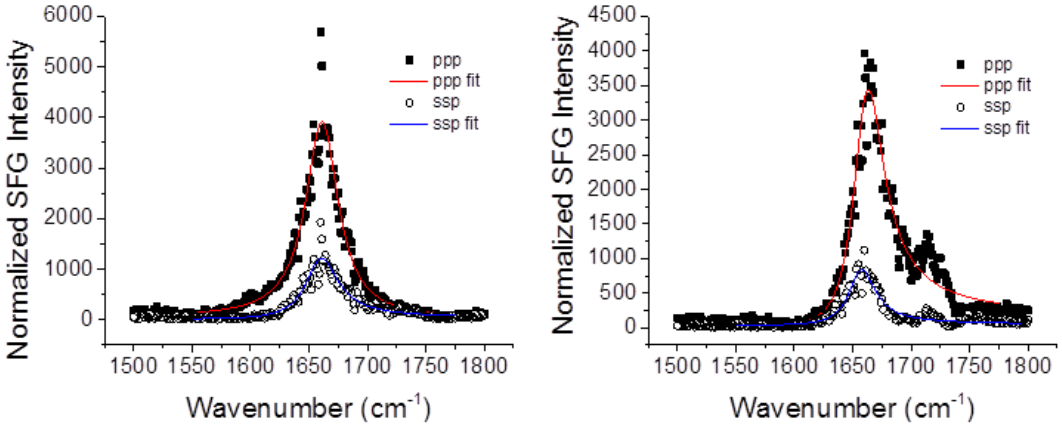

Figure 4.8: SFG signal detected in the amide I frequency region from ovispirin-1 associated with a dDPPE:dDPPG (3:2)-DPPE:DPPG(3:2) bilayer (left) and a dDPPE:dDPPG (3:2)-Lipid A from *Salmonella minnesota* R595 bilayer (right).

We successfully matched the charge density for lipid A from *Salmonella minnesota* with a mixture of DPPE:DPPG (3:2), and it was shown that the amide I region 1655 cm^{-1} signal as well as the outer leaflet C-H region spectra are relatively similar for the two systems at this concentration. Because of this, we think that the association we see is largely electrostatic.

Additionally, we performed SFG experiments to study the interactions between ovispirin-1 G18 with a dDPPE:dDPPG (4:1)-DPPE:DPPG (4:1) bilayer and a dDPPE:dDPPG (4:1)-lipid A bilayer. The SFG signal collected from the dDPPE:dDPPG (4:1)-lipid A bilayer in both the

CD and CH stretching frequency regions are similar to those of the dDPPG-DPPG bilayer, showing that the a dDPPE:dDPPG (4:1)-lipid A bilayer are ordered with quality (Figure 4.4). The SFG amide I signal at 1655 cm^{-1} (again indication of α-helical structure) was higher for the peptide on the lipid A containing bilayer versus on the DPPE:DPPG (4:1) bilayer (Figure 4.9). In this case, the charge for the PE:PG mixed system was -0.1/chain which is half of that for the 3:2 ratio and for lipid A from *Salmonella minnesota* R595. Based on this evidence, we felt the argument of the electrostatic interaction dominating (as also proposed from the study discussed above) in the peptide-lipid bilayer interaction is logical.

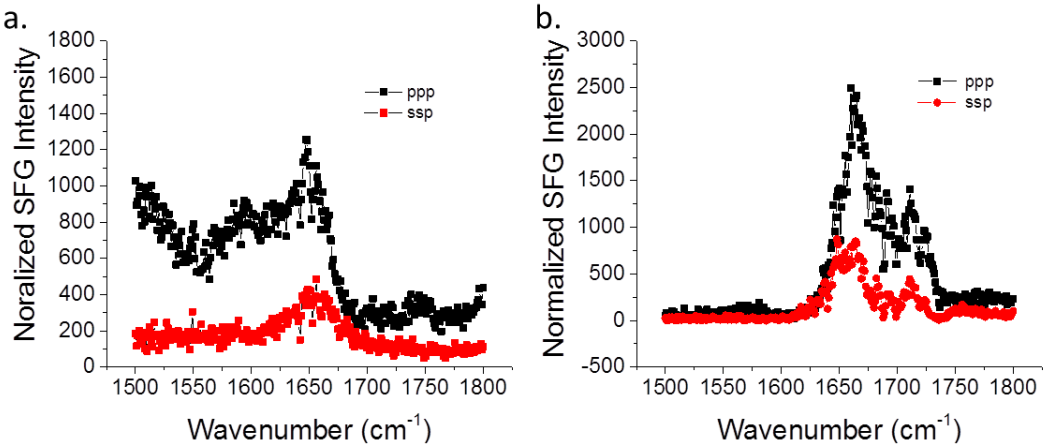

Figure 4.9: SFG signal detected in the amide I frequency region from ovispirin-1 associated with the dDPPE:dDPPG (4:1)-DPPE:DPPG(4:1) bilayer (left) and the dDPPE:dDPPG (4:1)-Lipid A from *Salmonella minnesota* R595 bilayer (right).

This also agrees with literature studies on interactions between lipid A and various peptides. Neville and coworkers [39] showed with that for monolayers of DPPC, DPPG and lipid A, protegrin-1 disrupted the DPPG monolayer at 20 mN m^{-1} the most, and inserted more into lipid A than into DPPC. When they increased the surface pressure to 30 mN m^{-1}, the peptide inserted less than at 20 mN m^{-1} into both DPPC and DPPG. They reported that the peptide interacted mainly with the head groups and that the anionic lipids had an extra adsorbed layer of

peptide in addition to that inserted into the monolayer, indicating the importance of electrostatics. Our above results showed increased peptide association at bilayers that are more negatively charged, which is supported by their results. We did not see a significant increase in leaflet disorder with DPPG compared to lipid A, but that could be because our surface pressure is closer to the 30 mN m^{-1} which they showed was able to decrease the amount of inserted peptide in the monolayers. Another study by Neville and coworkers [34] used lipid A monolayers and showed that as surface pressure is increased the ability for peptide to insert decreases and that peptides might rotate the lipid A molecules so that they can insert into the head group region, but did not cause extensive disorder to the monolayer. It is possible that with gel phase lipids that there could be head group interaction or insertion with little acyl tail disruption, but we would not be able to detect this. The CH_3 signal we observed would be the same before and after, which similar to their results [34]. However, another study shows that protegrin-1 interacts with lipid A monolayers similarly to with DPPG at a low pressure of 20 mN m^{-1}, but is able to disrupt a lipid A monolayer at 35 mN m-1 while the DPPG monolayer is not disrupted [73]. This study used the same concentration that Neville et al. [39] used, but they used a higher pressure with their lipid A (20 vs. 35 mN m^{-1}) and similar ones for DPPG. This suggests that maybe lipid A does not respond the same way as DPPG at higher pressures. Another study showed that LL-37's response to DPPG and lipid A at 30 mN m^{-1} were similar while the insertion/disruption in DPPC was minimal [74]. These peptides obviously rely on electrostatics for association and it appears as though lipid A is often very similar to DPPG in behavior, but the behavior depends on the peptide. Therefore, we think it is reasonable that we see similar response from DPPG and lipid A leaflets in our experiments, given that the charge of the leaflets are similar.

Peptide	Bilayer	Polarization	Peak center	Amplitude	Peakwidth	χ_{eff}	$\frac{\chi_{zzz}}{\chi_{xxz}}$

G18 (50µg/ml)	dDPPG-DPPG	ppp	1661 (0.3)	1834.3 (34)	15.6 (0.3)	117.6	1.80
		ssp	1659 (0.4)	1136.4 (24)	14.6 (0.4)	77.8	--
	dDPPG-Kdo2 Lipid A	ppp	1660 (0.5)	3265.5 (86)	16.7 (0.5)	195.5	1.85
		ssp	1659 (0.5)	1646.3 (57)	13.1 (0.6)	125.7	--
	dPE:dPG(3:2)-PE:PG(3:2)	ppp	1661 (0.5)	1063.2 (29)	17.1 (0.5)	62.2	2.16
		ssp	1659 (0.7)	588.2 (22)	17.2 (0.7)	34.2	--
	dPE:dPG(3:2)-Lipid A from *S. minnesota*	ppp	1660 (0.6)	912.2 (30)	16.1 (0.6)	56.7	2.38
		ssp	1656 (0.6)	389.0 (15)	13.8 (0.7)	28.2	--
I7 (50 µg/ml)	dDPPG-Kdo2 Lipid A	ppp	1618 (2.4)	69.3 (35)	6.2 (3.7)	--	--
		ssp	1620 (2.2)	36.3 (18)	5.2 (3.2)	--	--
		ppp	1660 (0.5)	2696.0 (57)	21.3 (0.5)	126.6	1.54
		ssp	1657 (0.4)	1446.4 (27)	17.6 (0.4)	82.2	--
G8 (50 µg/ml)	dDPPG-Kdo2 Lipid A	ppp	1610 (4.2)	78.4 (71)	11.1 (9.5)	--	--
		ssp	--	--	--	--	--
		ppp	1662 (0.6)	1812.6 (50)	18.3 (0.6)	99.1	1.67
		ssp	1660 (0.7)	873.2 (106)	14.7 (0.6)	59.4	--
I7 (3 µg/ml)	dDPPG-Kdo2 Lipid A	ppp	1618 (2.7)	85.1 (49)	8.0 (5.0)	--	--
		ssp	1620 (2.3)	27.2 (14)	3.4 (2.3)	--	--
		Ppp	1661 (0.5)	2602.6 (61)	19.5 (0.5)	--	--
		ssp	1660 (0.4)	1655 (36)	18.0 (0.5)	--	--
G8 (3 µg/ml)	dDPPG-Kdo2 Lipid A	ppp	1606 (2.7)	50.8 (26)	6.4 (4.1)	---	--
		ssp	--	--	--	--	--
		Ppp	1662 (0.5)	1926.2 (50)	18.2 (0.5)	105.8	1.72
		ssp	1660 (0.4)	963.5 (23)	15.7 (0.5)	61.4	--

Table 4.1: Fitting parameters of the SFG amide I spectra for ovispirin-1 isotope labeled peptides associated with dDPPG-DPPG, dDPPG-Kdo2 Lipid A, dDPPE:dDPPG (3:1)-DPPE:DPPG(3:1), dDPPE:dDPPG (3:1)-Lipid A from *Salmonella minnesota* R595. Fitting error is in parenthesis.

4.3.3 Isotope Labeled Peptide Experiments

4.3.3.1 dDPPG-Kdo2 Lipid A

As stated previously, the results we observed showed that more ovispirin-1 G18 associated on dDPPG-Kdo2 Lipid A bilayers compared to dDPPG-DPPG. Kdo2 Lipid A has a different structure compared to DPPG but the charge per acyl chain is similar. Kdo2 Lipid A contains the lipid A structure of *E. coli* and two 3-deoxy-a-D-mannooctulosonic acid (Kdo) groups. The lipid A is composed of a β-glucosamine-(1-6)-glucosamine-1-phosphate base [Aldrich] with four fatty acid chains attached through either ester or amide bonds. The base also contains two phosphoryl groups, carrying a negative charge each. The Kdo groups, which are part of a hydrophilic inner core, are free to interact with the peptide in solution and are one of the main differences between this lipid A and DPPG [14, 18].

As seen in Figure 4.6, the amide I intensity detected from ovispirin-1 G18 was higher on Kdo2 lipid A, which was unexpected because of the presence of the Kdo2 groups. To explore the possible reason for this, we used I7 and G8 isotope labeled ovispirin-1. I7 is in the hydrophobic region of the peptide and G8 is in the hydrophilic region. It has been shown previously [Ding, B.; Wang, Z.; Ho, J.; Laaser, J.E.; Zanni, M.T.; Chen, Z. Unique Site-specific Structural Information of a Biomolecule at Model Membrane Interface by Incorporating Isotope-labeled Sum Frequency Generation Probes, to be published] that the peak center and peak width of the isotope labeled amide $^{13}C=O$ stretching can be used to determine the local environments of the labeled units and the relative environment that a peptide is in. It was shown that ovispirin-1 I7 has a peak center: 1618 ± 2 cm^{-1} and peak width: 8 ± 3 cm^{-1} on DPPG. Similarly, the observed peak center and peak width for ovispirin-1 G8 were 1610 ± 2 cm^{-1} and 15 ± 5 cm^{-1}, respectively. Figure 4.10

shows the SFG amide I spectra collected from ovisipirin-1 I7 and ovispirin-1 G8 associated with the dDPPG-Kdo2 lipid A bilayer. The spectral fitting information is in Table 4.1 and shows the fitted peak center and peak width comparison in DPPG and Kdo2 lipid A. It is clear from these results that the peptide is in the same environment as in DPPG, and that the difference in signal intensity is not due to the peptides being interfered with or being caught in the Kdo2 groups.

Experiments were also done at 3 µg/ml and while the isotope labeled peaks were sometimes too small to be well fitted, the 1660 cm^{-1} peaks were well resolved. Figure 4.11 shows the 3 µg/ml amide I region. The I7 peak fit well and was determined to be similar to the DPPG case, so it is still in a hydrophobic environment. None of the G8 spectra were consistent at this concentration. This very low signal intensity could be due to the lower concentration, or it could be due to the peptide not being in a consistent environment. If the peptide had moved to a hydrophobic environment, we would expect its peak center to shift closer to 1618 cm^{-1} and its peak width to decrease (closer to 8 cm^{-1}). The peak center had a tendency to shift to an even lower frequency than 1608 cm^{-1} and the peak width was often very small and in the range of the hydrophobic I7 peak width. However, since both values did not shift in the expected way and the I7 residue seems to still be in the same environment, we are not convinced that the G8 residue definitively resides in another environment unless further studies are carried out.

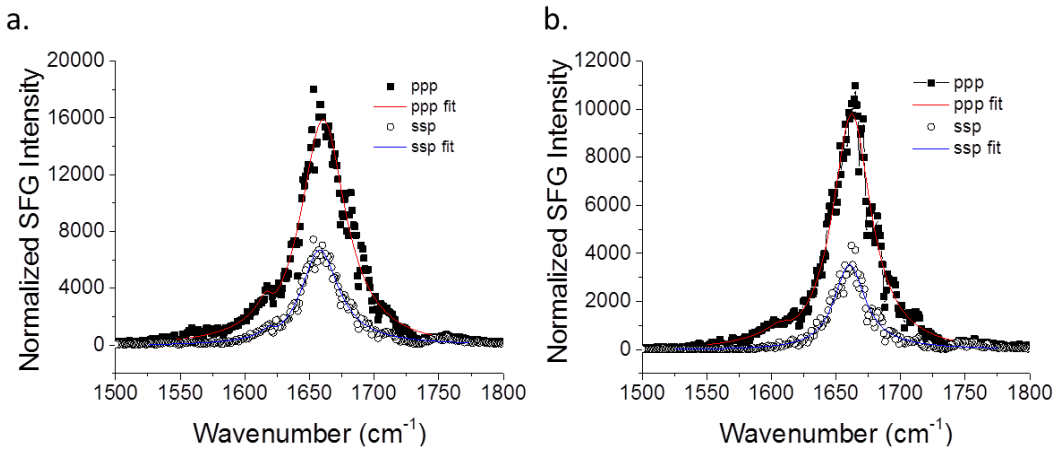

Figure 4.10: (a) Amide I region, dDPPG-Kdo2 Lipid A, 50 µg/ml ovispirin-1 I7 (b) Amide I region, dDPPG-Kdo2 Lipid A, 50 µg/ml ovispirin-1 G8

	I7 peak center (cm^{-1})	I7 peak width (cm^{-1})	G8 peak center (cm^{-1})	G8 peak width (cm^{-1})
DPPG (10 µg/ml)*	1618 ± 2	8 ± 3	1610 ± 2	15 ± 5
Kdo2 lipid A (50 µg/ml)	1618	6.24	1609	11
Kdo2 lipid A (3 µg/ml)	1618	9	--	--

Table 4.2: Peak width and peak centers for isotope labeled ovispirin-1 residues in DPPG and Kdo2 lipid A. *DPPG values were taken from Ding, B.; Wang, Z.; Ho, J.; Laaser, J.E.; Zanni, M.T.; Chen, Z. Unique Site-specific Structural Information of a Biomolecule at Model Membrane Interface by Incorporating Isotope-labeled Sum Frequency Generation Probes, to be published.

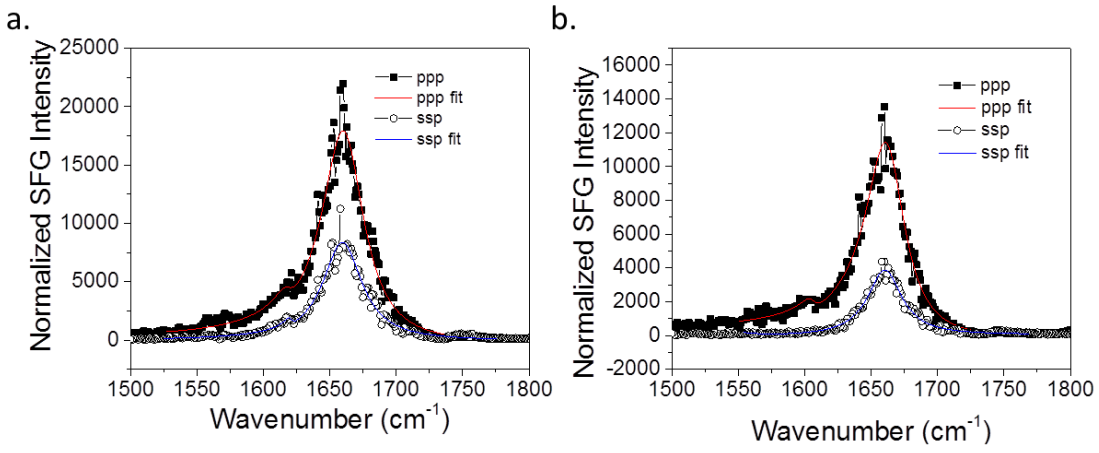

Figure 4.11: (a) 3 µg/ml ovispirin-1 I7 on dDPPG-Kdo2 lipid A (b) 3 µg/ml ovispririn-1 G8 on dDPPG-Kdo2 lipid A

Ovispirin-1 is well known to be a hemolytic and cytotoxic as well as possessing antimicrobial activity [60, 75]. Its MIC for many bacteria is well below the concentration used in this study and several are below 10 µg/ml. Cytotoxicity starts at approximately 25 µg/ml, depending on the cell type [60, 75]. Several studies mentioned earlier, using lipid A monolayers and a variety of peptides including LL-37 and protegrin-1, did see disruption in lipid A monolayers and DPPG at surface pressures similar to ours [39, 73, 74]. Because of these results in literature, we expected to see some activity in ovispirin-1's MIC range. Many of the peptides studied, such as LL-37, are known to start in carpet mode then insert into the bilayer depending on the concentration and lipid bilayer [56, 76, 77]. However, ovispirin-1 is thought to act through the carpet mechanism and lies parallel to the bilayer in the lipid head groups [61, 62]. This difference could be why we don't see substantial disruption of gel phase lipid bilayers by ovispirin-1. Strong interactions with the head groups, to the point where the acyl chains become disordered, may be required and it may be difficult to achieve this when interacting with well-ordered gel phase lipids.

Despite this fact, the peptide association at the bilayer should not be as affected by well-ordered acyl tails since association relies heavily on electrostatic effects. We did see that, in general, the amount of ovispririn-1 that associated at the bilayers of dDPPE:dDPPG-DPPE:DPPG (4:1) compared to dDPPG:dDPPE (4:1)-Lipid A from *Salmonella minnesota* and dDPPG-DPPG compared to dDPPG-Kdo2 were likely similar. The compared bilayers had very similar charge densities, which should have allowed any differences to be attributed to acyl chain/hydrophobic effects or to the different head groups on lipid A. However, we saw very similar results. Many studies concluded that the key to lipid A's resistance to permeability is due to the well-ordered and tightly packed acyl chains and head group [39, 45, 47, 48]. However, there are groups that attribute the resistance to the O-antigen chain or other parts of the polysaccharide core [23-25]. It is hard to say based on our results which of these cases are more likely since we saw no membrane disruption. It is possible that the mode of action and structure of the particular peptide determines which defense is more effective, and that is why there is a debate on which feature is more responsible.

4.4 Conclusions

In this study, we successfully showed that we can make supported lipid bilayer of gel phase inner leaflet and a gel phase lipid A outer leaflet. This new model is very promising as one to model outer cell membranes that include tightly packed lipid A molecules. We saw, through SFG experiments, that ovispirin-1 likely interacted through electrostatics on both Kdo2 lipid A and lipid A from *Salmonella minnesota* containing bilayers. This was demonstrated by the similar amide I peptide spectra intensities and ppp/ssp ratios on the phospholipid and lipid A outer leaflets when the net charges were approximately the same. When the charge is different, as we showed with the lipid A from *Salmonella minnesota* example, there is more peptide

association on the lipid A system because of a more anionic environment. We also used isotope labeling to investigate peptide orientation/environment and concluded that ovispirin-1 interaction with the Kdo2 lipid A containing bilayers was similar to the interaction with pure DPPG. By using the peak width and peak center results from the isotope labeled residue peak fitting, we determined that ovispirin-1 is probably in the same orientation in Kdo2 lipid A at 50 μg/ml as it is in DPPG at 10 μg/ml. Also, the data suggests that ovispirin-1 is still associated in this same orientation at 3 μg/ml on Kdo2 lipid A. This agrees with previous unpublished data that ovispirin-1 lies on the surface at all concentrations.

Because it is difficult to determine if lipid A is able to deter peptide pore formation when we used a peptide that lies down, it would be interesting to study a peptide that is known to insert into the bilayer and see the results on lipid A vs. DPPG containing membranes. Also, once a peptide that causes disruption/destruction is found, it would be interesting to add Ca^{2+} ions to see if SFG can determine if there are any differences in peptide-bilayer interaction since it is thought that certain ions can help make the lipid A layer more resistant to permeabilization [44, 46, 47]. Also, the lipid A/LPS leaflet could be varied to see the difference in peptide-lipid interaction with longer vs. shorter O-antigen chains. Additionally, it would be interesting to see if those interactions are affected by both a difference in O-antigen chains and in lipid A packing, or if the peptide induced disruption is generally only affected by one of the structural features.

4.5 References

1. Navarre, W.W.; Schneewind, O. *Microbiology and Molecular Biology Reviews* **1999**, *63*, 174-229.
2. Dirienzo, J.M.; Nakamura, K.; Inouye, M. *Annual Review of Biochemistry* **1978**, *47*, 481-532.
3. Nikaido, H. *Microbiology and Molecular Biology Reviews* **2003**, *67*, 593-656.

4. Hardaway, R.M. *American Surgeon* **2000**, *66*, 22-29.
5. Cohen, J. *Nature* **2002**, *420*, 885-891.
6. Raetz, C.R.H.; Whitfield, C. *Annual Review of Biochemistry* **2002**, *71*, 635-700.
7. Andra, J.; Lohner, K.; Blondelle, S.E.; Jerala, R.; Moriyon, I.; Koch, M.H.J.; Garidel, P.; Brandenburg, K. *Biochemical Journal* **2005**, *385*, 135-143.
8. Japelj, B.; Pristovsek, P.; Majerle, A.; Jerala, R. *Journal of Biological Chemistry* **2005**, *280*, 16955-16961.
9. Bhunia, A.; Chua, G.L.; Domadia, P.N.; Warshakoon, H.; Cromer, J.R.; David, S.A.; Bhattacharjya, S. *Biochemical and Biophysical Research Communications* **2008**, *369*, 853-857.
10. Bhunia, A.; Mohanram, H.; Domadia, P.N.; Torres, J.; Bhattacharjya, S. *Journal of Biological Chemistry* **2009**, *284*, 21991-22004.
11. Nagaoka, I.; Hirota, S.; Niyonsaba, F.; Hirata, M.; Adachi, Y.; Tamura, H.; Tanaka, S.; Heumann, D. *Clinical and Diagnostic Laboratory Immunology* **2002**, *9*, 972-982.
12. Rosenfeld, Y.; Papo, N.; Shai, Y. *Journal of Biological Chemistry* **2006**, *281*, 1636-1643.
13. Ruiz, N.; Kahne, D.; Silhavy, T.J. *Nature Reviews Microbiology* **2006**, *4*, 57-66.
14. Hancock, R.E.W. *Annual Review of Microbiology* **1984**, *38*, 237-264.
15. Alexander, C.; Rietschel, E.T. *Journal of Endotoxin Research* **2001**, *7*, 167-202.
16. Nikaido, H. *Science* **1994**, *264*, 382-388.
17. Wang, X.Y.; Quinn, P.J. *Progress in Lipid Research* **2010**, *49*, 97-107.
18. Caroff, M.; Karibian, D. *Carbohydrate Research* **2003**, *338*, 2431-2447.
19. Kabanov, D.S.; Prokhorenko, I.R. *Biochemistry (Moscow)* **2010**, *75*, 383-404.
20. Kontrohr, T.; Kocsis, B. *Journal of Biological Chemistry* **1981**, *256*, 7715-7718.
21. Wilkinson, S.G. *Progress in Lipid Research* **1996**, *35*, 283-343.
22. Kilar, A.; Dornyei, A.; Kocsis, B. *Mass Spectrom Rev* **2013**, *32*, 90-117.
23. Banemann, A.; Deppisch, H.; Gross, R. *Infection and Immunity* **1998**, *66*, 5607-5612.
24. Nikaido, H. *Biochimica Et Biophysica Acta* **1976**, *433*, 118-132.
25. Murray, G.L.; Attridge, S.R.; Morona, R. *Journal of Bacteriology* **2006**, *188*, 2735-2739.
26. Le Brun, A.P.; Clifton, L.A.; Halbert, C.E.; Lin, B.; Meron, M.; Holden, P.J.; Lakey, J.H.; Holt, S.A. *Biomacromolecules* **2013**, *14*, 2014-2022.
27. Kubiak, J.; Brewer, J.; Hansen, S.; Bagatolli, L.A. *Biophysical Journal* **2011**, *100*, 978-986.
28. Nomura, K.; Inaba, T.; Morigaki, K.; Brandenburg, K.; Seydel, U.; Kusumoto, S. *Biophys J* **2008**, *95*, 1226-1238.
29. Pontes, F.J.S.; Rusu, V.H.; Soares, T.A.; Lins, R.D. *Journal of Chemical Theory and Computation* **2012**, *8*, 3830-3838.
30. Tong, J.H.; McIntosh, T.J. *Biophysical Journal* **2004**, *86*, 3759-3771.
31. Mookherjee, N.; Wilson, H.L.; Doria, S.; Popowych, Y.; Falsafi, R.; Yu, J.J.; Li, Y.X.; Veatch, S.; Roche, F.M.; Brown, K.L.; Brinkman, F.S.L.; Hokamp, K.; Potter, A.; Babiuk, L.A.; Griebel, P.J.; Hancock, R.E.W. *Journal of Leukocyte Biology* **2006**, *80*, 1563-1574.
32. Kaconis, Y.; Kowalski, I.; Howe, J.; Brauser, A.; Richter, W.; Razquin-Olazaran, I.; Inigo-Pestana, M.; Garidel, P.; Rossle, M.; Martinez de Tejada, G.; Gutsmann, T.; Brandenburg, K. *Biophys J* **2011**, *100*, 2652-2661.
33. Mangoni, M.L.; Epand, R.F.; Rosenfeld, Y.; Peleg, A.; Barra, D.; Epand, R.M.; Shai, Y. *Journal of Biological Chemistry* **2008**, *283*, 22907-22917.

34. Neville, F.; Hodges, C.S.; Liu, C.; Konovalov, O.; Gidalevitz, D. *Biochimica Et Biophysica Acta-Biomembranes* **2006**, *1758*, 232-240.
35. Allende, D.; McIntosh, T.J. *Biochemistry* **2003**, *42*, 1101-1108.
36. Bhunia, A.; Domadia, P.N.; Bhattacharjya, S. *Biochimica Et Biophysica Acta-Biomembranes* **2007**, *1768*, 3282-3291.
37. Bhunia, A.; Ramamoorthy, A.; Bhattacharjya, S. *Chemistry* **2009**, *15*, 2036-2040.
38. Domadia, P.N.; Bhunia, A.; Ramamoorthy, A.; Bhattacharjya, S. *Journal of the American Chemical Society* **2010**, *132*, 18417-18428.
39. Neville, F.; Ishitsuka, Y.; Hodges, C.S.; Konovalov, O.; Waring, A.J.; Lehrer, R.; Lee, K.Y.C.; Gidalevitz, D. *Soft Matter* **2008**, *4*, 1665-1674.
40. Pristovsek, P.; Feher, K.; Szilagyi, L.; Kidric, J. *Journal of Medicinal Chemistry* **2005**, *48*, 1666-1670.
41. Rana, F.R.; Macias, E.A.; Sultany, C.M.; Modzrakowski, M.C.; Blazyk, J. *Biochemistry* **1991**, *30*, 5858-5866.
42. Delcour, A.H. *Biochimica Et Biophysica Acta-Proteins and Proteomics* **2009**, *1794*, 808-816.
43. Ruiz, N.; Kahne, D.; Silhavy, T.J. *Nature Reviews Microbiology* **2009**, *7*, 677-683.
44. Jeworrek, C.; Evers, F.; Howe, J.; Brandenburg, K.; Tolan, M.; Winter, R. *Biophysical Journal* **2011**, *100*, 2169-2177.
45. Kotra, L.P.; Golemi, D.; Amro, N.A.; Liu, G.Y.; Mobashery, S. *Journal of the American Chemical Society* **1999**, *121*, 8707-8711.
46. Matsuzaki, K.; Sugishita, K.; Harada, M.; Fujii, N.; Miyajima, K. *Biochimica Et Biophysica Acta-Biomembranes* **1997**, *1327*, 119-130.
47. Snyder, D.S.; McIntosh, T.J. *Biochemistry* **2000**, *39*, 11777-11787.
48. Snyder, S.; Kim, D.; McIntosh, T.J. *Biochemistry* **1999**, *38*, 10758-10767.
49. Ferris, F.G.; Beveridge, T.J. *Canadian Journal of Microbiology* **1986**, *32*, 594-601.
50. Schneck, E.; Papp-Szabo, E.; Quinn, B.E.; Konovalov, O.V.; Beveridge, T.J.; Pink, D.A.; Tanaka, M. *Journal of the Royal Society Interface* **2009**, *6*, S671-S678.
51. Nguyen, K.T.; King, J.T.; Chen, Z. *Journal of Physical Chemistry B* **2010**, *114*, 8291-8300.
52. Ye, S.J.; Nguyen, K.T.; Chen, Z. *Journal of Physical Chemistry B* **2010**, *114*, 3334-3340.
53. Yang, P.; Wu, F.G.; Chen, Z. *J Phys Chem C Nanomater Interfaces* **2013**, *117*, 3358-3365.
54. Yang, P.; Ramamoorthy, A.; Chen, Z. *Langmuir* **2011**, *27*, 7760-7767.
55. Nguyen, K.T.; Le Clair, S.V.; Ye, S.J.; Chen, Z. *Journal of Physical Chemistry B* **2009**, *113*, 12358-12363.
56. Ding, B.; Soblosky, L.; Nguyen, K.; Geng, J.Q.; Yu, X.L.; Ramamoorthy, A.; Chen, Z. *Scientific Reports* **2013**. *3*, 1-8, DOI: 10.1038/srep01854.
57. Ding, B.; Chen, Z. *J Phys Chem B* **2012**, *116*, 2545-2552.
58. Chen, X.; Wang, J.; Kristalyn, C.B.; Chen, Z. *Biophys J* **2007**, *93*, 866-875.
59. Ding, B.; Chen, Z. *Abstracts of Papers of the American Chemical Society* **2013**, *246*, 14625-14634.
60. Sawai, M.V.; Waring, A.J.; Kearney, W.R.; McCray, P.B.; Forsyth, W.R.; Lehrer, R.I.; Tack, B.F. *Protein Engineering* **2002**, *15*, 225-232.
61. Woys, A.M.; Lin, Y.S.; Reddy, A.S.; Xiong, W.; de Pablo, J.J.; Skinner, J.L.; Zanni, M.T. *Journal of the American Chemical Society* **2010**, *132*, 2832-2838.

62. Yamaguchi, S.; Huster, D.; Waring, A.; Lehrer, R.I.; Kearney, W.; Tack, B.F.; Hong, M. *Biophysical Journal* **2001**, *81*, 2203-2214.
63. *Avanti polar lipids, inc.* [cited 2014 04/01/2014]; Structure of Lipid A from Kdo2 Lipid A]. Available from: http://avantilipids.com/index.php?option=com_content&view=article&id=403&Itemid=123&catnumber=699500.
64. *Avanti polar lipids, inc.* [cited 2014 04/01/2014]; Structure of Lipid A from Salmonella Minnesota R595]. Available from: http://avantilipids.com/index.php?option=com_content&view=article&id=405&Itemid=318&catnumber=699200.
65. Buck, M.; Himmelhaus, M. *Journal of Vacuum Science & Technology A: Vacuum, Surfaces, and Films* **2001**, *19*, 2717-2736.
66. Chen, Z.; Shen, Y.R.; Somorjai, G.A. *Annual Review of Physical Chemistry* **2002**, *53*, 437-465.
67. Eisenthal, K.B. *Chemical Reviews* **1996**, *96*, 1343-1360.
68. Humbert, C.; Busson, B. **2011**, 279-321.
69. Lambert, A.G.; Davies, P.B.; Neivandt, D.J. *Applied Spectroscopy Reviews* **2005**, *40*, 103-145.
70. Moad, A.J.; Simpson, G.J. *Journal of Physical Chemistry B* **2004**, *108*, 3548-3562.
71. Shen, Y.R. *Nature* **1989**, *337*, 519-525.
72. Zhuang, X.; Miranda, P.B.; Kim, D.; Shen, Y.R. *Physical Review B* **1999**, *59*, 12632-12640.
73. Gidalevitz, D.; Ishitsuka, Y.J.; Muresan, A.S.; Konovalov, O.; Waring, A.J.; Lehrer, R.I.; Lee, K.Y.C. *Proceedings of the National Academy of Sciences of the United States of America* **2003**, *100*, 6302-6307.
74. Neville, F.; Cahuzac, M.; Nelson, A.; Gidalevitz, D. *Journal of Physics-Condensed Matter* **2004**, *16*, S2413-S2420.
75. Kalfa, V.C.; Jia, H.P.; Kunkle, R.A.; McCray, P.B.; Tack, B.F.; Brogden, K.A. *Antimicrobial Agents and Chemotherapy* **2001**, *45*, 3256-3261.
76. Wildman, K.A.H.; Lee, D.K.; Ramamoorthy, A. *Biochemistry* **2003**, *42*, 6545-6558.
77. Burton, M.F.; Steel, P.G. *Natural Product Reports* **2009**, *26*, 1572-1584.

CHAPTER 5

SUMMARY AND FUTURE DIRECTIONS

Cell membranes are complex structures that serve as a barrier between the inner contents of a cell and the outside environment. The composition of these complex structures varies depending on the cell type and the organism. For example, the outer leaflet of mammalian membranes is largely composed of zwitterionic PC phospholipids, sphingomyelin and cholesterol, but also contains other lipids and membrane proteins. In contrast, the outer plasma membrane leaflet of bacterial membranes is largely composed of zwitterionic PE lipids and a smaller amount of anionic PG lipids and cardiolipin. This is important information to keep in mind when studying AMPs. AMPs are a potential alternative to traditional antibiotics and are attractive because they are generally thought to interact with and disrupt lipids in the cell membrane, rather than other constituents on cell membranes or inside the cell. The cell membrane is believed to be more difficult to alter, in an attempt to gain resistance, compared to other structures that are often targeted by antibiotics. If the goal is to further develop therapies based on these AMPs, it is important that we understand how and why AMPs work. Because cell membranes are so complicated, it is beneficial to study the AMPs interacting with cell membrane models to gain more information. In order to get the most accurate and relevant information,

models as close as possible to actual cell membranes should be used. Many past studies have used relatively simple model bilayers, and the goal of this thesis is to compare the peptide-bilayer interactions of these simple model membranes to more complicated and hopefully more realistic models.

In Chapter 2, we used SFG to investigate the interaction of an AMP, LL-37, with bilayers consisting of POPC and CHO. Cholesterol is thought to cause fluid bilayers, such as POPC, to be more gel-like which contributes to a higher resistance to disruption by membrane active peptides. In our experiments, we compared the interaction of LL-37 on POPC:CHO (1:1) to pure POPC and POPC:POPG:CHO (0.7:0.3:1) to POPC:POPG (7:3) bilayers. It was found that the addition of CHO to POPC bilayers attenuated LL-37's ability to associate on the bilayer. We saw no peptide signal, but it was confirmed that some peptide molecules did interact with the cholesterol containing bilayer. After adding an anionic lipid, POPG, more LL-37 molecules were able to associate with the bilayer, which was indicated by a small peptide signal in the amide I range, but this amount was still much smaller than the amount associated on the POPC:POPG (7:3) bilayer. These results clearly show that the addition of cholesterol to zwitterionic POPC bilayers results in a reduced association of LL-37 peptides. The likely reason that cholesterol inhibits peptide association and disruption is because it causes the bilayer to become more rigid and well packed which makes it more difficult for interaction, possibly because it is more energetically difficult. A similar effect was seen in our lab when studying another AMP, alamethicin. Alamethicin had low peptide signal when associated with gel phase lipids and higher signal when associated with fluid phase lipids.

In the future, it would be interesting to expand these studies. As was mentioned before, the composition of membranes depends on the cell type, and that also applies to the CHO

content. It would be interesting to conduct a study over a range of cholesterol percentages. Additionally, cholesterol is known to interact more favorably with sphingomyelin molecules. Together, cholesterol and sphingomyelin are believed by many to be the main components of "lipid rafts". Including these structures has been shown in some studies to change the way that peptides interact with the bilayer compared to phospholipid-cholesterol bilayers. Therefore, it would be interesting to investigate this more complex system using SFG.

In Chapter 3, we focused on more complex bacterial membranes instead of mammalian membranes. The most commonly used lipids for our peptide-bilayer studies for modeling bacterial membranes are POPG and POPC:POPG mixtures. Such bilayers have been widely used as cell membrane models in the literature. However, the overall surface charge of POPG is much higher than that found on an actual bacterial membrane and the lipid head group interactions between POPC and POPG are not the same as between the PE and PG head groups more commonly found in bacterial membranes. Therefore, we studied the differences in the interactions between several membranes active peptides with bilayers composed of dDPPG-POPG and dDPPG-*E. coli* polar lipid extract. We presented an asymmetric bilayer setup to study the differences in interaction between the two model systems and the peptides MSI-594, ovispirin-1, magainin 2, melittin, and LL-37. It was found that the interaction results for each peptide were different and depended on the peptide's charge/residue and interaction mechanism. In particular, we showed that the time dependent interaction of peptide and lipid bilayer is one of the large and most important differences between the two different lipid systems.

Overall, it was shown that pure POPG is not a sufficient model of bacterial cell membranes for the purposes of investigating detailed peptide-lipid interaction mechanisms. For example, there were multiple cases where the pure POPG outer leaflet did not model the

interaction kinetics or the leaflet disruption in the same manner as the *E. coli* polar lipid extract. In order to determine the entire story of a peptide's interaction in detail, we must take all of the data into consideration. If some of this data is not correct, either due to different electrostatic interactions, or possibly because of different lipid interactions (like the different interactions between PE with PG lipids compared to the interaction of PC with PG lipids), we might draw a different conclusion. Therefore, while it is suitable to use POPG as a simple model to test if a peptide will associate with anionic lipids, one should take into consideration the caveats related to using it as the only model. With this in mind, the use of a more complex bilayer, like the *E. coli* polar lipid extract, is likely a better option for modeling bacterial membranes. This is extremely important because the interaction kinetics should be of great interest when considering new antibiotic therapies. The work we presented will hopefully be generally interesting for designing better testing regimens for future antimicrobial compounds.

Future work in this area for our group could entail comparing both POPG and *E. coli* polar lipid extracts to mixtures of PG/PE/cardiolipin lipids to determine if particular peptides interact more similarly with the POPG or the *E. coli* lipid mixture. These studies could determine whether it is possible to use a phospholipid mixture to model the bilayer and if so, one could then customize the composition depending on what bacteria they intended to model.

Chapter 4 focused on studying model cell membranes that mimic bacterial outer cell membranes and their interaction with isotope labeled samples of the membrane active peptide, ovispirin-1. We established that we were able to make stable bilayers of dDPPG-Kdo2 Lipid A and dDPPE:dDPPG(3:1)-Lipid A from *Salmonella minnesota* R595. These bilayers are asymmetric like in the previous chapter and allow us to study the outer leaflet of interest. We then found that ovispirin-1 G18 disrupted the outer leaflet of both dDPPG-DPPG and dDPPG-

Kdo2 Lipid A bilayers similarly. However, there were more peptides associated to the Kdo2 Lipid A containing system. This difference was likely because of a slightly higher anionic charge on Kdo2 vs. DPPG. Using isotope labeled ovispirin-1 I7 and G8, we were able to determine that the isotope labeled residues were in generally the same environment on both dDPPG-DPPG and dDPPG-Kdo2 Lipid A bilayers. We studied ovispirin-1 G18 interacting with dDPPE:dDPPG(3:1)-DPPE:DPPG(3:1) and dDPPE:dDPPG (3:1)-Lipid A from *Salmonella minnesota* R595. It was observed that the amide I peptide signal was approximately the same on both bilayers when the charge of both outer leaflets was the same. When the charge of the lipid A leaflet was more negative than the phospholipid mixture, more peptides associated to the lipid A leaflet. This experiment suggests that the previous Kdo2 system's higher peptide association is due to the charge difference. The similar peptide signals for lipid A from *Salmonella minnesota* R595 and the phospholipid mixture suggest that the peptides were similar in number on the bilayer surfaces and they had similar orientations. Overall, I showed that we can make asymmetric surface supported bilayers with lipid A molecules, and that isotope labeled ovispirin-1 molecules, which lay down on the bilayer surface, interact similarly with lipid A containing bilayers and with the mixed phospholipid bilayers. To our knowledge, this is the first time that SFG has been used to study outer cell membrane models.

Future studies in this area could include studying a peptide that is known to insert into the bilayer. Ovispirin-1 is generally thought to lay down on the bilayer and act through the carpet mechanism regardless of the bilayer composition. Therefore, if a peptide that acts through a pore forming mechanism is used, we might be able to discern if the more tightly packed lipid A acyl chains inhibit the peptide from causing disruption as easily as on phospholipid bilayers. Also, the lipid A molecules studied here contained only part of or none of the core oligosaccharide region

and no O-antigen chain. In future studies, it would be interesting to study more complete LPS molecules instead of just the lipid A portion, as there is still some discrepancy as to whether the tightly packed acyl chains or the O-antigen chain contribute to LPSs ability to protect gram negative bacteria from outside threats.

In summary, we used SFG to study three different complex bilayer systems modeling mammalian membranes, bacterial plasma membranes, and bacterial outer cell membranes. The results obtained show that simple phospholipid models are not adequate for modeling mammalian membranes or bacterial membranes because some bilayer qualities that influence peptide interaction are not properly expressed. For example, the omission of cholesterol or other bilayer components can cause the peptide to interact differently with a bilayer, which in turn can cause one to draw incorrect conclusions about the toxicity of a drug in question. Also, using the incorrect lipids in a model bacterial membrane can cause similar problems as the simple model. POPG is highly anionic while actual membranes are less negatively charged and also contain PE lipids that oppose positive curvature (though to be induced by toroidal pore forming AMPs). Additionally, some contain LPS which is thought to protect the cell from drugs crossing the outer membrane. Without considering these other components, it is unlikely that preliminary tests of future antimicrobial drugs will be accurate. Therefore, it is important to continue studying more complex lipid bilayers in order to develop the most useful models for studying bilayer and bilayer-molecule interactions.